GEOLOGY OF THE NEOGENE BASIN FILL ON THE INDIAN WELL WILDERNESS 7.5' QUADRANGLE, CENTRAL RIO GRANDE RIFT, NEW MEXICO

by

Colin Cikoski

Submitted in partial fulfillment

of the requirements for the degree of

Master of Science in geology

New Mexico Institute of Mining and Technology

Department of Earth and Environmental Science

Socorro, New Mexico

August, 2010

ABSTRACT

Mid-Miocene to Recent sediments on the Indian Well Wilderness (IWW) quadrangle record a complicated sedimentologic and structural history of evolving depositional systems, syndepositional orthogonal fault sets, multiple phases of faulting, and changing basin geometry. Sediments accumulated in two basins of the Rio Grande rift: the Miocene Bosque basin (new informal name) and the younger Plio-Pleistocene Socorro basin, which overprints and masks the older basin. Gravity data, bedding attitudes, and previous work indicate the Bosque basin is a southeast-tilted half-graben bounded by a north-northeast-trending "master" fault that runs along the base of Little San Pascual Mountain (LSPM).

Bosque basin sediments are dominated by northeast- to east-derived piedmont deposits originating from an ancestral LSPM highland. Lowermost sediments also contain bouldery material derived from local intrabasinal fault blocks. East-derived sediments record two distinct source areas in the eastern highland: a northern source that delivered mainly rhyolitic ignimbrite clasts and a southern area that produced a mix of andesitic lava and ignimbrite clasts. Rare Permian limestone and "red bed" clasts are also found in deposits from the southern source and in upper deposits from the northern source. At this time (circa 10 Ma), the Chupadera Mountains, which today bound the west side of the basin, were largely or completely buried.

At the toe of the southern part of the piedmont, a large dune field developed that lapped eastward against the piedmont, occasionally advancing and overtaking the piedmont, presumably during dry spells. Alluvial-eolian interactions between the fan and the erg resulted in a particularly sand-rich distal piedmont facies, which was reworked by westerly winds to feed the dune field.

The eastern piedmont gradually retreated, and sometime after 8.5 Ma a western piedmont prograded into the area, perhaps prior to the arrival of the ancestral Rio Grande (ARG) or exhumation of the Chupadera Mountains. Western piedmont deposits overlie eastern piedmont deposits with an irregular angular unconformity, indicating a highly erosive contact, but local southward paleocurrents on either side of the contact suggest a somewhat gradual shift from eastern piedmont to western piedmont dominance.

Between 4 and 7 Ma, the ARG entered the area and the Chupadera Mountains were largely exhumed, establishing the depositional setting seen today, with a western piedmont from the Chupadera Mountains dominating the sedimentation but interacting with an axial fluvial facies at the east and south ends of the quadrangle. Sediments continued to accumulate in the now-Socorro basin, until about 800 ka, at which point the ARG and its tributaries entrenched episodically, incising in a series of steps that resulted in a flight of terraces and fans.

Interestingly, intrabasinal structures are dominantly northwest-trending, despite the large north-northeast-striking faults bounding the basin. Faults in the general area are categorized as 1) north-northeast-striking, down-to-the-west, basin-bounding faults; 2) shallowly- to moderately-dipping down-to-the-southwest; 3) moderately-dipping down-to-the-northeast; and 4) steeply-dipping down-to-the-southwest. The one exception is a

southwest-dipping apparent reverse fault, which nearby bedding attitudes suggest was originally a down-to-the-northeast normal fault that fault block rotation tilted to an apparent reverse orientation. Category 1 and 2 faults appear syndepositional with mid-Miocene sedimentation and concurrent with stratal tilting; category 3 and 4 faults appear to post-date stratal tilting, and hence seem to be a part of a younger generation of faulting. Fault orientations are likely controlled by pre-existing Precambrian and Laramide weaknesses, and are probably influenced by the location of the basin at a "shoulder" in the rift. This "shoulder" is formed by the northwest margin of the Jornada stable block, a small (~65 X 75 km) block of relatively strong lithosphere that has resisted extensional deformation and forced a right-lateral transfer of extensional strain just south of the study area. Broad, northwest-striking, map-scale folds are also found in the area, which are attributed to ramp-flat fault geometries and blind slip on buried faults.

Today, sediments of the Bosque basin are exposed only along a northwest-trending swath apparently controlled by flexural uplift of the footwall block of the Bosque del Apache (BDA) fault. Sediments are only exposed on the footwall of the fault, but disappear from the surface again away from the fault to the southwest. This is attributed to the slight (0.5°) southwestward dip of the erosional upper contact of the Miocene basin fill, which projects the contact into the subsurface away from the BDA fault. This, in turn, is attributed to Plio-Pleistocene flexural uplift of the footwall block. Fault scarps in Quaternary sediments along the BDA fault indicate it is still active today.

The area has known groundwater and hydrothermal resources, as well as seismic hazards, to which the results of this study can be applied. In addition, the study suggests that pre-existing structures and crustal properties exert strong control on the development

of rift basins.

Keywords: Rio Grande rift, extensional basins, Santa Fe Group, Popotosa Formation

ACKNOWLEDGEMENTS

This research was funded by the USGS EdMap and StateMap programs. I would like to thank Tom Melanson, Colin Lee, and the rest of the Bosque del Apache National Wildlife Refuge staff for access to the Indian Well and Chupadera Wildernesses. I also thank Tom Waddell for permission to map on the Armendaris Ranch, and Alan Olson and Butch Hammack for access to the Highland Springs Ranch. Lisa Peters and the students at the New Mexico Geochronology Research Laboratory ran all of the $^{40}Ar/^{39}Ar$ analyses presented here. The New Mexico Bureau of Geology and Mineral Resource provided field vehicles.

The advice and guidance of Richard Chamberlin was instrumental to this thesis. I learned more about field geology and mapping from field trips and discussions with him than from any other instructor in my seven years of studies. Dave Love, Bruce Harrison, and Peter Mozley also provided important insights into the geology of the area.

TABLE OF CONTENTS

PAGE

ABSTRACT.....

ACKNOWLEDGEMENTS..... ii

TABLE OF CONTENTS..... iii

LIST OF FIGURES..... viii

LIST OF TABLES..... xii

LIST OF PLATES..... xiii

INTRODUCTION..... 1

Geologic setting..... 4

Previous work in the southern Socorro and Bosque basins..... 5

Purpose of the study..... 12

Geographic setting..... 13

Methods of investigation..... 13

STRATIGRAPHY..... 18

Pre-Santa Fe Group..... 18

Precambrian and Paleozoic rocks..... 18

Precambrian..... 18

Paleozoic sedimentary rocks 20
Datil Group 22
Mogollon Group 22
Santa Fe Group 25
Popotosa Formation 27
Rhyolite tuff-dominated conglomerates and associated alluvial sandstones (Tpt1, Tpt2) 31
Eolian sandstones (Tpe) and mixed eolian and alluvial sandstones (Tps), with minor conglomerates 34
Andesitic lava-dominated conglomerates, with associated alluvial and eolian sandstones (Tpa) 38
Interbedded tuff- and lava-dominated conglomerates with associated alluvial sandstones (Tpfi) 40
Tuff-dominated conglomerates and associated alluvial sandstones toward the top of the Popotosa (Tpft1, Tpft2) 42
Mixed clast suite conglomerates and alluvial sandstones in the north of the field area (Tpfn, Tpfb) 44
Volcanic units interbedded in the Popotosa Formation (Tbo, Tbt1, Tbt2) 45
Middle Santa Fe Group transitional unit (Tsp) 49
Sierra Ladrones Formation 51
Sierra Ladrones ancestral Rio Grande deposits (QTsf) 53
Sierra Ladrones piedmont deposits (QTsp) 57
Post-Santa Fe Group deposits 60

Piedmont deposits (Qvn1 though Qvn5, Qvs1, Qvs2, Qpu, Qt, Qa, Qae, Qai) 62
Older piedmont deposits (Qvn_, Qvs_, Qt, Qpu) 63
Younger piedmont deposits (Qa, Qai, Qae) 65
Axial fluvial (Qvof, Qf) and transitional (Qvot) deposits 65
Older Rio Grande deposits (Qvof) 65
Younger Rio Grande deposits (Qf) 66
Transitional deposits (Qvot) 66
Colluvial deposits (Qc, Qls) 67
Apache #1-A oil test well 67
PROVENANCE STUDIES OF POPOTOSA STRATA 72
Clast suites 72
Sandstone petrography 75
PALEOGEOGRAPHY 81
Pre-Santa Fe Group 81
Syn- and post-Santa Fe Group 82
Popotosa paleogeography 84
Transitional paleogeography 91
Sierra Ladrones to present (paleo)geography 93
Piedmont replacement through Santa Fe Group time 93
STRUCTURE 101
Review of local structure 101
Precambrian 101
Laramide, excluding volcanism 102

Cenozoic volcanism 103
Previous work on rift structures in the area 104
Rift structures of the IWW basin fill 107
Faulting 107
Folding 112
Interpretation of IWW basin fill rift structures 113
Faulting 113
Multiple phases of faulting 114
Reactivation of multiple weakness planes 118
"Rift shoulder" effect 119
Folding and stratal rotations 125
Flexural uplift in the footwall of the Bosque del Apache fault 129
APPLIED GEOLOGY 131
Resource potential 131
Seismic risk 132
SUMMARY 134
Eocene to present geologic history 134
IMPLICATIONS FOR RIFT BASIN DEVELOPMENT 140
REFERENCES 142
APPENDIX I – FREQUENCY DATA FOR PALEOCURRENT AND PALOWIND ROSE DIAGRAMS 152
APPENDIX II – CLAST COUNT DATA 153
APPENDIX III – SANDSTONE PETROGRAPHY 156

APPENDIX IV – $^{40}AR/^{39}AR$ GEOCHRONOLOGY 158

LIST OF FIGURES

PAGE

Figure 1 – Map of Neogene rift basins, including those of the Rio Grande rift. 2

Figure 2 - Geologic and physiographic features of the area around the study area 3

Figure 3 - Geographic features of the area around the study area 6

Figure 4 - Distribution of outcrops of Miocene basin fill in the Socorro area..... 7

Figure 5 - Map locating previous studies in the general area of this study 8

Figure 6 - Shaded relief map of the area around the study area, overlain by Bouger gravity contours 10

Figure 7 - Index map showing informal names of faults used in this thesis.....11

Figure 8 - Google™ Earth view of the southern Socorro basin from the south 12

Figure 9 - An example image from the ArcScene program 14

Figure 10 - Simplified stratigraphic columns for Mogollon Group and older units from surrounding highlands..... 19

Figure 11 - Correlation chart for the units used on the geologic map 20

Figure 12 - Schematic depiction of domino-style faulting 26

Figure 13 - A picture of the oreodont fossil recovered from the field area..... 30

Figure 14 - Rose diagrams of paleocurrent indicator attitudes for a) Tpt1 and b) Tpt2 ... 32

Figure 15 - Rose diagram of attitudes of the dip directions of eolian cross-stratifications, indicating paleowind direction 35
Figure 16 - Rose diagram of paleocurrent indicator attitudes for the Tpa map unit 38
Figure 17 - Rose diagram of paleocurrent indicator attitudes for the Tpfi map unit 40
Figure 18 - Cross-sections illustrating the possible interpretations of the two outcrops of basalt located in the immediate footwall of the Bosque del Apache fault 48
Figure 19 - Rose diagram of paleocurrent indicator attitudes for the Tsp map unit 50
Figure 20 - Rose diagrams of paleocurrent indicator attitudes for a) QTsf and Qvof and b) QTsp 54
Figure 21 - Photo of a QTsf concretion. 55
Figure 22 - Photo of an ancestral Rio Grande bluff line in the southwest of the field 56
Figure 23 - Outcrop-scale exposure of the angular unconformity separating east-tilted Popotosa eolian sandstones from gently-dipping Sierra Ladrones piedmont gravels 58
Figure 24 - Rose diagram of all paleocurrent indicator attitudes from the Popotosa Formation exposed in the study area 59
Figure 25 - Stages of carbonate horizon development 60
Figure 26 - ArcScene image demonstrating how the piedmont wraps around the Chupadera Mountains. 64
Figure 27 - Simplified lithologic log for the Apache 1-A oil test well with the interpretation presented here. 68
Figure 28 - Schematic diagrams depicting two scenarios that could explain the juxtaposition of tuff-dominated and lava-dominated regions in the eastern highland source area for the upper Popotosa Formation 74

Figure 29 - Thin section locations overlain on the geologic map 76
Figure 30 - Scatter plots showing the modal abundances of four phases in the thin sections described in the text 78
Figure 31 - Inferred paleogeography for the area in the early Oligocene 83
Figure 32 - a) Interpreted paleogeography for basal Popotosa time, between about 16 and 15 Ma 85
Figure 33 - Interpreted paleogeography for the study area and surroundings in later Popotosa time, between about 15 and 8 Ma 87
Figure 34 - Interpreted paleogeography for the study area and surroundings during the transitional period 92
Figure 35 - Generalized paleogeography for Sierra Ladrones and post-Santa Fe Group times, beginning between 4 and 7 Ma 94
Figure 36 - Block diagrams depicting the lateral migration of sedimentary facies due to tectonic surface tilting in a half-graben 97
Figure 37 - Stratal tilt versus age graph of Cather et al. (1994) for strata in the northern Socorro basin 105
Figure 38 - Generalized block diagrams demonstrating how contemporaneous fault block rotation and deposition results in ‘fanning’ of stratal dips 113
Figure 39 - Map of faults in the study area, with colors to distinguish their relative ages 116
Figure 40 - Shaded relief map overlain by Bouger gravity contours, faults from the field area, and the approximate extent of the Jornada stable block 119
Figure 41 - A) Generalized geologic map for the overlapping synthetic accommodation

zone described by Mack and Seager (1995). B) Model for the generation of NE-trending normal faults in the accommodation zone 121

Figure 42 - Summary figure from Hudson et al. (1998), showing vertical axis rotations, derived from paleomagnetic data, of small fault blocks in a left laterally sheared transfer zone 122

Figure 43 - a) One of McClay et al.'s (2002) experimental set-ups in plan view. b and c) Results of the experiment depicted in 43a 124

Figure 44 - Summary diagram from Janecke et al. (1998) demonstrating the most common mechanisms for generating both longitudinal and transverse folds in extensional settings 126

Figure 45 - Green-line topographic map of the IWW quadrangle with the BDA and nearby faults, as well as the location of a well that delivers 33°C water from 252 ft 132

Figure 46 - Block diagrams schematically summarizing the geologic evolution of the area 135

Figure 47 - Block diagrams demonstrating how flexural uplift due to slip along the BDA fault could result in exposure of Miocene basin fill in this area 139

LIST OF TABLES

PAGE

Table 1: Fault plane data 110

LIST OF PLATES

Plate 1: Geologic map ..... In Pocket

Plate 2: Cross-sections ..... In Pocket

Plate 3: Clast count pie diagrams ..... In Pocket

INTRODUCTION

This study focuses on the Santa Fe Group and post-Santa Fe sediments on the Indian Well Wilderness (IWW) quadrangle. These sediments accumulated in half-graben basins of the Rio Grande rift (RGR), a north-trending narrow belt of continental extension dividing northern and central New Mexico approximately in half (Figure 1). Today, these sediments are within the southern portion of the Socorro basin, a Plio-Pleistocene sedimentary basin that is superimposed on older basin(s) of Miocene age. Prior to this study, the mapped area received only local attention, and this work is the first to study all the Plio-Pleistocene and Miocene sediments exposed on the quadrangle.

Several previous workers studied the rift basins north of Socorro in detail and documented multiple phases of tectonic activity and changing depositional settings (summarized in Cather et al., 1994a). The basins north and south of Socorro are separated by the Socorro accommodation zone (SAZ; Figure 2) of Chapin (1989), which acted as both a structural and topographic divide for most of the area's rift history (Chamberlin, 1980). As such, the results of the research to the north can only tentatively be extrapolated southward. Although several graduate students examined the mountains south of the SAZ (e.g., theses by Roth [1980], Petty [1979], and Osburn [1978] in the southern Magdalena Mountains, by Eggleston [1982] in the central Chupadera Mountains, and by Geddes [1963] on Little San Pascual Mountain), this is the first

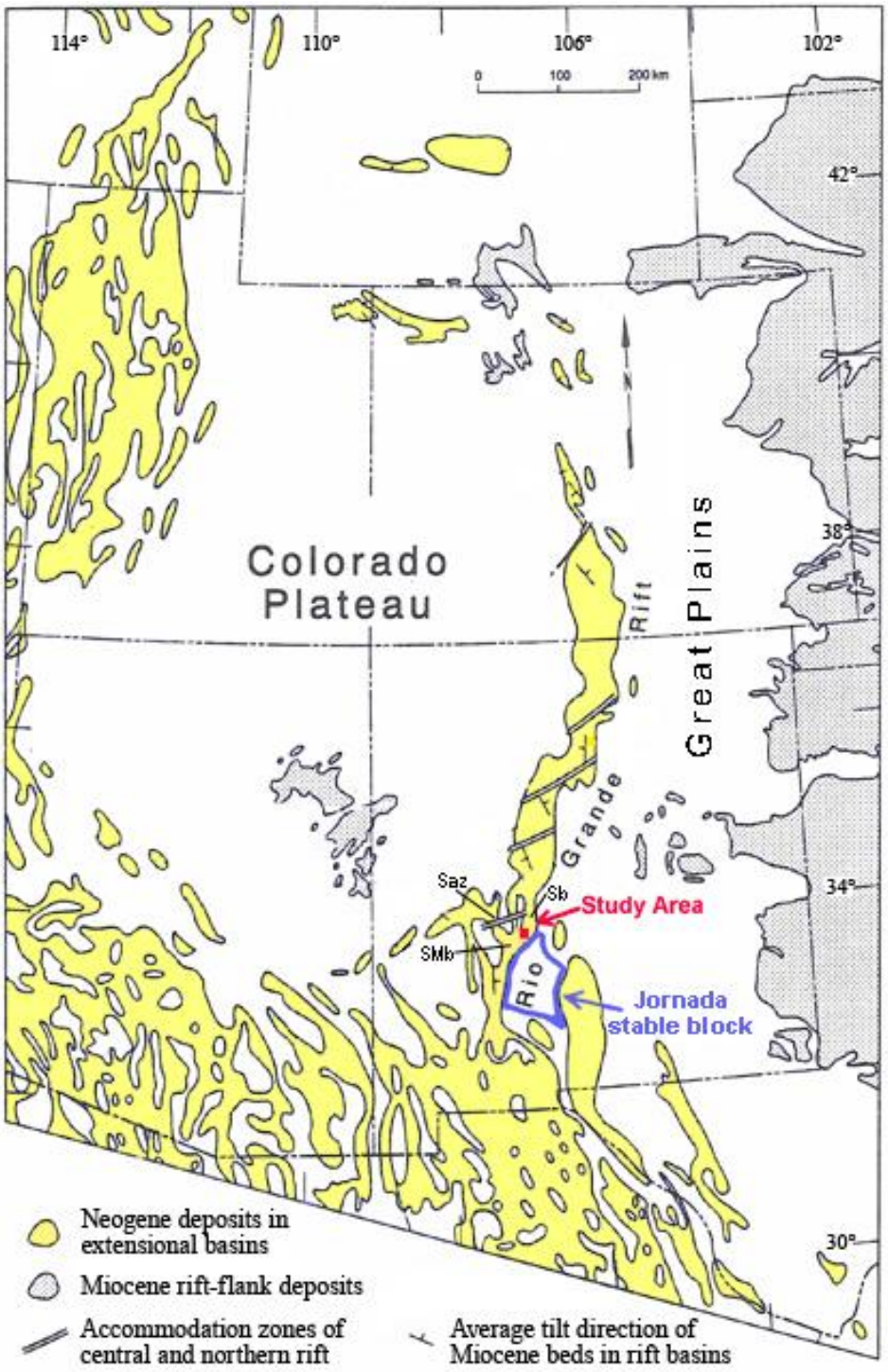

Figure 1 – Map of Neogene rift basins, including those of the Rio Grande rift (north-trending tongue of basins in the center). Abbreviations: Saz: Socorro accommodation zone; Sb: Socorro basin; SMb – San Marcial basin. Adapted from Chapin and Cather, 1994.

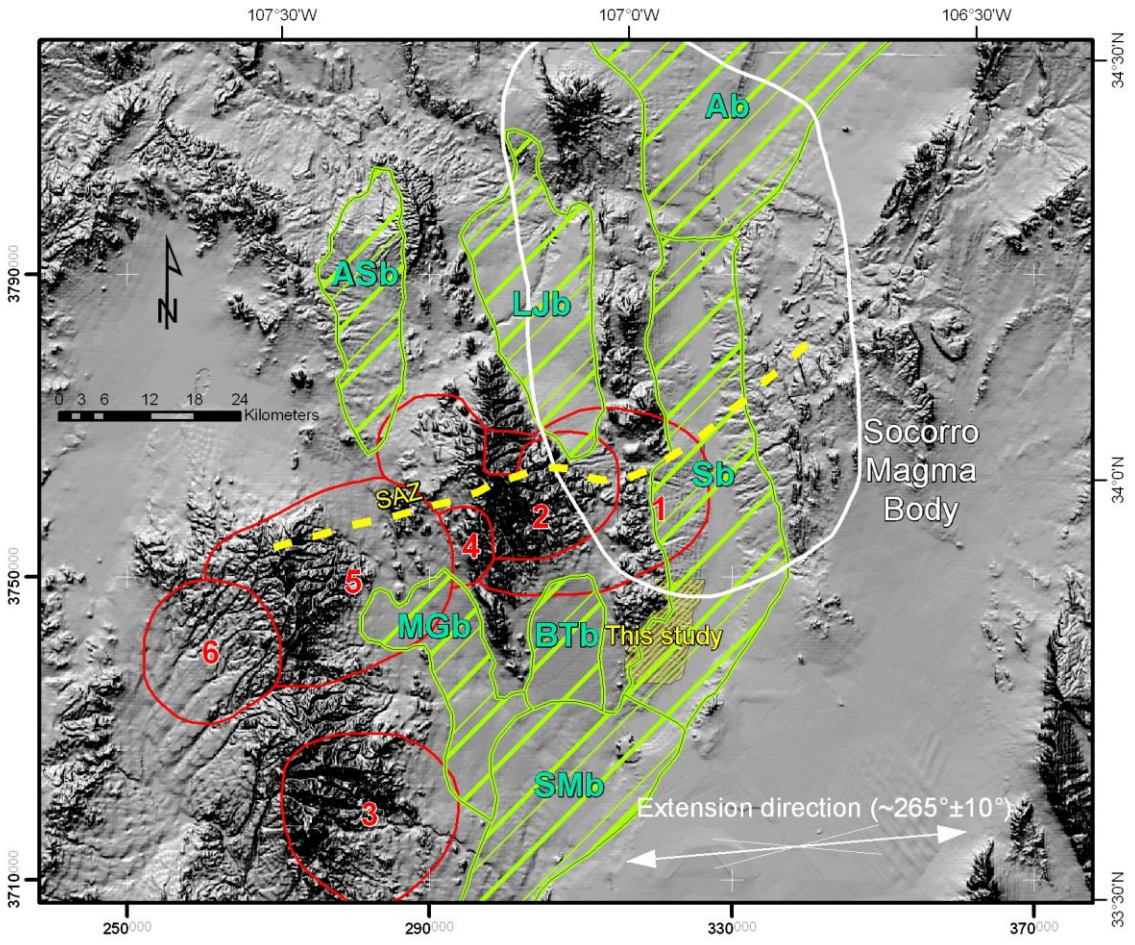

Figure 2 - Geologic and physiographic features of the area around the study area. White line delineates the extent of the Socorro Magma Body as per Balch et al. (1997), red lines delineate calderas, green hachured areas located Rio Grande rift basins, and the yellow dashed line approximately locates the Socorro Accommodation Zone. Caldera margins and SAZ location after Chamberlin et al. (2004). Extension direction is the local (around Socorro basin) vector determined by Chamberlin et al. (2007). Yellow hachured area is the field area of this study. Abbreviations: Ab – Albuquerque basin, ASb – Abbey Springs basin, BTb – Broken Tank basin, LJb – La Jencia basin, MTb – Milligan Gulch basin, SAZ – Socorro Accommodation Zone, Sb – Socorro basin, SMb – San Marcial basin. Caldera numbers: 1 – Socorro caldera, 2 – Sawmill Canyon caldera, 3 – Nogal Canyon caldera, 4 – Hardy Ridge caldera, 5 – Mount Withington caldera, 6 – Bear Trap Canyon caldera. 40,000-meter UTM NAD27 grid.

detailed study on the basin fill itself.

Basin fill mapping is important from both pure and applied standpoints. The basin fill records the paleogeographic, paleoclimatic, and structural evolution of the basin, providing important insights into the development of the rift as a whole. From an applied standpoint, the basin fill can host useful groundwater and geothermal resources, and provides the record for evaluating active faults. Thus, this research may be beneficial to a number of users.

Geologic setting

The RGR (Figure 1) consists of a north-trending, right-stepping, en echelon series of mainly half-graben basins separated by transfer or accommodation zones (Chapin and Seager, 1975). In New Mexico, the rift separates the largely undeformed Colorado Plateau from the Great Plains province, and grades southward into the Basin and Range. Many of its basins received considerable attention either in recent years (e.g., San Luis and Española basins: see Smith, 2004; Albuquerque basin: see Connell, 2004; Engle, Palomas, and basins further south: see Lozinsky, 1986, and Mack, 2004) or in the past ("Popotosa basin" of Bruning [1973]: see Cather et al., 1994a). A significant gap in our understanding exists, however, between the studies of Cather et al. (1994a) and Lozinsky (1986), in which lie the southern Socorro and San Marcial basins. This study addresses the former.

The Socorro basin is a Pliocene to recent half-graben rift basin extending from the town of San Acacia in the north to the southern terminus of the Chupadera Mountains, and is bounded on the west by the Chupadera-Socorro-Lemitar mountain chain and on

the east by uplifted pre-Cenozoic sedimentary strata (Figures 2, 3). It is a hydrologically open basin, connected to the San Marcial and Albuquerque basins to the south and north, respectively, by the Rio Grande. It is divided roughly in half by the SAZ, an east-northeast trending zone marked by recurrent volcanism and subhorizontal strata separating west-tilted strata to the north from east-tilted strata in the south (Chapin, 1989). These regions are informally referred to here as the northern and southern Socorro basins, respectively.

The Socorro basin, as well as the La Jencia, Milligan Gulch, Broken Tank, and San Marcial basins around it, overprints multiple Miocene basins with boundaries that are not necessarily reflected in the modern topography (cf. Cather et al., 1994a). Strata from these basins are locally found at the surface in and around present-day highlands (Figure 4). This thesis concerns deposits of both the Socorro basin and an earlier Miocene basin overprinted by the Socorro basin; I will informally refer to the later as the Bosque basin.

Previous work in the southern Socorro and Bosque basins

Although many workers have examined the sediments of the northern Socorro basin, most crucially Bruning (1973), Chamberlin (1980), and Cather et al. (1994a), only large-scale and local work has been done in the southern Socorro basin. In compiling a geologic map of Socorro County, Osburn (1984) performed local, coarse-scale mapping of the basin fill and basement rocks in this area. Chamberlin et al. (2002) and Cather (2002) began detailed mapping of the basin fill, covering the areas north and northeast of the IWW quadrangle, respectively. Hendrickx and Harrison (2000), Chamberlin et al. (2006), and Chamberlin (unpublished) conducted local detailed studies on the quadrangle

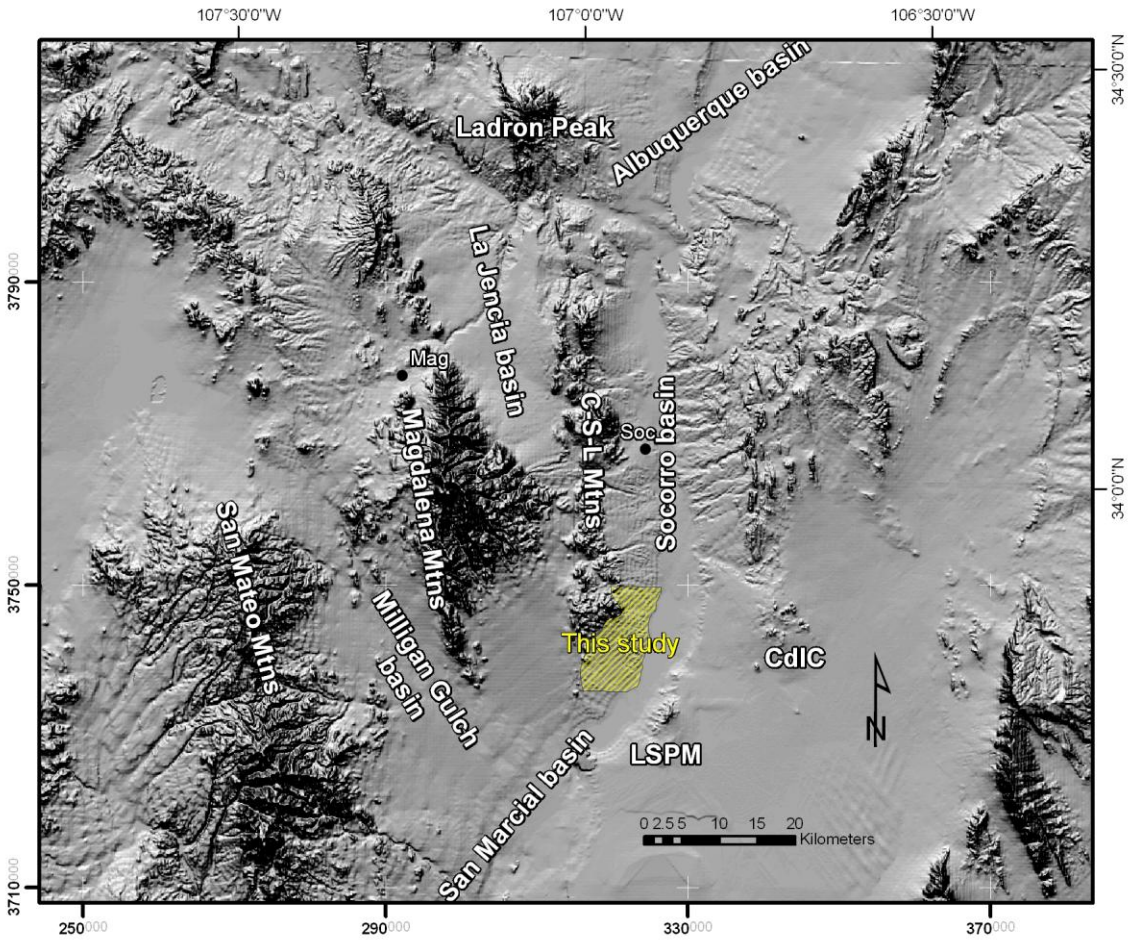

Figure 3 - Geographic features of the area around the study area. Abbreviations: CdlC: Cerro de la Campana; C-S-L Mtns: Chupadera-Socoro-Lemitar mountain range; LSPM: Little San Pascual Mountain; Mag: town of Magdalena; Soc: town of Socorro. 40,000-meter UTM NAD27 grid.

itself. Also of importance to this study are the results of Eggleston (1982) and Geddes (1963), who mapped the mountains to the northwest and southeast of the field area. See Figure 5 for a map of nearby previous studies.

Previous work around the field area suggested the IWW-area basins would be southeast-tilted half-graben dominated by down-to-the-northwest normal faulting. Geddes (1963) mapped and measured a gravity profile around Little San Pascual

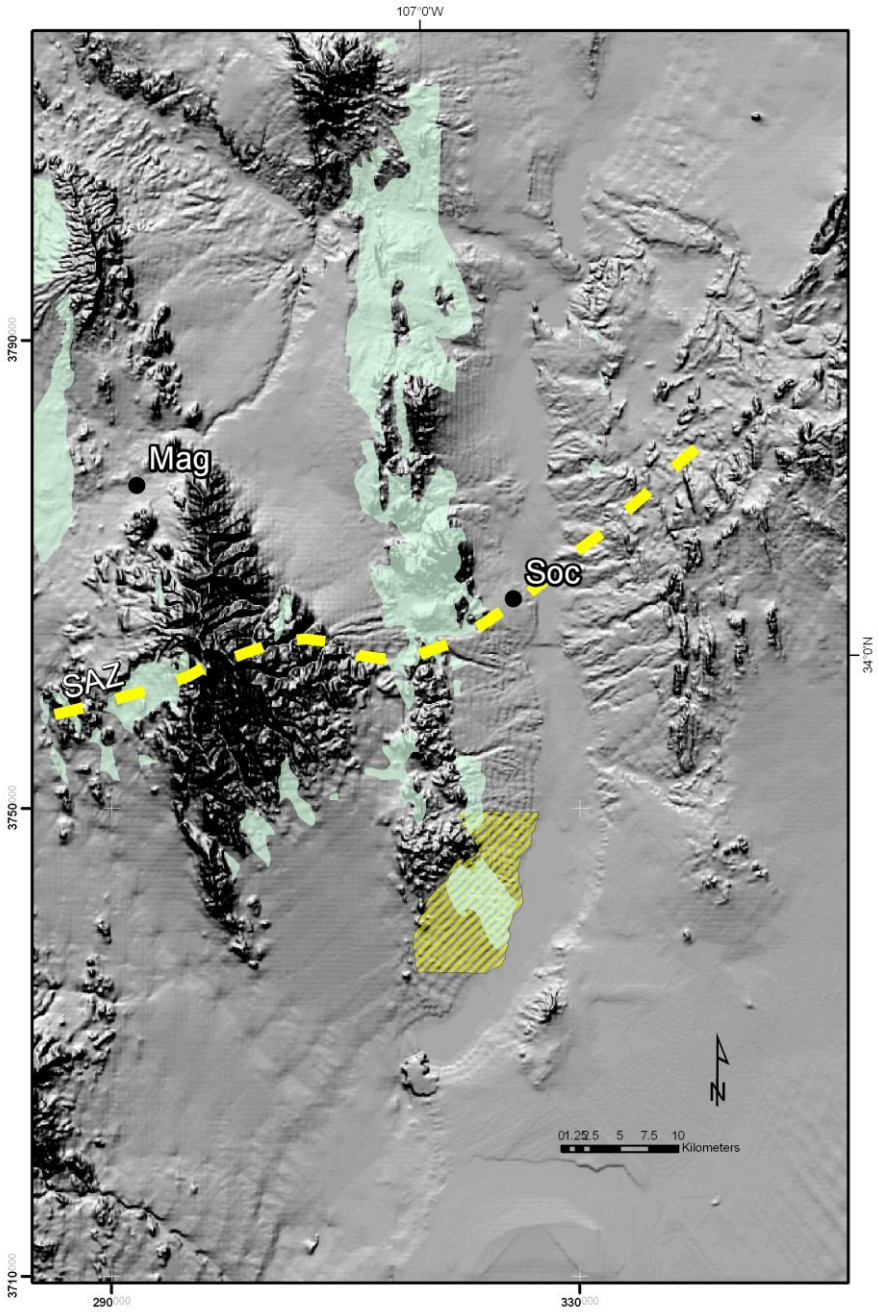

Figure 4 - Distribution of outcrops of Miocene basin fill in the Socorro area. Teal shading locates areas of Miocene basin fill at the surface, after NMBGMR (2003) and Cather et al. (2004). Yellow dashed lines locates the Socorro accommodation zone (SAZ), and the field area is hatched in yellow. Soc: town of Socorro; Mag: town of Magdalena. 40,000-meter UTM NAD27 grid.

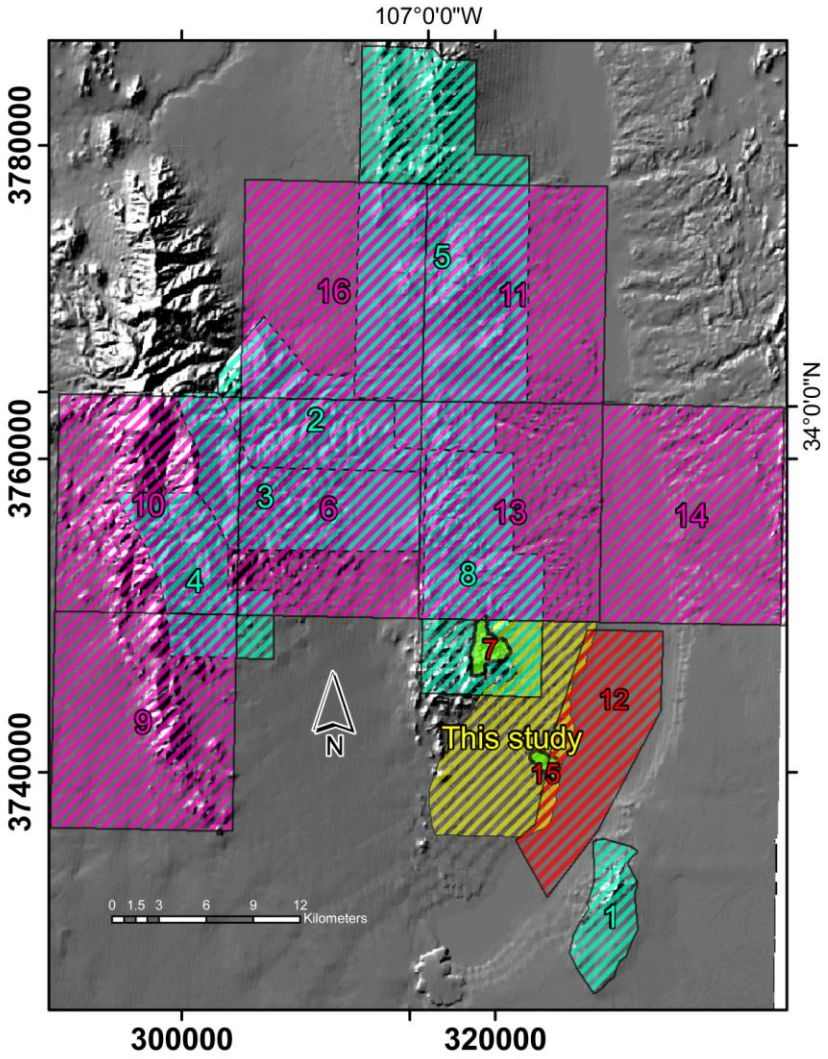

Figure 5 - Map locating previous studies in the general area of this study. Yellow hatched area is the study area, purple hatch lines locate New Mexico Bureau of Geology and Mineral Resource geologic maps, light blue hatches locate theses and dissertations, green hatched areas are local studies on the quadrangle itself, and the red hatches area is the Rio Grande floodplain on the BDA NWR. Osburn's (1984) study encompasses the extent of this map. 20,000-meter UTM NAD27 grid. Key to numbers:

1 - Geddes, 1963
2 - Osburn, 1978
3 - Petty, 1979
4 - Roth, 1980
5 - Chamberlin, 1980
6 - Osburn et al., 1981
7 - Kent, 1982
8 - Eggleston, 1982
9 - Osburn et al., 1985
10 - Osburn et al., 1988
11 - Chamberlin, 1999
12 - Hendrickx and Harrison, 2000
13 - Chamberlin et al., 2002
14 - Cather, 2002
15 - Chamberlin et al., 2006
16 - Chamberlin and Osburn, 2006

Mountain (LSPM) to the southeast of the basin, and found the mountain dominated by Paleozoic limestones and lesser clastic sedimentary rocks, folded into a northeast-striking anticline, and bound on the west by a large down-to-the-northwest normal fault. Mapping in the central Chupadera Mountains to the northwest of the field area, Eggleston (1982) similarly found that the largest faults nearest this study's field area were north-northeast-striking with down-to-the-northwest sense of movement, and that the strata were rotated to the southeast, in agreement with dominantly down-to-the-northwest faulting. Gravity data by Keller (1983) corroborates these results, locating a steep, northeast-trending gravity gradient at the base of LSPM (Figure 6), and suggesting that Geddes' mountain front fault is the basin-bounding "master" fault.

In contrast, local preliminary work on the quadrangle itself found only northwest-striking structures. Both Chamberlin et al. (2006) and Chamberlin (unpublished) mapped down-to-the-northeast normal faults, referred to here as the Solitude and Bosque del Apache (BDA) faults, respectively (see Figure 7). The later in particular appeared to be a major fault, juxtaposing late Miocene sediments intercalated with the 8.6 Ma basalt of Broken Tank against Plio-Pleistocene sediments; drill hole observations near the town of Socorro suggests this requires perhaps as much as 340 meters of offset (R.M. Chamberlin, pers. comm.). Neither study attempted to address the relationship of these northwest-striking structures to the large north-northeast-trending faults described above.

Interestingly, preliminary work also found the Miocene sediments on the study area to be dominantly west-transported (Chamberlin et al., 2006), in contrast to the present depositional environment dominated by east-transported sediments. Today, the study area is dominated by the eastern piedmont of the southern Chupadera Mountains,

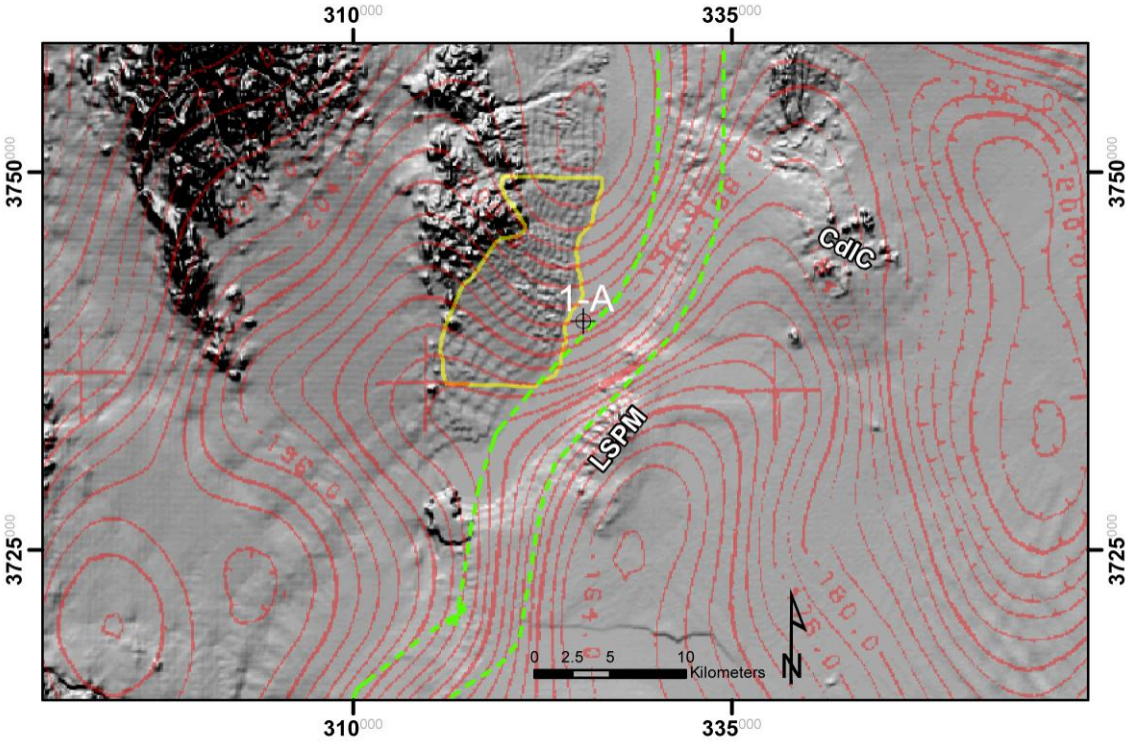

Figure 6 - Shaded relief map of the area around the study area, overlain by Bouger gravity contours (red lines, interval of 2 mGal) from Keller (1983). Study area outlined in yellow. Green dashed lines bound a sinuous steep gravity gradient, decreasing to the west, that is here interpreted to be a major down-to-the-west and -northwest basin-bounding fault system. "1-A" locates the Apache oil test well 1-A, the well log of which is discussed in detail in its own section. Abbreviations used for geographic features: CdlC: Cerro de la Campana; LSPM: Little San Pascual Mountain. 25,000-meter UTM NAD27 grid.

with some Rio Grande sediments on the east and south ends (Figure 8). The sediments examined by Chamberlin et al., however, suggest that in Miocene time the same area was dominated by the piedmont of some ancestral LSPM highland. The cause of this significant piedmont replacement was not examined.

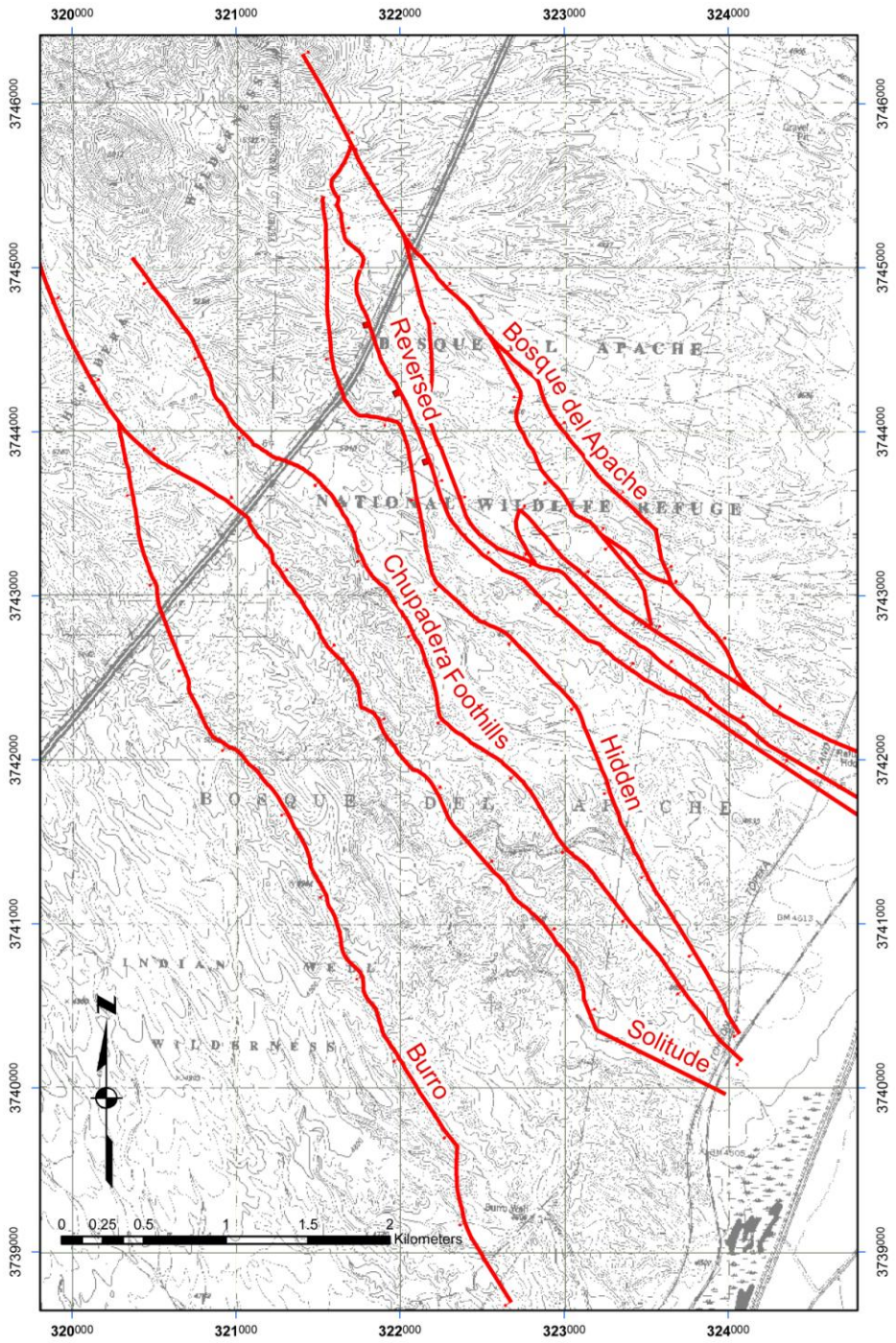

Figure 7 - Index map showing informal names of faults used in this thesis. “Bosque del Apache fault” and “Chupadera Foothills fault” are generally abbreviated to “BDA fault” and “CF fault,” respectively. 1000-meter UTM NAD27 grid.

Figure 8 - Google™ Earth view of the southern Socorro basin from the south, looking up the Rio Grande. Notice that today the study area is dominated by the Chupadera Mountains piedmont, and the eastern piedmont is laterally restricted to the base of Little San Pascual Mountain.

Purpose of the study

Results from the previous work raise several questions:

- How are the northeast-trending, apparently basin-bounding faults related to the northwest-trending structures found within the basin? Are they different-age structures accommodating a changing stress field, or contemporaneous structures resulting from a complex field? Are northeast-trending structures found in the basin as well?
- How and why does the depositional setting shift from footwall piedmont-dominated in Miocene time to hanging wall piedmont-dominated, as seen today?

The purpose of this study was to collect the data necessary to try to answer these questions. In addition, previous work established the potential for low temperature geothermal resources (cf., Barroll and Reiter, 1995) and seismic hazards (cf. Machette et

al, 1998) in the area, which the results of this study could be applied to.

Geographic setting

The field area consists of the piedmont of the Indian Well Wilderness (IWW) quadrangle (Figure 2, 3, and 8), where rift basin fill as old as middle Miocene is exposed. The IWW quadrangle lies in south-central New Mexico along the Rio Grande, approximately 17 km due south of the town of Socorro. It is mostly undeveloped, as almost half of it lies on wilderness land of the Bosque del Apache National Wildlife Refuge (BDA NWR) and the rest is rangeland. The quadrangle contains the southern tip of the Chupadera Mountains, their eastern piedmont, and Rio Grande floodplain.

Due to the undeveloped nature of the area, access is provided by only a few roads. I-25 cuts southwestward across the quad, almost splitting it in half, while NM-1 skims the eastern and southeastern edge. A dirt power-line road provides additional access to the area west of NM-1. Dirt roads also enter the quadrangle from the west to provide access to the westernmost edge of the quadrangle, near Willow Springs. Most of the field area lies within the Indian Well or Chupadera Wildernesses, where motorized vehicles are forbidden and research permits are required for access.

Methods of investigation

The primary form of research was general geologic mapping at a scale of 1:24,000, performed on 1:24,000 USGS topographic maps. This was supplemented with clast counts of conglomerate clast lithologies to determine the nature of clast lithology variability; visually estimated modal abundances of sandstone thin sections to determine the relationship between fluvial sandstones, eolian sandstones, and associated

conglomerates; and $^{40}Ar/^{39}Ar$ age determinations.

I performed most mapping by making foot traverses through arroyos, where the older basin fill is best exposed, although Quaternary mapping consisted mainly of aerial photo and topographic data interpretation. As the older basin fill consists mainly of three lithologies (conglomerate, alluvial sandstone, eolian sandstone), foot traverses mainly involved examining how the relative proportions of the three lithologies varied across the landscape, with contacts placed where change appeared most rapid. This unfortunately resulted in many approximately located contacts, as the relative proportions generally changed gradually, or poor exposure obscured the variability. I located Quaternary contacts mainly by analysis of aerial photos and 10m DEM data. I correlated Quaternary piedmont deposits by visually projecting piedmont surfaces in the program ArcScene (e.g., Figure 9), then correlating deposits which appeared to have originally been a part of a continuous piedmont. Contacts and correlations were locally field checked as a part

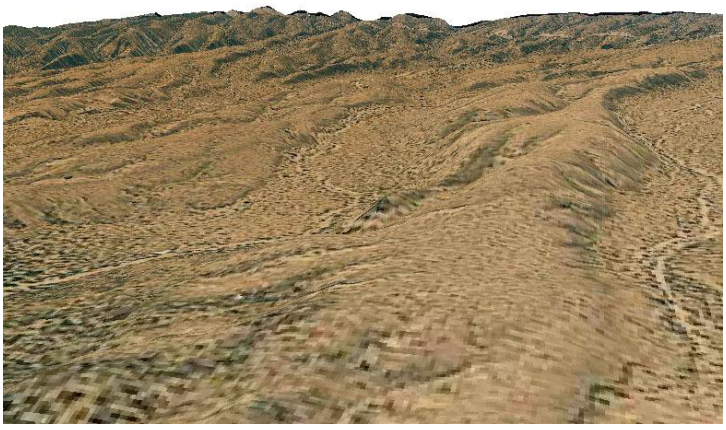

Figure 9 - An example image from the ArcScene program. The program "drapes" georeferenced images, in this case an aerial photo, over the DEM of the area, giving the image a 3rd dimension. Notice that the tops of piedmont deposits can be visually followed and correlated.

of foot traverses. The resulting geologic map is presented as Plate 1, and cross-sections extrapolated from the map are presented as Plate 2.

I determined paleocurrent and paleowind directions predominantly from clast imbrications and the dip directions of eolian cross-strata, respectively. Paleocurrent directions determined from imbrications are generally the average of six or more individual clast measurements at any given outcrop. Measurements were only taken where a dominant imbrication direction could be determined. I believe these averages are within 20° of the true paleocurrent direction, but it is important to bear in mind that the paleocurrent preserved by the imbrication is only a snapshot of the local, instantaneous current direction. The local paleocurrent may be as much as another 45° removed from the overall paleocurrent direction. Imbrication data is supplemented by measurements of the strike directions of paleochannels and lateral accretion cross-strata. Everywhere these measurements were taken, imbrications were observed to determine the paleocurrent direction along the strike of the feature. Paleowind directions determined from eolian cross-strata are the dip directions of the steepest eolian cross-strata in any given outcrop. Typically, the attitudes of multiple cross-strata were measured, but only the steepest is presented on the map. I only measured attitudes of cross-strata with greater than ~30° primary dips, in part to prevent accidently measuring alluvial cross-strata attitudes and in part because of the belief that the steeper cross-strata are more likely to record the prevailing wind direction and not a local wind direction. These measurements are likely within 30° of the true paleowind direction. Both paleocurrent and paleowind data are presented throughout the thesis in rose diagrams; tabulated frequency data is presented in Appendix 1.

Clast count methodology was modeled after Dickinson (2008), but restricted by the nature of the exposures in the principal area of interest. I was particularly interested in the change in clast suite along a transect paralleling Cross-section A-A', where a largely unfaulted, relatively well-exposed up-section transect can be examined for stratigraphic changes in clast suite (e.g., unroofing sequences). The bulk of the transect lies within a sandstone-dominated region, however, where conglomerate beds are typically thin and have limited exposure. The small size of the exposures prevented using methods such as counting all clasts within a certain area or counting only certain gravel sizes. Instead, I simply drew a vertical line at an arbitrary spot in each conglomerate bed and counted every clast from that line onward in one direction until at least 100 clasts were counted (with one exception). Where exposure and access to exposure permitted, I generally counted well over 100 clasts (average and median of 182 clasts, range of 53 to 352 clasts). Initially, clasts were categorized into fairly restricted groups, such as "crystal-rich intermediate lava" or "La Jencia tuff," but the rarity of clasts in many of these groups required that the final dataset use broader categories. In addition, I could not consistently differentiate the various tuff units (e.g., La Jencia, Vicks Peak), and therefore lumped all tuffs into one category. In the end, the categories used were andesitic lava, rhyolitic tuff, scoria, basalt, Abo, limestone, and 'other'. The 'other' category includes rare vein quartz, chert, and volcaniclastic sedimentary clasts. Modal clast count data is included in tabular form as Appendix 2, and pie diagrams of clast counts from across the area are presented on Plate 3.

Visual estimates of modal abundances of various phases were performed on eleven sandstone thin sections from along the clast count transect as well as from around

the basalt of Broken Tank and the east end of map unit Tsp. Thin sections were made of both alluvial and eolian sandstones. Modal abundances of phases were visually estimated at two or three locations in each thin section, usually at 4X magnification but also at 10X for thin sections of fine-grained sand. The data from the various locations on each thin section was then averaged, and the resulting data is presented in tabular and graphical form as Appendix 3. Phases were identified by optical properties from Klein (2002).

$^{40}Ar/^{39}Ar$ ages were determined by the New Mexico Geochronology Research Laboratory, a part of the New Mexico Bureau of Geology and Mineral Resources. Dating procedures and results are summarized in Appendix 4.

STRATIGRAPHY

Figure 10 graphically summarizes the stratigraphy of the highlands around the study area, while Figure 11 is a correlation chart of the map units used in this study.

Pre-Santa Fe Group

Although mapping stressed Santa Fe Group sediments and volcanics, some pre-Santa Fe Group units are present in the map area, and the pre-Santa Fe Group stratigraphy is important to the interpretation of clast suites in the conglomerates of the basin fill. Therefore, a simplified stratigraphy is presented here, largely borrowed from other studies, to provide a background for clast suite interpretation.

Precambrian and Paleozoic rocks

For mapping purposes, all pre-Tertiary rocks are lumped together into pre-Tertiary, undivided (pTu).

Precambrian

The Precambrian rocks exposed on the mapping area and further northwest in the Chupadera Mountains are discussed in Condie and Budding (1979) and Bowring et al. (1983) and mapped in detail by Kent (1982). Granites, siliceous metavolcanics, pelitic and feldspathic schists, and quartz veins and pegmatites comprise the Precambrian

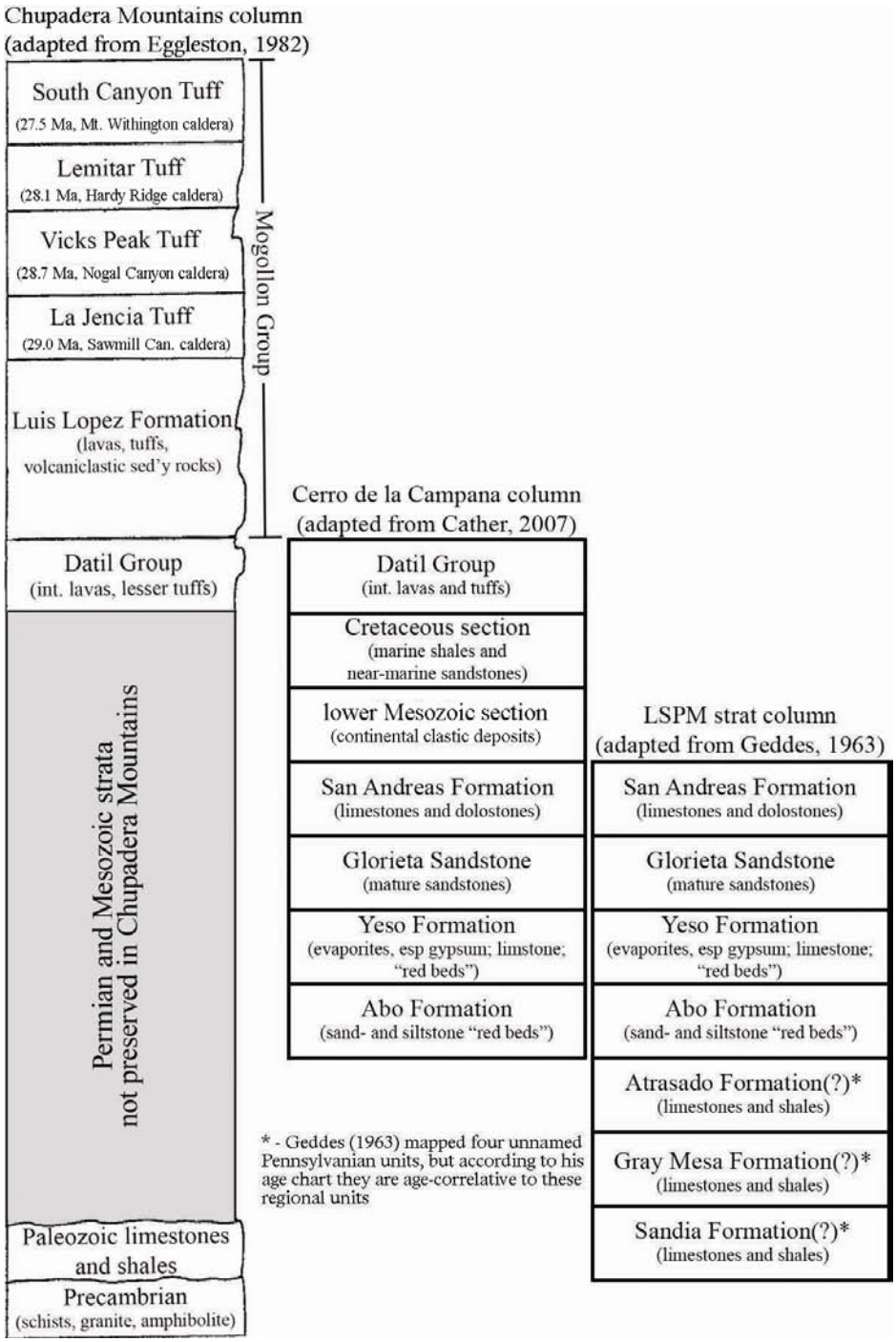

Figure 10 - Simplified stratigraphic columns for Mogollon Group and older units from surrounding highlands. Notice that none of the "red bed" bearing units are present in the Chupadera Mountains, indicating any "red bed" clasts must come from east of the field area from an ancestral LSPM highland. Ages and source calderas are given for the Mogollon tuff units. Abbreviations: Can. – Canyon, Mt – Mount.

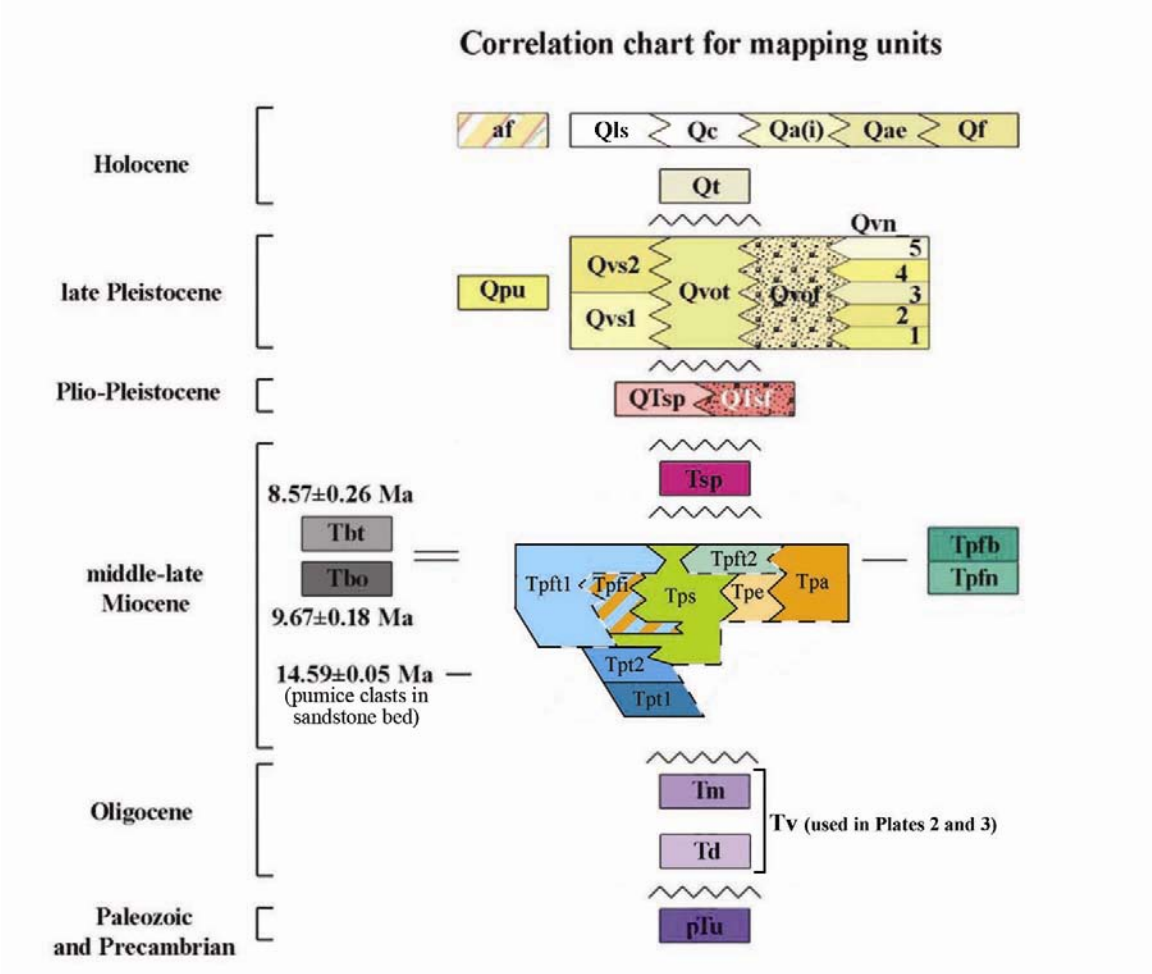

Figure 11 - Correlation chart for the units used on the geologic map (Plate 1).

section, and thin carbonatite dikes are also found in the area (Kent, 1982). The reader is referred to the works cited above for more detail on the Precambrian geology of the area.

Paleozoic sedimentary rocks

In the field area, up to 70 meters of limestones and minor shales and sandstones overlie the Precambrian rocks in the Chupadera Mountains that are interpreted as the Caloso and Sandia Formations (Eggleston, 1982). The Mississippian Caloso Formation comprises the basal 11 meters of section, and consists of several limestone horizons with

thin interbedded shales and minor sandstones (Armstrong, 1958; Krukowski, 1990). A thick sequence of Atokan shales and limestones comprises the rest of the section (Kottlowski, 1960, 1963), and probably belongs to the Sandia Formation (Kottlowski, pers. comm., cited in Eggleston, 1982). These Paleozoic rocks are directly overlain with angular unconformity by pre-Santa Fe Group mid-Cenozoic volcanic and volcaniclastic rocks.

Outside the mapping area, particularly to the east, the Paleozoic section is far thicker and overlain by Mesozoic strata. This difference in stratigraphy has two important implications: first, that the Chupadera Mountains area was severely eroded prior to Tertiary volcanism, while the area to the east was not, and second that post-Sandia Formation Paleozoic and Mesozoic clasts found in Santa Fe Group conglomerates could not originate from the Chupadera Mountains. In fact, post-Pennsylvanian strata are rare and thin in all the highlands west of the Rio Grande around the field area (R.M. Chamberlin, pers. comm., 2007), and generally in these areas Tertiary volcanics and volcaniclastics directly overlie either Precambrian or pre-Permian rocks (cf. NMBGMR, 2003). This observation will become important later when discussing the provenance of Popotosa conglomerates. The former implication, that the Chupadera Mountains area was severely eroded prior to Tertiary volcanism, supports the conclusions of Eardley (1962), who postulated the area west of the Rio Grande around Socorro was a Laramide highland that was unroofed down to the Precambrian in the Eocene (Cather, 2004).

While the Paleozoic section east of the field area is dominated by limestones similar to those in the Chupadera Mountains, it also includes distinctive siltstone and sandstone “red beds” of the Abo and Yeso Formations (Figure 10; cf. Geddes, 1963;

Cather, 2002, 2007). The red beds, particularly those of the Abo Formation, locally have prominent reduction spots (cf. Bensing et al., 2005), which were used in the field to help identify Abo Formation clasts in Popotosa conglomerates. The reader is referred to Geddes (1963), Siemers (1978), Krukowski (1990), and papers in Lueth et al. (2009) for more detail on the Paleozoic section of Socorro County.

Datil Group

The Datil Group (Td) consists of all volcanic strata younger than the Baca Formation up to and including the Hells Mesa Tuff (nomenclature after Cather et al., 1994b). For mapping purposes, the Datil Group is not divided into individual units, and small exposures of volcaniclastic conglomerates and sandstones are included in the unit. In the southern Chupadera Mountains, the Datil Group map unit consists of dark gray to dark red, porphyritic to aphanitic, variably altered andesitic lava flows, and at least two lithic- and phenocryst-rich ash flows. The basal contact of the Datil Group is not exposed in the study area, but is most likely an unconformable contact with underlying Paleozoic or Precambrian rocks (Eggleston, 1982).

Mogollon Group

The Mogollon Group (Tm) consists of volcanic strata of the Mogollon-Datil volcanic field younger than the Hells Mesa Tuff (32.3 Ma: modified from Chamberlin et al., 2004; nomenclature after Cather et al., 1994a) but older than the Santa Fe Group (approximately 24 Ma: Bruning, 1973). For mapping purposes, the Mogollon Group is not divided into individual units. In the field area, the Mogollon Group includes the Lemitar, Vicks Peak, and La Jencia Tuffs as well as the Luis Lopez Formation

(nomenclature after Osburn and Chapin, 1983). As these units were not the focus of this study, they are only briefly addressed here. The reader is referred to Chamberlin (1980), Eggleston (1982), McIntosh et al. (1991), and Chamberlin et al. (2002; 2004) for more detail. Ages presented here differ from the above references as they have been modified to accommodate the Fish Canyon Tuff sanidine monitor age of 28.02 Ma of Renne et al. (1998).

The Luis Lopez Formation of Chamberlin (1980) is the heterogeneous moat-fill of the Socorro caldera, part of which occupied the northwestern corner of the mapped area. Regionally, it consists of basaltic, andesitic, and rhyolitic flows and an ash-flow tuff interbedded with three sedimentary intervals (Eggleston, 1982; Chamberlin et al., 2004). In the field area, only the basal sedimentary and medial pumiceous tuff members (nomenclature after Chamberlin et al., 2004) of the Formation are present. The former is locally composed of approximately 240 m of upward-fining conglomerates to sandstones to mudstones, apparently derived from erosion of the southern caldera wall (Eggleston, 1982). Clasts are primarily andesitic lavas, probably derived from nearby Datil Group lavas. The pumiceous tuff is a poorly welded lithic- and crystal-rich ash-flow deposit (Eggleston, 1982) dated at 30.2 Ma (modified from Chamberlin et al., 2004).

The La Jencia Tuff, which dominates the Mogollon Group in the field area, is a densely welded, light gray to brick red, phenocryst-poor and pumice-rich rhyolitic ignimbrite with a distinctly rheomorphic (flow-banded) medial zone (Chamberlin et al., 2002). Formerly termed the A-L Peak Tuff (cf. Chamberlin, 1980) but renamed by Osburn and Chapin (1983), it is up to 518 m thick in the study area (Eggleston, 1982). Within the Socorro Caldera, it overlies the Luis Lopez Formation; south of the caldera, it

unconformably overlies Datil Group lavas and tuffs (Chamberlin and Cikoski, on-going mapping). Its medial rheomorphic zone grades up- and down-section into non-flow-banded, eutaxitic tuff (Chamberlin et al., 2002). It has a mean bulk sanidine $^{40}Ar/^{39}Ar$ age of 28.98 ± 0.08 Ma (modified from McIntosh et al., 1991), and was erupted from the Sawmill Canyon caldera (Chamberlin et al., 2002; Chapin et al., 2004a).

The Vicks Peak Tuff is a densely welded, light gray to pale red, phenocryst-poor rhyolitic ignimbrite with typically large (up to 30 cm long) pumice lapilli (Chamberlin et al., 2002). It overlies the La Jencia Tuff in the field area, but elsewhere the tuff is truncated or removed by pre-Lemitar Tuff erosion (cf. Ferguson, 1985), and immediately north of the field area the tuff is only locally preserved on the down-thrown (west or southwest) side of north- to northwest-striking normal faults (Chamberlin et al., 2002). The preserved thickness is up to 125 meters, but the original, pre-erosion thickness is unknown. It has a mean $^{40}Ar/^{39}Ar$ age of 28.70 ± 0.06 Ma (modified from McIntosh et al., 1991).

The Lemitar Tuff is a distinctly compositionally zoned rhyodacitic to high-silica rhyolitic ignimbrite that grades from a phenocryst-poor lower member to a phenocryst-rich, quartz-poor medial member to a phenocryst-rich, quartz-rich upper member (Eggleston, 1982). It is light gray to dark red and generally densely welded (Chamberlin et al., 2002), with a mean $^{40}Ar/^{39}Ar$ age of 28.10 ± 0.12 Ma (modified from McIntosh et al., 1991). It overlies the Vicks Peak Tuff in the field area with apparent unconformity. Its thickness is unknown as the top is nowhere preserved, but to the north of the field area the unit is up to 240 meters thick (Chamberlin et al., 2002).

A fourth tuff, the South Canyon Tuff, is also common to the region, although not

present in the map area. It is found in the clast suite of some Popotosa conglomerates, and so is briefly described here. It is partially to densely welded, light gray to pale red, phenocryst-poor to moderately phenocryst-rich, pumiceous rhyolite ignimbrite (Chamberlin et al., 2002). It has a mean $^{40}Ar/^{39}Ar$ age of 27.52 ± 0.12 Ma (modified from McIntosh et al., 1991). In the Chupadera Mountains, it overlies the Lemitar Tuff with apparent unconformity, and is up to 50 meters thick (Chamberlin et al., 2002).

Santa Fe Group

The Santa Fe Group consists of all sedimentary basin fill and intercalated volcanics associated with the Rio Grande rift up to and including the highest aggradational surface of the basin fill (Baldwin, 1963; Hawley et al., 1969). Note that this definition excludes volcanic strata contemporaneous with early rifting but not associated with a thick sedimentary fill (cf. Chamberlin, 1980). This definition also excludes the terrace and fan deposits associated with Pleistocene to present entrenchment of the Rio Grande and its tributaries. The base of the Santa Fe Group is placed on the top of the Oligocene volcanic pile of the Mogollon Group (Hawley et al., 1969), effectively restricting the Group to the early Miocene to Pleistocene. Formation- and member-rank subdivision of the Santa Fe Group varies across the RGR; this thesis uses the nomenclature entrenched in the local literature (cf. Chamberlin, 1999, 2004; Chamberlin et al., 2002; Cather 2002, 2007), which divides the Group into the earlier Popotosa Formation of Denny (1940) and the younger Sierra Ladrones Formation of Machette (1978). In addition, the Santa Fe Group on the IWW quadrangle includes two basalt flows that are found within the Popotosa Formation and a transitional deposit of uncertain

correlation.

In general, the Santa Fe Group consists of intermontane deposits accumulating in half-graben depressions derived from tilted block uplifts, resulting mainly from domino-style extension (*sensu* Chamberlin, 1980, 1983; Figure 12). Older basin fill accumulated in closed basins, resulting in intertonguing "fanglomerates" and basin-floor playa deposits (Bruning, 1973). As the Miocene basins filled and the structurally high topographic barriers between them became buried, a through-flowing ancestral Rio Grande (ARG) developed that linked the series of north-trending, en echelon basins, including the Socorro basin, and the basin-floor playa facies was replaced by an axial fluvial facies. This change in depositional setting distinguishes the Sierra Ladrones Formation from the Popotosa Formation (Machette, 1978).

In this definition lies a significant difficulty: the formation designation of any given Santa Fe Group piedmont deposit is given by the nature of the basin-floor deposits with which it intertongues. It may not, however, be possible to determine the basin-floor deposit associated with any given piedmont facies bed. Thus, the two units are commonly distinguished based on auxiliary observations. For example, the contact between the

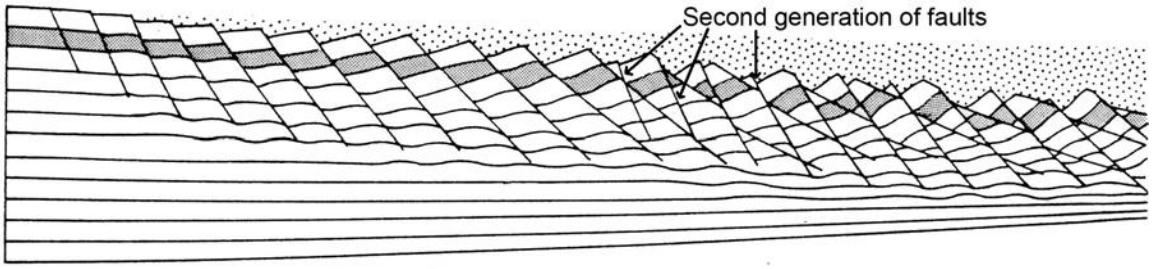

Figure 12 - Schematic depiction of domino-style faulting, after Morton and Black (1975). Degree of extension increases from left to right. Notice that fault blocks rotate with increased extension, and that, after a certain amount of rotation, a second generation of faults develops that cuts and overprints the original faults.

Sierra Ladrones and Popotosa is often an extensive and significant angular unconformity (cf. Machette, 1978), although not always (Cather et al., 1994a). Clast suites and paleocurrents may also identify the shift from closed to integrated drainage, but only if the changes can be conclusively linked to the existence of an ARG. In the field area, a significant change in paleocurrents occurs immediately above the Popotosa section, but no evidence for a coeval through-flowing ARG could be found. Therefore, a transitional unit of uncertain correlation is identified and described.

Popotosa Formation

The Popotosa Formation, as defined by Denny (1940) and redefined by Bruning (1973) and Machette (1978), is the lower unit of the Santa Fe Group in the Socorro basin (Chapin and Seager, 1975; Chamberlin, 1980). In the type location, it consists of volcanic-rich conglomerates, conglomeratic sandstones, and mudstones. It is generally interpreted as a series of basin-margin fans intertonguing with a basin-floor playa in broad, closed basins (Bruning, 1973), but work by Chamberlin (1980, 1983) and Cather et al. (1994a) suggests a more complicated history with at least two distinct phases of deposition. North of the SAZ, early deposition (about 27 to 16 Ma, Cather et al., 1994a) was dominated by debris flows originating from the SAZ topographic high ("lower Popotosa" of Chamberlin, 1980), except in the northern Lemitar Mountains, where west-transported debris flows are found near(?) the base of the section (Cather et al., 1994a). Sediments accumulated on a complex topography formed by narrowly-spaced early rift faults and pre-Santa Fe Group erosion (Chamberlin, 1980), and the unit is commonly bounded by angular unconformities both above and below (Cather et al., 1994a). Later

deposition (16 to 10 Ma, Cather et al., 1994a) largely followed the model of Bruning (1973), with a broad, basin-floor playa intertonguing with west- and east-derived alluvial fans and braid plains (Cather et al., 1994a). The change in depositional environment appears to result from an increase in the rate of tectonism and subsidence. To the north of the study area, the top of the Popotosa is commonly an angular unconformity of 10° to 15° (Cather et al., 1994a).

The Popotosa Formation on the IWW quadrangle is here informally divided into members based on:

1) dominant lithologies (sandstone vs. conglomerate),
2) transport processes (dominantly eolian sandstones vs. mixed alluvial and eolian sandstones),
3) clast suite (rhyolite tuff dominance vs. andesitic lava dominance, vs. a mixed clast suite),
4) presence of distinct marker beds (the pumiceous sandstone sequence of Tpt2), and
5) stratigraphic/geographic location (the isolated northern Popotosa [Tpfn] and the Tpft_ units located toward the top of the section).

These divisions commonly also correlate with differences in paleocurrent directions and sedimentary structures, and may indicate changes in basin geometry and events in the geologic past (cf. Chamberlin, 1980, 2004).

Ten informal members are mapped in the field area, and described in detail below. Figure 11 is a correlation chart displaying the interpreted relationships between these ten members, as well as showing the stratigraphic locations and $^{40}Ar/^{39}Ar$ ages of interbedded basalt flows (Tbt, Tbo) and of dated reworked pumices. In brief, these units

locate:

1) rhyolite tuff-dominated conglomerates and lesser alluvial sandstones (Tpt1, Tpt2),
2) andesitic lava-dominated conglomerates and associated alluvial and eolian sandstones (Tpa),
3) interbedded tuff- and lava-dominated conglomerate beds with associated sandstones (Tpfi),
4) tuff-dominated conglomerates and associated sandstones in the upper Popotosa (Tpft1, Tpft2),
5) eolian sandstones and lesser conglomerates (Tpe),
6) mixed eolian and alluvial sandstones with lesser conglomerates (Tps), and
7) mixed clast suite conglomerates and associated sandstones isolated in the north of the field area, near outcrops of the basalt of Olney Ranch (Tpfn, Tpfb).

(Note that "tuff" here is used to refer to welded ash-flow tuffs [ignimbrites] with enough induration and erosion-resistance to survive transport and persist as a clast.)

Age control for the Popotosa Formation in the field area is provided by water-laid pumices in sandstones at the base of Tpt2, by an oreodont skeleton found in Tpa, and by the basalts of Olney Ranch (Tbo) and Broken Tank (Tbt), found with beds of Tpfn (Tbo) and Tpft1 and Tps (Tbt). The basal pumiceous sandstone found in Tpt2 yielded sanidines from pumices with an average single-crystal $^{40}Ar/^{39}Ar$ age of 14.59 ± 0.05 Ma (Appendix 4; Morgan et al., 2009a). This age provides a lower bound for the age of the sandstone bed, and approximately dates the bed itself assuming the pumices neither spent an appreciable amount of time in transport nor are reworked from a significantly older deposit. These assumptions are supported by the narrow peak of the age probability

distribution plot (see Appendix 4), which indicates little mixing of sanidine crystals of different ages. Large amounts of time in transport and reworking of older deposits would both likely result in higher degrees of mixing and a broader peak on the plot.

Early in the mapping process, a relatively complete oreodont skeleton (Figure 13) was recovered from the Tpa map unit between the Chupadera Foothills (CF) and Hidden faults (see Figure 7). Morgan et al. (2009a) determined the fossil to be the late Miocene (11 to 9 Ma) species *Merychyus major major*, which constrains the age of these strata.

Upper Popotosa age constraint is provided by the basalt of Olney Ranch (Tbo) and the basalt of Broken Tank (Tbt). The basalt of Olney Ranch is found in the far north of the field area, overlying beds of Tpfn. Although samples of the basalt from the field

Figure 13 - A picture of the oreodont fossil recovered from the field area, after the arroyo wall was carefully cut back to better expose the remains. Jaw is about 25 cm long. Photo location: 0323577 m E, 3741082 m N.

area have not been dated, samples from the Luis Lopez quadrangle to the north yielded an average $^{40}Ar/^{39}Ar$ age of 9.67 ± 0.18 Ma (Chamberlin et al., 2002), placing an upper bound on the age of deposition of Tpfn. In contrast, Chamberlin et al. (2006) dated samples of the basalt of Broken Tank from the field area itself, obtaining an $^{40}Ar/^{39}Ar$ plateau age of 8.57 ± 0.26 Ma (Appendix 4). The basalt of Broken Tank is found towards the top of the Popotosa section, interbedded with both Tps and Tpft1 beds.

Cross-section reconstructions suggest the dated pumices are located in the middle third of the Popotosa section, the oreodont fossil was extracted from the upper third, and the basalts are found at the top.

Rhyolite tuff-dominated conglomerates and associated alluvial sandstones (Tpt1, Tpt2)

All along the northwest side of the study area, pebble to boulder conglomerates with a rhyolite tuff-dominated clast suite overlie the volcanic pile of the Chupadera Mountains and constitute the basal exposed Popotosa of the Miocene Bosque basin (Cross-section A-A', Plate 2).

The lower unit, Tpt1, is dominated by conglomerate beds and has only minor sandstone and rare mudstone beds. Conglomerate beds have poor to moderate sorting, with angular to rounded clasts, medium to thick bedding, and rare cross-stratification. Sorting improves up-section, while clast size generally decreases and sandstones and cross-stratification become more common. Less abundant types of clasts also change with stratigraphic, and geographic, location; basalt clasts are found in the lowermost beds, and are particularly common in the immediate footwall of the Chupadera Foothills (CF) fault, whereas andesite lava clasts appear toward the top of the section (Plate 3). Clast

imbrications indicate paleocurrent directions range from northwest to due south, with southwestward currents being most common (Figure 14a).

The base of Tpt1 is distinctly bouldery all along the Chupadera Mountain front. Boulders are subangular to rounded and composed of rhyolitic tuff and basalt. Boulders become less common up-section.

No depositional basal contact of Tpt1 is exposed in outcrop, in part because the lower half of the section is particularly poorly exposed, most likely due to poor

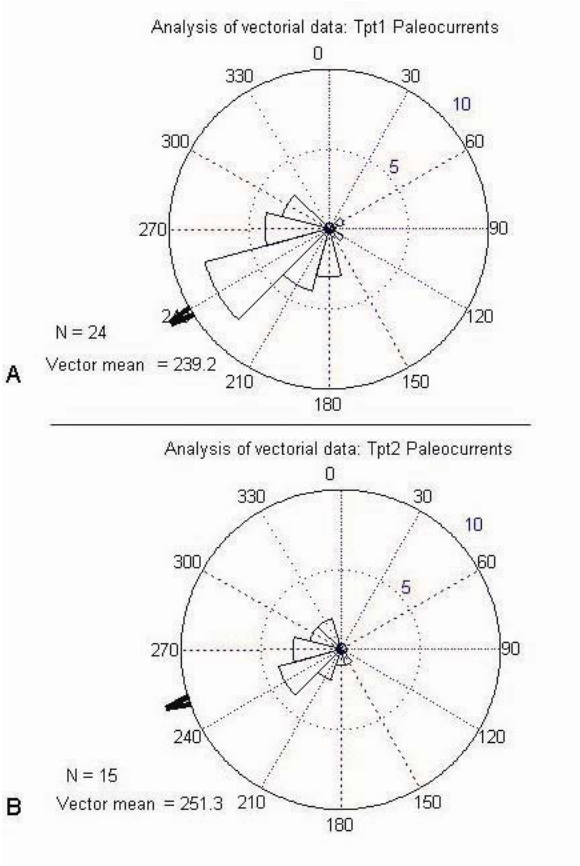

Figure 14 - Rose diagrams of paleocurrent indicator attitudes (mainly imbrications) for a) Tpt1 and b) Tpt2. "N" refers to the number of measurements, and the arrow indicates the vector mean of the attitudes. Rose diagrams by Vector_Stats of Jones (2006). Data tabulated in Appendix 1.

cementation and induration. The similarity between foliation attitudes in the underlying volcanic pile and bedding attitudes in the basal Tpt1, however, suggests the contact between the two is a paraconformity, with either slight or no angular unconformity.

The upper unit, Tpt2, is distinguished from Tpt1 by the presence of four pumiceous sandstone sequences that occur over a stratigraphic interval of 50 to 70 meters. The top and bottom of the unit are defined by the lowermost and uppermost pumiceous sequence, respectively. This unit continues some of the stratigraphic trends from Tpt1, namely the upwards fining, increase in sandstone beds, and increase in andesitic lava abundance in the clast suite. Cross-stratification is common. Conglomerate beds are dominantly pebbly but locally cobbly, with moderate to poor sorting and subangular to rounded clasts. Like Tpt1, imbrications suggest paleocurrents from northwestward to southward, with west-southwest being most common (Figure 14b). All exposed sandstone beds have an alluvial origin, evidenced by low-angle cross-stratification, poor sorting, and coarse grain sizes. Mudstone beds are thin and discontinuous. The unit is generally moderately-well exposed, except in the southwest of the field area, where Quaternary piedmont deposits blanket the surface.

The basal contact of Tpt2 is sharp by definition and conformable, but not necessarily well located, as the four pumiceous sandstones that define the unit are only locally all present (cf. Plate 1). Similarly, the upper contact is sharp and conformable but not always well located. They are well located on either side of the CF fault, but further north and south both faulting and Quaternary cover limit the number of exposed pumiceous sandstone beds.

Fortunately, enough exposure exists adjacent to the CF fault to establish abrupt

thickening of the Tpt_ units across the fault, attributed to syndepositional slip. Cross-sections (Plate 2) suggest Tpt1 thickens from 200 to 380 m, while Tpt2 thickens from 50 to 70 m. Cross-sections also suggest stratal thickening probably continued up through deposition of Tpfi (Cross-section C-C', Plate 2), but at that time syndepositional faulting appears to have ceased. Unit thicknesses may increase further to the southeast if slip along the LSPM mountain front fault zone was syndepositional as well (cf. Cross-section A-A').

Interpretations of the clast suite changes and depositional settings of these units are discussed in the "Provenance studies" and "Paleogeography" sections.

Eolian sandstones (Tpe) and mixed eolian and alluvial sandstones (Tps), with minor conglomerates

Dominating much of the center of the field area, and occurring at several stratigraphic levels (see Figure 11), are sandstone-dominated intervals with lesser, generally discontinuous conglomerate beds and thin mudstones. I interpreted sandstone beds as either alluvial or eolian in origin based on angle and height of cross-stratification, as well as on degree of sorting and grain size: beds with large, relatively high-angle (~30° primary dips and above) cross-strata and/or uniformly medium sand grains were considered eolian, while those with low-angle (~20° and below) cross-strata, poor sorting, and coarse sand grains were considered alluvial. I mapped regions dominated by eolian sandstones as Tpe, and those with a mix of eolian and alluvial sandstones as Tps.

The former unit, Tpe, consists almost entirely of eolian sandstones, with minor, laterally restricted conglomerates and rare alluvial sandstones and mudstones. To the

southwest of the Solitude fault, beds are well exposed, typically medium to thick, and commonly have well-developed, high-angle, large-scale cross-stratification. Sand grains are very well sorted, medium in size, and largely of volcanic composition. Where poorly exposed, to the northeast of the Solitude fault, beds are typically massive, and difficult to distinguish from alluvial sandstones except for the sorting and grain size. Dip directions of cross-strata suggest paleowind directions between west-southwest and northwest, with true west as the prevailing measurement (Figure 15). Alluvial sandstones are typically thin with low-angle, small-scale cross-stratification and rare pebbles. Mudstone beds are thin to medium and commonly wedge-shaped, presumably due to dune field topography. Conglomerate beds are generally pebbly to locally cobbly, with moderately sorted subangular to rounded clasts of dominantly andesitic lava composition (Plate 3), like the conglomerates of map unit Tpa (described below). Conglomerate beds are commonly channel-shaped.

Outcrop- and map-scale observations suggest only lateral boundaries are exposed

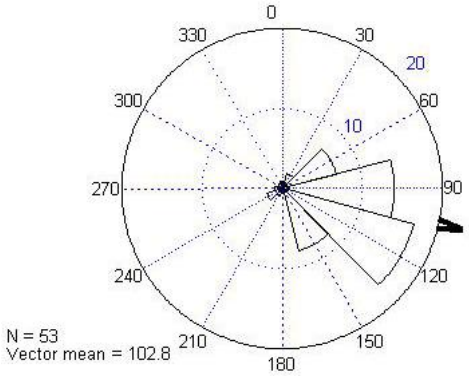

Figure 15 - Rose diagram of attitudes of the dip directions of eolian cross-stratifications, indicating paleowind direction. “N” is the number of measurements, and the arrow represents the vector mean of the attitudes. Rose diagram by Vector_Stats of Jones (2006). Data tabulated in Appendix 1.

in the field area for unit Tpe, such that the lower and upper bounds are unknown. To the southwest of the Solitude fault, intercalated eolian and alluvial sandstones, with a progressive increase in alluvial sandstones to the northwest, suggests either an interbedded stratigraphic contact or a lateral facies change contact with unit Tps; it is interpreted here as a facies change, with the contact placed at a marked increase in alluvial sandstone abundance. Map-scale patterns, and the presence of eolian sandstones throughout map unit Tpa, suggest a similar lateral contact with Tpa; the Tpe/Tpa contact is placed at a marked increase in abundance of conglomerate beds.

Tps is composed of alluvial and eolian sandstones as well as lesser conglomerates of variable clast suite. The eolian sandstones are similar to those of Tpe, of both well and poorly exposed varieties. Alluvial sandstones are thin to medium bedded, with local low-angle cross stratification and poor sorting, often with coarse sand grain sizes and pebbles to rare boulders. Rare out-sized clasts occur throughout the section, most likely resulting from low energy alluvial action removing smaller gravels and leaving behind cobbles and boulders surrounded by sand. Rhizoconcretions and massive beds indicate bioturbation is not uncommon, particularly in the lower part of the section. Conglomerate beds are thin to medium bedded and tabular to channel-shaped, and composed of subangular to rounded, poorly to moderately sorted pebbles to cobbles of variable clast suite, discussed below. Conglomerate beds are most prevalent at the base of the section.

Both stratigraphic and lateral contacts are recognized in the field area for Tps (e.g., Cross-sections A-A’ and D-D’, Plate 2). Stratigraphic contacts with Tpt2 and Tpfi appear conformable; a similar conformable contact with Tpft1 is inferred. The lateral contact with Tpe is discussed above; the lateral contact with Tpfi is interpreted from the

bedding attitudes in the area just northeast of the CF fault in the center of the area, around 0322000 m east, 3743000 m north. These bedding attitudes indicate that Tps and Tpfi beds on either side of the contact project toward each other, suggesting a lateral contact. Poor exposure in this area would allow for a fault contact, however.

Conglomerate bed clast suites vary considerably across unit Tps. In particular, I examined the change in clast suites along an up-section, or southeastward, transect to the southwest of the Solitude fault (Plate 3). Immediately above Tpt2, the clast suites are dominated by rhyolitic tuffs, but andesitic lava clasts increase in abundance up-section/southeastward until they constitute approximately half of the gravels. Clasts of red siltstone and sandstone with rare, distinctive reduction spots, interpreted as Abo Formation, also appear up-section/to the southeast. As noted above and illustrated in Figure 10, the up-section transition from rhyolitic tuffs to andesitic lavas, and on into the Permian System, would constitute an unroofing sequence, but alternatively the change in clast suite could result from two gravel sources with different clast suites mixing together in the center of the basin. The significance of the clast suite trends are discussed in more detail under the "Clast suite" heading of the "Provenace studies" section.

Exposed thicknesses of these units are 320 m for Tps, and 100 m for Tpe, although cross-section reconstructions, particularly A-A', suggest the units may be much thicker. Interpretations of these units for depositional environments are discussed in the "Paleogeography" section.

Andesitic lava-dominated conglomerates, with associated alluvial and eolian sandstones (Tpa)

Along the southeast margin of the field area, andesitic lava-dominated conglomerates compose the bulk of the sediments, with lesser interbedded sandstones and rare mudstones.

Tpa conglomerates contain poorly to moderately sorted, angular to subrounded pebbles to cobbles of dominantly varicolored andesitic porphyry lavas and moderately abundant ignimbrites, with lesser scorias and rare clasts of Abo Formation and limestone. The ratio of lavas to tuffs increases up-section, while Abo and limestone clasts also increase in abundance (Plate 3). Beds are generally massive and tabular around the Solitude and Burro faults, becoming more cross-stratified, channel shaped, and better sorted toward the northeast. Imbrications indicate paleocurrents between northwest and southwest, with most measurements between west-southwest and due west (Figure 16).

I interpreted sandstone beds as either eolian or alluvial in origin based on the

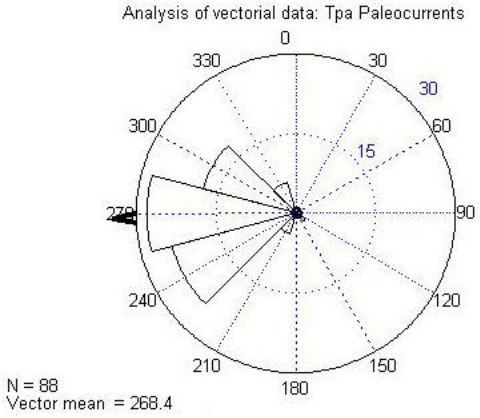

Figure 16 - Rose diagram of paleocurrent indicator attitudes (mainly imbrications) for the Tpa map unit. “N” is the number of measurements, and the arrow indicates the vector mean of the attitudes. Rose diagram by Vector_Stats of Jones (2006). Data tabulated in Appendix 1.

criteria given in the description for map units Tps and Tpe. Eolian sandstones are identical to those described in the Tpe description, with thick, well-cross-stratified beds southwest of the Solitude fault and massive, poorly exposed beds to the northeast of the fault. Alluvial sandstone beds are generally thin and pebbly, with common, faint, low-angle, small-scale cross-stratification. Thin mudstone beds are generally associated with sandstone intervals, particularly eolian intervals, and are often wedge shaped, presumably as a result of dune field topography.

Particularly coarse material is found in the far south of this unit's exposure near Elmendorf. Sediments here are pebbly to bouldery and poorly sorted, fining to the north and east.

The basal and upper contacts of this unit are not exposed in the field area, and any contacts to the east have been removed by the Rio Grande. The northwestern contact with map unit Tpe is exposed in the area, and is suggested to be a lateral, interfingering contact. This is mainly based on the attitudes of paleowind and paleocurrent indicators, which indicate that the dunes were migrating east onto west-flowing streams. This suggests the eolian and alluvial deposits would intertongue with one another, forming a dynamic boundary that likely migrated with tectonism and climate change.

Although the exposed thickness of Tpa is only 120 m, Cross-section A-A' suggests the unit may be much thicker, as it is directly adjacent to the syndepositional basin-bounding fault system (syndepositional slip along the basin margin fault is discussed in the "Structure" section). Interpretations of clast suite changes and depositional setting are discussed in the "Provenance studies" and "Paleogeography" sections.

Interbedded tuff- and lava-dominated conglomerates with associated alluvial sandstones (Tpfi)

Near the center of the field area, commonly associated with map unit Tps, a section of interbedded rhyolitic tuff-dominated and andesitic lava-dominated conglomerates is found. Interbedded with these conglomerates are uncommon sandstones and rare thin mudstone beds.

Tpfi is dominated by pebble to cobble conglomerates with poor to moderate sorting and subangular to rounded clasts. Tuff-dominated beds are generally poorer sorted and coarser. Beds are thin to medium, and lack sedimentary structures besides imbrications, which indicate dominantly southwestward transport (Figure 17). Southward and southeastward imbrications are found near 322750 m east, 3743250 m north, which is interpreted to be the stratigraphic top of the unit. Sandstone beds are poorly exposed, but generally are similar to the alluvial Tpa sandstones and are thus interpreted as alluvial in origin.

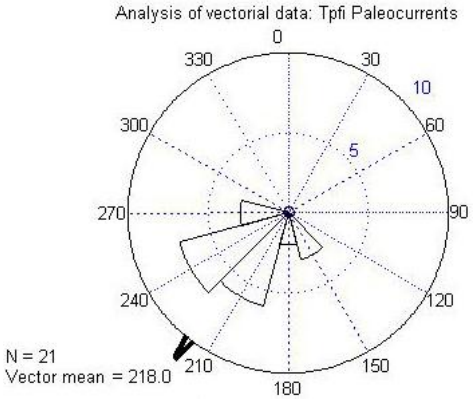

Figure 17 - Rose diagram of paleocurrent indicator attitudes (mainly imbrications) for the Tpfi map unit. "N" is the number of measurements, and the arrow indicates the vector mean of the attitudes. Rose diagram by Vector_Stats of Jones (2006). Data tabulated in Appendix 1.

Stratigraphic contacts with map unit Tps are exposed in the field area, while lateral contacts with map units Tps and Tpft1 are inferred from bedding attitudes and stratigraphy. The stratigraphic contacts with unit Tps are relatively well exposed by I-25 on either side of the CF fault, where they appear conformable. A lateral contact with Tps is interpreted from bedding attitudes in outcrops of Tpfi and Tps on either side of the contact near 0322000 m east, 3743000 m north, which project into each other. Exposure in this area is poor, however, and a fault could lie between the outcrops. The inferred lateral contact with Tpft1 and stratigraphic contact with Tsp are discussed in those units' descriptions, below.

Cross-section D-D' shows considerable changes in unit thickness across the field area from southwest to northeast. These I interpret from map patterns to be the result of 1) syndepositional slip along the CF fault and 2) apparent thickening due to proximity to the source area. Syndepositional slip along the CF fault is virtually certain given the definitive thickening of Tpt1 and Tpt2 across that fault. Cross-section D-D' demonstrates that fault-related thickening of strata could continue up to the upper contact of Tpfi, at which point further thickening would be incompatible with normal slip on the CF fault (e.g., if Tps above Tpfi in the cross-section were thickened, the upper contact would have to move upward and above the same contact on the footwall of the CF fault). Therefore, syndepositional faulting is a reasonable explanation for the increase in thickness from 95 to 220 m across the CF fault. Thickening toward the northeast is explained as increased proximity to the source of the conglomerates resulting in a greater volume of coarse material. Imbrications indicate paleocurrents to the southwest, such that deposits to the northeast are closer to the source. Assuming the deposit fines in the direction of transport,

a greater abundance of coarse material should be expected up-stream, resulting in an apparent thickening of this conglomeratic unit. Due to poor exposure and faulting, the exact thickness cannot be measured, but the minimum exposed thickness is 95 m.

The significance of this unit and its interbedded clast suites is discussed in the "Provenance studies" section.

Tuff-dominated conglomerates and associated alluvial sandstones toward the top of the Popotosa (Tpft1, Tpft2)

Near to and in the immediate footwall of the BDA fault, rhyolitic tuff-dominated conglomerates and interbedded sandstones form the dominant lithologies. These beds are presumed to be the uppermost Popotosa in the study area, based on bedding attitudes and cross-sections, as well as the presence of the 8.57 Ma basalt of Broken Tank, which intercalates with the northwestern unit.

Both units are composed of pebble to cobble conglomerates and poorly exposed sandstone and rare mudstone beds. The conglomerates are typically moderately sorted with subangular to rounded clasts of dominantly rhyolitic tuff composition. This dominance is clear and definitive in Tpft1; in Tpft2, dominance is only slight (Plate 3). Andesitic lavas constitute the bulk of the remainder of clasts, with rare Abo Formation rounding out the clast suite. Limestone is also present, though rare, in Tpft2. Beds are thin to medium, tabular and cross-bedded in Tpft1, and channel-shaped and massive in Tpft2. Sandstones appear alluvial, with rare, faint, low-angle, small-scale cross-stratification and coarse sand to pebbly sand composition. Units also contain rare, thin mudstone beds, commonly associated with sandstone intervals.

For the northwestern unit, Tpft1, only the upper contact with Tsp is exposed, but in addition a lateral contact with Tpfi is inferred. The stratigraphic contact with Tsp is discussed in that unit's description, below. The lateral contact with Tpfi is suggested by the stratigraphy, as both Tpfi and Tpft1 appear to overly the basal-Popotosa Tpt1\Tpt2\Tps sequence. This suggests the deposits were coeval and may have interacted somehow. In fact, I suggest that the alluvial system responsible for the tuff-dominated Tpft1 beds may also be the source of the tuff-dominated beds in Tpfi. This idea is consistent with the southwestward-directed paleocurrent measurements common to Tpft1, which suggest that streams passing through the Tpft1 area could have continued on into the Tpfi area. This is discussed in more detail below in the "Provenance studies" section.

The 8.57 Ma basalt of Broken Tank (Tbt) intercalates with conglomerates of Tpft1, placing a late Miocene age constraint on these deposits.

For the southeastern unit, Tpft2, no contacts are exposed, but lateral contacts with both Tpft1 and Tpa are inferred. Geographically, Tpft2 lies between those two units, and in terms of clast suite Tpft2 also lies somewhere between the lava-dominated Tpa and tuff-dominated Tpft1. I suggest that Tpft2 reflects a mixing zone, where the separate lava- and tuff-dominated alluvial systems to the south and north, respectively, converge to produce a roughly 60/40 tuff/lava clast suite. Under this interpretation, the contacts between Tpft2 and Tpa and Tpft1 would be lateral, probably interfingering contacts.

Exposed thicknesses for these units are about 280 m and 70 m for Tpft1 and Tpft2, respectively. Thicknesses are not well constrained, however, as the basal contact of neither unit is exposed, and neither is the upper contact of Tpft2.

Mixed clast suite conglomerates and alluvial sandstones in the north of the field area (Tpfn, Tpfb)

In the northwestern corner of the field area, well removed from the rest of the Popotosa section, is a sequence of pebble to boulder conglomerates with no clear relationship with the rest of the section. One unit (Tpfn) is a pebble to cobble conglomeratic unit with no distinct clast suite overlain by the basalt of Olney Ranch. The other unit (Tpfb) is a very distinctive basaltic boulder conglomerate.

Tpfn consists mainly of conglomerates with lesser conglomeratic sandstones, sandstones, and rare mudstones. Conglomerates consist of poorly to moderately sorted, subangular to rounded pebbles to cobbles and rare boulders of mostly rhyolitic tuffs and andesitic lavas, and uncommon to rare scorias and basalts. Imbrications suggest southwestward paleocurrents. Aside from imbrications, both conglomerates and sandstones are generally massive and thin to medium bedded. Sandstone beds are interpreted to be alluvial in origin based on grain size and sorting. Overall, the unit fines upward, with more pebble conglomerate and sandstone beds toward the top. Tpfn is at least 140 m thick.

Tpfb consists of a relatively narrow band (up to 10 meters thick) of basaltic boulder-rich conglomerate. Basalt boulders are subangular to subrounded and up to 0.5 m in diameter, and generally medium grey, dense and aphanitic, though some are black and vesicular. The bed also contains rhyolitic tuff pebbles and cobbles and rare andesitic lava pebbles. Sedimentary structures are lacking.

No contacts are exposed in the field area, but these units can be projected northward onto the Luis Lopez quadrangle, where basal contacts are present. “Tpfn” and

"Tpfb" here correlate to "Tpf" and "Tpfb" of Chamberlin et al. (2002) to the north. There, Tpfb is demonstrated to be a conformable band within the conglomerates of Tpf, and Tpf is shown to disconformably overlie the volcanic pile with as much as 100 meters of erosional relief. Upper contacts are more difficult to ascertain. In the field area, Tpfn is capped conformably by the basalt of Olney Ranch, but on the Luis Lopez quadrangle, the same basalt only locally caps Tpf. Elsewhere, deposits of Tpf surround flows of the younger basalt of Broken Tank, which suggests that deposition of Tpf continued after eruption of the basalt of Olney Ranch, such that this basalt is also intercalated with Tpf. In other locations on the Luis Lopez quadrangle, Tpf is capped by mudstones and lithic arenites suggested to be a facies that is transitional between the Tpf piedmont and a playa or axial river ("Tpt" of Chamberlin et al., 2002).

Local capping by the basalt of Olney Ranch restricts the age of Tpfn in the field area to older than 9.67 Ma (age from Chamberlin et al., 2002).

Interpretation of the depositional environment of Tpfn is discussed in the "Paleogeography" section. Chamberlin et al. (2002) suggest the Tpfb unit could be a local mass wasting deposit, derived from uplifted flows of the basalt of Olney Ranch. Indeed, the basaltic boulders found within the deposit are similar to the Olney Ranch flows, and uplift could have occurred along their Extraño fault, as the boulder bed is only found in the hanging wall of the fault and the flow is missing from the footwall.

Volcanic units interbedded in the Popotosa Formation (Tbo, Tbt1, Tbt2)

Two basaltic flows occur intercalated with the upper Popotosa Formation, the basalt of Olney Ranch (Tbo) and the basalt of Broken Tank (Tbt_). Neither was studied in

detail in this project, but Chamberlin (1980) and Chamberlin et al. (2002) present petrographic, geochemical, and geochronologic data. Most of the below discussion is borrowed from those studies, but with additional details from this field area.

The older basalt of Olney Ranch is a medium to dark gray, fine-grained tabular trachybasalt found in the north-central of this area and further northwest on the south end of the Luis Lopez quadrangle (Chamberlin et al., 2002). In the field area, it is up to 12 m thick, grading upwards from dense, uncommonly vesicular and medium gray to vesicular and dark gray. On the Luis Lopez quadrangle, the same basalt bears a 3-6 meter thick basal zone that is distinctly porphyritic, with fine- to medium-grained phenocrysts of tabular plagioclase and subhedral olivine (Chamberlin et al., 2002). The basalt has not been dated in the field area, but two widespread outcrops to the north yielded an average $^{40}Ar/^{39}Ar$ date of 9.67 ± 0.18 Ma (Chamberlin et al., 2002).

Based on map patterns that indicate exhumed paleotopography and on paleocurrent indicators from overlying and underlying Popotosa beds, Chamberlin et al. (2002) inferred that the basalt of Olney Ranch flowed westward through a Miocene paleovalley from a now-concealed source south of San Antonio. The southwestward-pointing imbrications observed in this area are in agreement with this hypothesis. Paleotopography surrounding Tbo has not been observed in the area, however, such that the suggestion of a paleovalley cannot be addressed.

The basalt of Broken Tank (formerly the basalt of Bear Canyon of Chamberlin [1980] and Osburn and Chapin [1983]) is a dark gray to black to dark reddish brown trachybasalt found in the immediate footwall of the BDA fault and further north in the Luis Lopez and Socorro quadrangles (Chamberlin, 1980, 1999; Chamberlin et al., 2002).

In the field area, it is up to 8 m thick, fine-grained diabasic to slightly porphyritic, dense to amygdaloidal, and unaltered to propylitically altered. Thin sections samples reveal sub-ophitic textures and rare micro-phenocrysts of olivine. Studies to the north demonstrate that at least one locality it has a slightly porphyritic basal zone with sparse, fine-grained phenocrysts of plagioclase, clinopyroxene, and olivine or iddingsite, overlain by a dense ophitic to subophitic core (Chamberlin et al., 2002). To the north, where multiple flows are stacked around Walnut Creek and Broken Tank, maximum thickness is around 30 meters (Chamberlin et al., 2002).

Chamberlin et al. (2002) suggest the basalt flowed westward down piedmont slopes and paleovalleys from a source near San Antonio into the Chupadera Mountains area, then northward toward Bear Canyon, where it spilled onto playa deposits. This interpretation is based on outcrop distribution, thickness variations, and paleocurrents from underlying Popotosa conglomerates. Paleocurrent observations made around outcrops of the basalt in the field area are consistent with this interpretation.

Outcrops of the basalt of Broken Tank are here separated into map units Tbt1 and Tbt2 based on the sediments with which the outcrop is intercalated. Tbt1 is found intercalated within west-transported pebble conglomerates and yielded a whole rock $^{40}Ar/^{39}Ar$ age of 8.57 ± 0.26 Ma (Chamberlin et al., 2006). Tbt2 is found intercalated with fine-grained sandstones and mudstones to the southeast of Tbt1, and although whole rock $^{40}Ar/^{39}Ar$ dating was attempted the sample was too altered to yield a reliable date (R.M. Chamberlin, pers. comm., 11/2009). The two are lithologically identical, in both hand sample and thin section, but bedding attitudes and the different depositional environments associated with the two suggest they may not be the same flow. Figure 18 illustrates

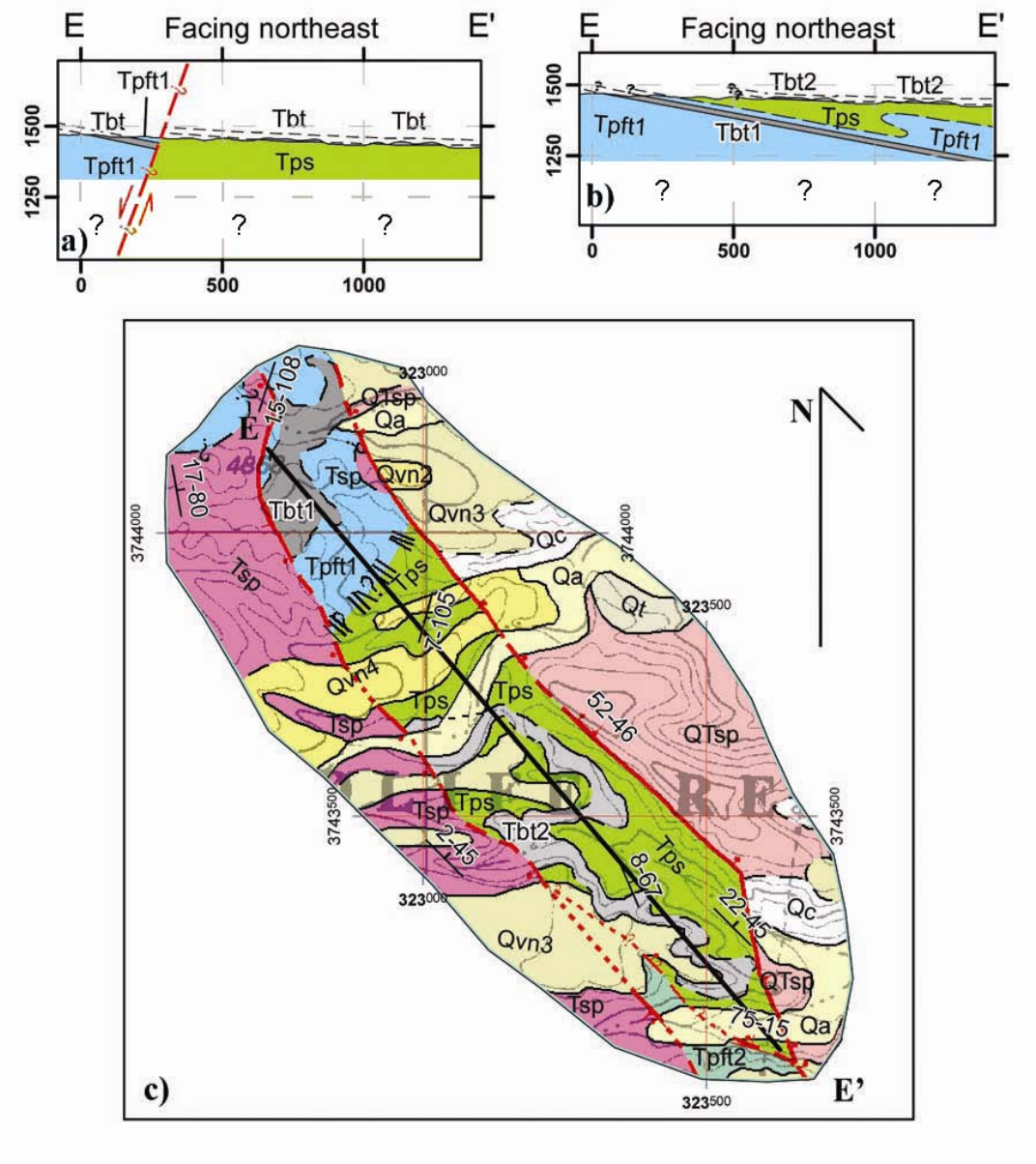

Figure 18 - Cross-sections illustrating the possible interpretations of the two outcrops of basalt located in the immediate footwall of the Bosque del Apache fault. a) The two outcrops could be the same basalt flow, if structure in between the two (most likely a fault) caused the juxtaposition of conglomerates and sandstones, followed by offset of the basalt flow. b) Alternatively, the two outcrops could be individual flows, Tbt1 and Tbt2, separated by enough time for the depositional environment to change from conglomerate-dominated to sandstone-dominated. Both cross-sections are 1:24,000 true scale (no vertical exaggeration). c) Blow-up of the part of the geologic map containing the basalt outcrops. The location of the cross-section depicted in 18a and b is shown with a black line. Colors, abbreviations, and symbols for both cross-sections and the map are the same as the geologic map, Plate 1.

these two possibilities with cross-sections through the area with exposures of the basalt, showing how the basalt outcrops and the sediments found around these outcrops may be related. I favor the interpretation that the two basalts are the same flow, and my cross-sections and correlation charts reflect this, but I cannot prove this hypothesis.

Middle Santa Fe Group transitional unit (Tsp)

Exposed in the middle of the field area, in what appears to be a region of horst and graben in the immediate footwall of the BDA fault, is a conglomeratic unit that fits neither the local Popotosa description nor the Sierra Ladrones definition; it is therefore described as a transitional "middle Santa Fe Group" deposit of uncertain correlation.

Tsp consists of poorly exposed pebble conglomerate beds grading to sandstones and rare mudstones to the southeast. Conglomerates contain moderately to moderately-well sorted, subangular to rounded clasts of light bluish gray to light purple rhyolitic tuff and rare andesitic lavas, scorias, rounded basalts, and vein-like quartz. Imbrications suggest southward to eastward paleocurrents, with eastward to southeastward dominating (Figure 19). Both conglomerates and sandstones are poorly cemented and generally massive to weakly planar bedded. Sandstones are interpreted as alluvial in origin based on their poor sorting and the presence of rare gravels within the beds. Mudstones are thin and planar.

Only the basal contact with Tpft1 is exposed in the field area, but it is obscured by poor exposure and by the similarity between Tsp and Tpft1 beds. Pebble imbrication direction is the only characteristic that truly distinguishes the two units, and since imbrications are not obvious in every outcrop it is difficult to establish with certainty the

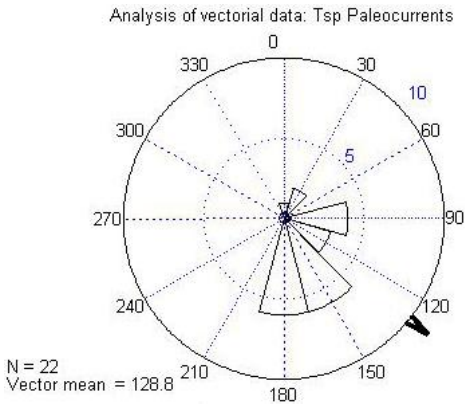

Figure 19 - Rose diagram of paleocurrent indicator attitudes (mainly imbrications) for the Tsp map unit. "N" is the number of measurements, and the arrow indicates the vector mean of the attitudes. Rose diagram by Vector_Stats of Jones (2006). Data tabulated in Appendix 1.

map pattern of the contact. However, I could not find any outcrops containing both eastward- and westward-directed imbrications, suggesting the contact is not interbedded. Bedding attitudes of clearly Tsp beds are consistently shallower than those of nearby Tpft1 beds, suggesting the contact exhibits angular unconformity of about 6 to 10°. "Dashing in" a contact between Tsp and Tpft1 outcrops results in an irregular contact, which could be the result of erosional paleorelief. These observations combined suggest the Tsp basal contact is an irregular angular unconformity.

Further suggesting an erosional basal contact is the similarity of clast suites between Tsp and Tpft1. Although this could result from similar tuff units being exposed in both the eastern and western highlands, it is more likely the result of reworking of Tpft1 clasts by southeast-flowing streams into the Tsp deposits. This process would require erosion of Tpft1 deposits, resulting in an unconformable basal contact. This erosion may have occurred to the northwest of the study area, however.

On the other hand, local southward paleocurrents in Tsp around the contact, as

well as toward the top of Tpfi, suggest the contact is somewhat gradational. The nature of the Tsp basal contact, and in particular its significance in terms of geologic history, is discussed in more detail in the "Piedmont replacement" section, below.

Thickness of unit Tsp cannot be determined exactly as the upper contact is not exposed, but the preserved thickness is at least 95 m.

Tsp is distinguished from the Popotosa Formation because the southeastward paleocurrents contrast with the dominantly west and southwestward paleocurrents of the Popotosa; it is distinguished from the Sierra Ladrones Formation because of its significantly different clast suite and the lack of evidence for a through-flowing ARG during Tsp time. As discussed below, the Sierra Ladrones piedmont facies in the area of the BDA fault is composed mainly of dark red to blood red tuffs, most likely La Jencia Tuff, with rare schists, a completely different clast suite from Tsp. Furthermore, although the Tsp conglomerates intercalate with sandstones to the southeast, the sandstones bear no evidence of being ARG (i.e., no exotic pebbles such as chert, quartzite, or granite). Therefore, Tsp is interpreted and described as a transitional unit, lying between the two formations.

Sierra Ladrones Formation

As defined by Machette (1978), the Sierra Ladrones Formation is the uppermost unit of the Santa Fe Group in the Socorro basin (Chamberlin, 1980). In the type area, it consists of sands, muds, and gravels associated with alluvial fan, piedmont, overbank, and axial-fluvial (i.e., ancestral Rio Grande [ARG]) deposits, the presence of the later distinguishing the Sierra Ladrones from the Popotosa (Machette, 1978; Chamberlin,

1980). Therefore, the base of the unit is placed at the first appearance of ARG deposits. The top is placed at the maximum aggradational surface prior to the present phase of Rio Grande valley entrenchment (Hawley et al., 1969). Where preserved in the Socorro basin, this highest surface is termed the Las Cañas surface after McGrath and Hawley (1987). Near Socorro, the base of the Sierra Ladrones is bracketed by the 6.88 ± 0.02 Ma basaltic trachyandesite of Sedillo Hill of Chamberlin and Osburn (2006) and the 3.7 ± 0.1 Ma basalt of Socorro Canyon of Chamberlin (1999, with age from R.M. Chamberlin, unpublished data, cited in Chapin et al., 2004b; both ages are $^{40}Ar/^{39}Ar$ ages). No nearby age constraints exist for the top of the formation, but magnetostratigraphic research on stratigraphically-equivalent units to the south (Camp Rice Formation of the Las Cruces basin) and north (Sierra Ladrones of the Albuquerque basin) suggest entrenchment began around 800 ka (Mack et al., 1993; Pazzaglia and Hawley, 2004; Connell et al., 2005). Morgan et al. (2009b) describe fossil fauna removed from ARG deposits in the walls of Tiffany Arroyo, immediately south of the study area, and assigned them a late early Blancan age, between about 3.2 and 2.2 Ma, which is consistent with the age bounds described above.

The Sierra Ladrones Formation in this study area is represented by three facies: the axial ancestral Rio Grande facies, a piedmont facies, and a transitional facies. They are distinguished from each other based on sedimentology, clast suite, and geographic location. As the transitional facies only occurs as small exposures, it is mapped with the ARG facies.

Variations in the thickness of the Sierra Ladrones Formation across the field area are an interesting characteristic of the study area geology. Thickness changes appear to be

particularly related to the BDA fault. Although the base of the deposit is not exposed immediately north of the fault, a deep water well drilled near the city of Socorro intersected 340 meters of ARG sands before bottoming in muds (R.M. Chamberlin, pers. comm. 04/2009), suggesting 340 meters is a maximum thickness for the area. In contrast, the formation is locally absent in the immediate footwall of the fault, and only reappears 2 km away as thin caps on small, isolated buttes. The unit thickens to the south, however, until the base of the deposit projects into the subsurface (cf. both the true-scale and vertically exaggerated versions of Cross-section C-C' on Plate 2). The maximum thickness attained in the south of the field area is unknown. The implications of these thickness variations are discussed under the "Flexural uplift" heading of the "Structure" section.

Sierra Ladrones ancestral Rio Grande deposits (QTsf)

Outcropping sporadically all along the eastern side of the field area are sands, pebbly sands, and pebble deposits with rounded gravels of exotic compositions. Due to low erosion resistance and only local cementation, they are very poorly exposed, and sometimes only locatable by small pockets of exotic clasts or particularly sandy colluvium on hillsides. Because poor exposure precludes accurately defining individual deposits' extents, QTsf is mapped discontinuously throughout, with a westernmost limit of ARG deposits defined by extrapolating between the westernmost outcrops.

QTsf consists mainly of moderately to well sorted sands, pebbly sands, and rare pebble beds of rounded quartz and quartzite, (Pedernal) chert, and granite and angular to rounded volcanics, as well as unmappable exposures of greenish muds and reddish-

orange muddy sands. The sands are generally a peppered or speckled light gray color, with the speckling resulting from varicolored lithics. Beds are thin and massive or cross-bedded, with weak imbrications suggesting southwest to southward paleocurrents (Figure 20a). Deposits are locally cemented as concretions (Figure 21) or where immediately overlying better-cemented units of low permeability that cause perching of water and preferential cementation. Muds and muddy sands are massive.

These deposits are interpreted to be the product of the ARG as the rounded exotic

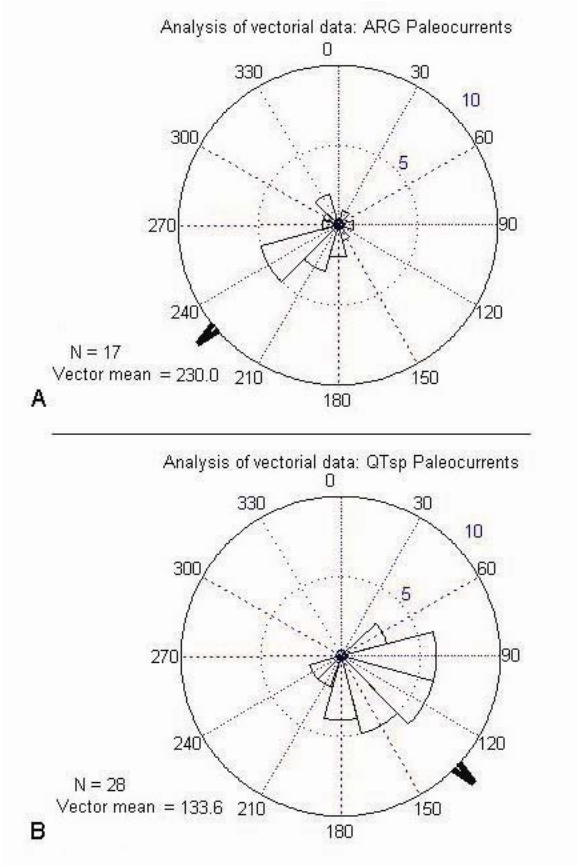

Figure 20 - Rose diagrams of paleocurrent indicator attitudes (mainly imbrications) for a) QTsf and Qvof and b) QTsp. "N" is the number of measurements, and the arrow indicates the vector means of the attitudes. Rose diagrams by Vector_Stats of Jones (2006). Data tabulated in Appendix 1.

Figure 21 - Photo of a QTsf concretion formed by very localized cementation of the deposit. Photo location: 0324470 m E, 3745955 m N.

clasts (e.g., quartzite and Pedernal chert) indicate a far extrabasinal source and are consistent with the typical ARG clast suite of lithologies derived from northern New Mexico highlands. In addition, the clast suite is similar to that of young, definitively Rio Grande deposits, and there exists no other major river or any evidence of a paleoriver in the area that could have delivered these lithologies. Sands, pebbly sands, and pebbles are most likely ARG channel deposits. Greenish muds are likely abandoned channel fill or flood plain deposits, while reddish-orange muddy sands could be overbank/distal fan transition deposits, like Qvot, described below.

Both stratigraphic and lateral contacts are found in the field area, but only south of the BDA fault. Here, the base of QTsf is exposed in outcrop to be a mild angular unconformity with underlying Popotosa strata. In the same area, a buttress unconformity with QTsp (Sierra Ladrones piedmont facies) is suggested by a continuous northeast-trending bluff line (Figure 22), a feature originally incorrectly interpreted by Machette et

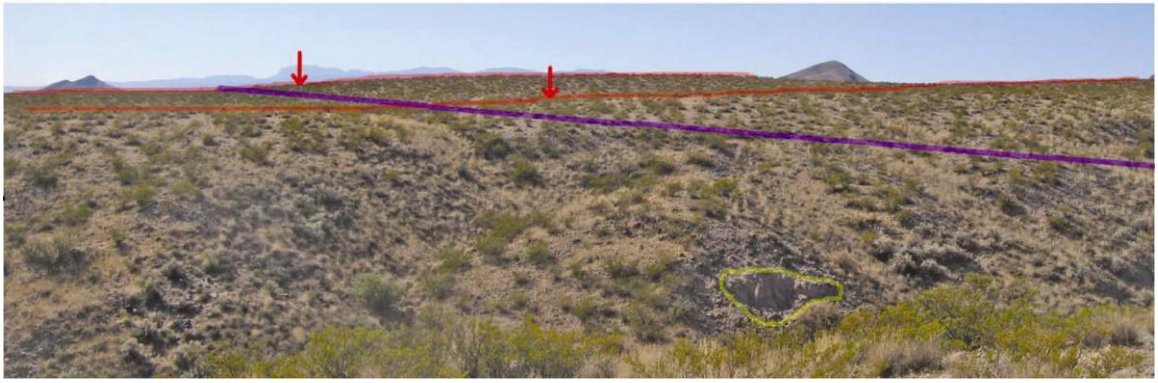

Figure 22 - Photo of an ancestral Rio Grande bluff line in the southwest of the field area, facing west-southwest. Red lines highlight topographic ridges, while the red arrows located the center point of a continuous scarp that is the bluff line; purple line parallels the scarp. Exotic ARG clasts can be found all over the surface below the scarp, but nowhere above, indicating the scarp is a buttress unconformity, juxtaposing ARG and piedmont deposits. Highlighted in yellow are Popotosa alluvial sandstones that dip about 10° to the east, in contrast to the nearly horizontal post-Popotosa deposits above. Sandstone outcrop is about 2 meters tall. Photo taken near 0322100 m E, 3740100 m N.

al. (1998) as a Quaternary fault scarp. Observations to the north of the field area suggest that interfingering lateral contacts between QTsf and QTsp also exist (cf. Chamberlin et al., 2002), though they have not been found in outcrop in the study area.

Post-Santa Fe Group ARG deposits are also found in the study area, which I separated from Sierra Ladrones ARG based on clast suite and geomorphology. Obsidian is found as a rare constituent of the clast suite of some ARG deposits, the majority of which is presumed to be the 1.43 Ma Rabbit Mountain obsidian ($^{40}Ar/^{39}Ar$ age from Love et al., 2004). Although this obsidian is found in Sierra Ladrones ARG, it is restricted to the top of the formation (R.M. Chamberlin, pers. comm. 2009). Conversely, all post-Santa Fe Group ARG deposits have rare obsidian in them, although the scarcity of the obsidian makes it easy to overlook. For mapping purposes, I labeled all ARG deposits with obsidian pebbles post-Santa Fe Group. I admit this convention may result in

miscorrelated deposits, but believe it is a fair convention for addressing the difficult task of distinguishing between Sierra Ladrones and post-Sierra Ladrones ARG deposits. I mapped all deposits on clearly inset surfaces as post-Santa Fe Group, regardless of clast suite, however.

Sierra Ladrones piedmont deposits (QTsp)

Located mostly in the north-center of the area are deposits consisting of poorly sorted angular to subrounded sands to cobbles and locally boulders with various clast suites reflecting source areas in the Chupadera Mountains. In general, from north to south the clast suite grades from common red rhyolitic tuffs and rare basalts, schists, and limestones to common gray, light bluish gray, and light purple tuffs and rare andesitic lavas and scorias. Clast sizes decrease to the south and east away from the mountain front, and sand beds become more prevalent. Imbrications suggest paleocurrents that parallel present drainages, i.e. south and east away from the mountain front (Figure 20b). Well-developed (Stage III+ and greater) carbonate horizons are found throughout as a part of both buried and active soil profiles. The basal contact, where exposed to the south of the BDA fault, is an angular unconformity with underlying Popotosa strata (Figure 23). The clast suites, paleocurrent directions, and decrease in grain size to the south and east all indicate these are piedmont deposits of the Chupadera Mountains.

Above, I noted the potential difficulty of distinguishing Sierra Ladrones and Popotosa piedmont facies; in this area, the two are generally easily separated by paleocurrent directions, bedding attitudes, and clast suites. The Sierra Ladrones piedmont emanated from the Chupadera Mountains, such that paleocurrent indicators show fanning

Figure 23 - Outcrop-scale exposure of the angular unconformity (thin red line) separating east-tilted Popotosa eolian sandstones from gently-dipping Sierra Ladrones piedmont gravels. Black backpack on arroyo floor for scale. Photo facing south, and taken at 0320717 m E, 3741253 m N.

vectors outward from the mountain front to the south and east (Figure 20b). The Popotosa Formation piedmont deposits, in contrast, are generally westward to southwestward, toward or across the mountain front (Figure 24); the major exception to this is the uppermost Popotosa, where southward to southeastward paleocurrents are observed (i.e., in Tpfi). Bedding attitudes also often distinguish the two, as most places Popotosa beds have shallow to moderate dips whereas the overlying piedmont deposits slope to the southeast at nearly original piedmont gradients. In these areas, prominent angular unconformities can locally be found in outcrop (Figure 23). Again, however, there are exceptional areas, such as along the floodplain southwest of the Solitude fault, where Popotosa beds are gently dipping to horizontal. Finally, clast suites can often distinguish the two, especially around the CF fault and further north, where the Sierra Ladrones and younger piedmont deposits consist of red tuffs and rare schists that contrast

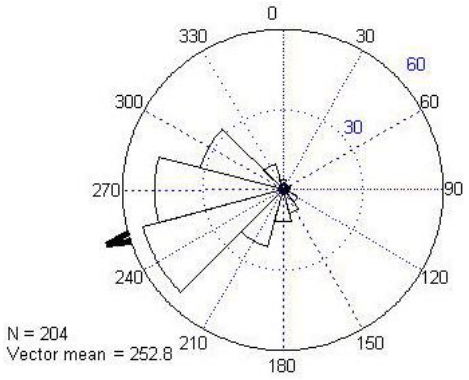

Figure 24 - Rose diagram of all paleocurrent indicator attitudes from the Popotosa Formation exposed in the study area. "N" is the number of measurements, and the arrow indicates the vector mean of the attitudes. Rose diagram by Vector_Stats of Jones (2006). Data tabulated in Appendix 1.

strongly with the light bluish grey and light purplish tuffs of the Popotosa conglomerates. The most difficult area for distinguishing between Popotosa and later piedmont deposits is along the mountain front southwest of the CF fault, where poor exposure and colluvial mixing of clast suites masks the contact between the two.

Sierra Ladrones piedmont and post-Santa Fe Group piedmont deposits can be very difficult to distinguish. Here, the two are distinguished based on carbonate horizon development and the elevations of geomorphic surfaces. Pedogenic carbonate horizons develop along a well-documented series of stages (Figure 25; Gile et al., 1965; Machette, 1985). The time required to achieve each stage varies with a number of factors, but in Socorro County thick (2+ m) horizons of the last three stages are generally not found in deposits younger than Sierra Ladrones in age (cf. Goldstein, 2001). For mapping purposes, I chose to interpret all deposits with Stage III+ or greater carbonate horizons greater than 2 m thick as Sierra Ladrones deposits. Sierra Ladrones piedmont deposits can also be identified based on the elevation of the geomorphic surface overlying the

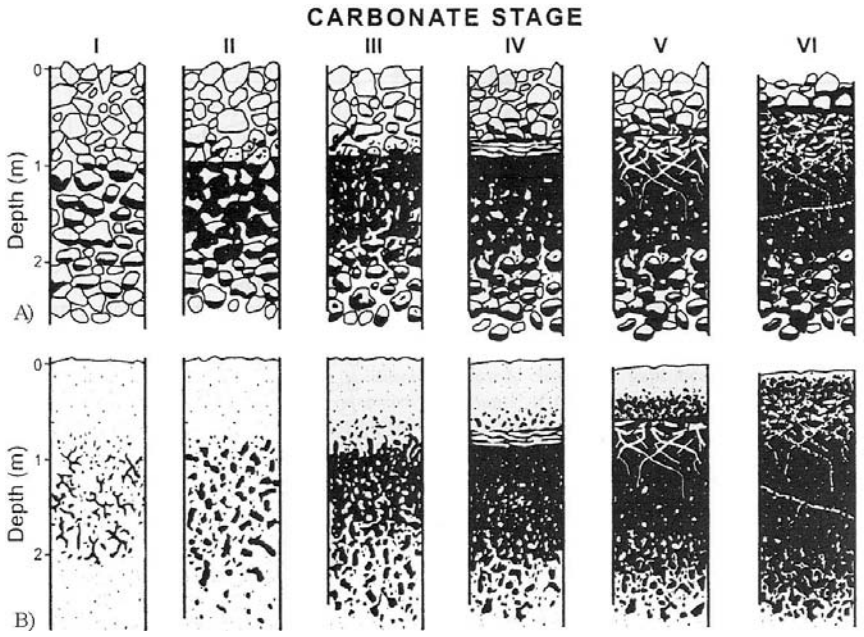

Figure 25 - Stages of carbonate horizon development, from Schaetzl and Anderson (2006), for a) a gravelly parent material and b) a non-gravelly parent material. Although carbonate is white in the field, it is here represented by black masses. Stages I through III demonstrate increasing amounts of carbonate on clasts and within the matrix material; Stage IV is distinguished by the presence of laminar layers of carbonate at the top of the horizon, and Stages V and VI demonstrate alternating periods of fracturing and precipitation of carbonate in the fractures.

deposit. As the formation is defined as including all piedmont deposits associated with an ARG up to and including the highest aggradational surface, deposits that are capped by the highest surfaces in the area are interpreted as Sierra Ladrones in age, while deposits capped by inset surfaces are interpreted as post-Santa Fe.

Post-Santa Fe Group deposits

All deposits that accumulated during the present phase of Rio Grande entrenchment are simply termed post-Santa Fe. No formal stratigraphic names have yet been proposed for these deposits, and no names are applied here. The post-Santa Fe in

this area is dominated by Chupadera Mountain piedmont deposits (Qvn_, Qvs_, Qpu, Qt, Qa_). Rio Grande alluvium (Qvof, Qf), a piedmont/fluvial transitional deposit (Qvot), and colluvium (Qc, Qls) are also delineated.

While the timing of initial entrenchment is now well constrained to about 800 ka, the cause is not known. Four commonly considered hypotheses are 1) integration of the San Luis basin in south-central Colorado with the Rio Grande, 2) integration of the Rio Grande with the Gulf of Mexico, 3) regional uplift, and 4) regional climate change (Connell, 2004). Recent dating of lacustrine geomorphic surfaces associated with Lake Alamosa by Machette et al. (2007), however, indicates that the San Luis basin did not integrate with the Rio Grande until after 440 ka, well after entrenchment began. Thus, this first theory must be discounted. Any one or a combination of the other three may be the cause of entrenchment.

Following entrenchment, the Rio Grande and its tributaries oscillated between periods of aggradation and incision, producing a flight of terraces and fans. The controls on these cycles are not known for certain, but climate/glacial cycles are most often invoked as an explanation (e.g., Connell, 2004; Pazzaglia and Hawley, 2004). Integration of the San Luis basin with the Rio Grande likely also influenced the pattern.

I obtained no precise age constraints on post-Santa Fe deposits from the field area, but mapping by myself and Chamberlin et al. (2002) correlates my Qvn3 with the Qvo3 of Chamberlin (1999), whose surface Phillips et al. (2003) dated by ^{36}Cl to be 122 ± 18 ka. This age correlates well with age constrains on other surfaces in the rift. Basalt flows lying within and on top of the Los Duranes Formation of Connell et al. (2007), a Rio Grande terrace deposit in the Albuquerque area, constrains the age of the top of that

formation to between 98 and 156 ± 20 ka (Connell, 2004). Pazzaglia and Hawley (2004) suggest the top of the Picacho alluvium of Gile et al. (1981) is 140-200 ka. Dethier and McCoy (1993) estimated the age of their Qt3 at 170 ± 40 ka based on amino acid racemization, and Formento-Trigilio and Pazzaglia (1998) estimated their Qt4 to be around 150 k.yr. old. Further support for possible correlation between these units is the extent of each. Qvn3 is by far the most extensive post-Santa Fe piedmont deposit in this field area, just as Qvo3 is to the north on the Luis Lopez and Socorro quadrangles (see Chamberlin, 1999, and Chamberlin et al., 2002). Formento-Trigilio and Pazzaglia (1998) suggest their Qt4 is the most extensive terrace surface in their field area, while Pazzaglia and Hawley (2004) suggest the Los Duranes Formation is also an unusually widespread deposit. These similarities suggest this deposit and its overlying geomorphic surface may have regional significance.

Piedmont deposits (Qvn1 though Qvn5, Qvs1, Qvs2, Qpu, Qt, Qa, Qae, Qai)

Post-Santa Fe piedmont deposits dominate all but the center of the field area. Each consists of poorly to moderately sorted, angular to rounded, sand to boulders of lithologies from upstream bedrock units in the Chupadera Mountains, local Popotosa strata (where exposed), and Rio Grande alluvium (where reworked by tributary streams). Except locally, rhyolitic tuffs dominate the clast suites, with less common andesitic lavas and scorias and rare basalts, schists, limestones, Abo Formation, quartzites, and cherts. General trends in clast suite parallel those of the Sierra Ladrones piedmont deposits, i.e. red tuffs and rare schists and basalts in the north, grayish tuffs and lesser lavas in the south. These general trends are highly influenced by locally reworked strata, however.

Where sandy Popotosa strata are exposed, eolian sands are uncommonly found burying the piedmont deposits; I do not know whether any eolian sands are actually interbedded with the piedmont deposits, however. Where eolian sands are mappable, they are mapped as Qae.

Piedmont deposits are divided based on relative age, geographic location, and sedimentology. The Qvn and Qvs series consist of middle Pleistocene to early Holocene(?) piedmont deposits of the north and south of the area, respectively, which are further subdivided based on relative age inferred from surface elevations. Qt and Qpu are terrace and fan deposits, respectively, which could not be correlated to the other piedmont series. Qa, Qae, and Qai are the late Holocene(?) to historic deposits of arroyo floors and sand sheets.

Older piedmont deposits (Qvn_, Qvs_, Qt, Qpu)

Pleistocene to early Holocene(?) piedmont deposits are mapped as a member of Qvn_, of Qvs_, or as Qt or Qpu depending on correlation to other deposits and geographic location. Deposits in the Qvn_ and Qvs_ series are differentiated based on relative age inferred from surface elevations. Qpu, Qvs_, and Qt deposits are each 0 to at least 5 m thick, while Qvn_ deposits are 0 to 25 m or more thick.

I initially attempted to map all piedmont deposits as a part of a single series of different aged deposits (cf. Chamberlin et al., 2002), but age-ranking every deposit in the area based on surface elevations proved difficult. I correlated and relative-dated piedmont deposits by visually projecting piedmont surfaces in ArcScene (e.g., Figure 9), correlating deposits which appeared to have originally been a part of a single continuous piedmont.

This process worked well in the northern half of the study area, where five piedmont surfaces could be identified and correlated to the surfaces of the Qvo_ units of Chamberlin et al. (2002) to the north. Unfortunately, around the center of the area, where Popotosa strata are exposed and break up the Quaternary, the piedmont surfaces bend around the southern terminus of the Chupadera Mountains (Figure 26), and I was not able to correlate units across this bend. Therefore, I divided the piedmont deposits into northern (Qvn_) and southern (Qvs_) facies. More difficulties arose when attempting to delineate individual Qvs units, as the piedmont deposits in the south of the area appear to have less regular surface elevations. Thus the southern piedmont was only divided into two units based on surface elevation and surface preservation, each of which may correlate to one or more Qvn deposit. I tentatively correlate Qvs2 with Qvn3 based on the widespread distribution, lateral continuity, and surface preservation of both. Future work could test this correlation by comparing the soil development on well-preserved surfaces of both. Within each piedmont series, age decreases with increasing suffix, i.e. Qvn1 is

Figure 26 - ArcScene image demonstrating how the piedmont wraps around the Chupadera Mountains, facing east at the north end of the field area and south-southeast at the south end.

the oldest while Qvn5 is the youngest. I also could not correlate some mountain front fans (Qpu) and small piedmont terraces (Qt) to the Qv_ units, and hence mapped them separately.

Younger piedmont deposits (Qa, Qai, Qae)

Historic and late Holocene(?) deposits on the piedmont are mapped as Qa (active alluvium, undivided), Qai (incised alluvium), or Qae (active alluvium and eolian sand, undivided). Contacts between these three are all gradational. Qai is located in gullies incised into Qa deposits. Incision appears to be the result of base level changes, as the gullies shallow upstream to merge with the surrounding Qa deposit, suggest headward propagation of incision. Interestingly, these deep gullies only occur to the far south and far north of the field area. Qae is located around exposed Popotosa sandstones, particularly eolian sandstones, where the abundant sand supply is reworked into eolian sheets. All younger piedmont deposits are 0 to at least 5 m thick.

Axial fluvial (Qvof, Qf) and transitional (Qvot) deposits

All along the eastern edge of the area as well as in the south-central are post-Santa Fe Rio Grande deposits. In the south-central, there is also a significant width of piedmont/axial-fluvial transitional deposits.

Older Rio Grande deposits (Qvof)

Middle to late Pleistocene terrace deposits and alluvium of the Rio Grande are mapped as Qvof, and consist of poorly to moderately well sorted sands and pebbles of

common rounded quartzite and (Pedernal) chert, rare rounded granite and obsidian, and varying amounts of locally-derived, angular to rounded volcanics. Obsidian is presumed to be dominantly Rabbit Mountain obsidian, which, as described above, is precisely dated at 1.428 ± 0.003 Ma (Love et al., 2004) and used in this area to distinguish between Santa Fe Group- and post-Santa Fe Group-aged Rio Grande deposits. Deposits are 0 to 5 m thick.

Younger Rio Grande deposits (Qf)

Late Pleistocene to Holocene terrace deposits and alluvium of the Rio Grande are mapped as Qf, and consist of muds and pebbly sands. Pebbly sands are similar to those described under Qvof. Along the east edge of the area, Qf intertongues with Qa, Qae, and Qai. The bases of these deposits are nowhere exposed, but the deposits are 0 to at least 25 m thick.

Transitional deposits (Qvot)

In the south-central part of the area, a wide zone of reddish beige to light orange muddy sands lie between the piedmont and axial fluvial deposits and is interpreted to be a piedmont/axial fluvial transitional deposit. Qvot consists of locally gypsiferous, uncommonly pebbly, massive to weakly bedded sands and muds. In the far south, the deposit grades continuously into Qvof deposits by decreasing in mud content, increasing in pebble content, and gradually changing color. Further north, exposures along broad arroyos demonstrate interfingering lateral contacts with both Qvof and Qvs_ beds. Qvot is likely a combination of distal fan and axial floodplain sediments. The bases of these deposits are nowhere exposed, but the deposits are 0 to at least 20 m thick.

Colluvial deposits (Qc, Qls)

Colluvium (Qc) is locally mapped where it appears to conceal important features or deposits. In this area, this is mainly where uncemented and easily eroded ARG deposits underlie more erosion-resistant piedmont deposits, resulting in burial of ARG outcrops by reworked coarse piedmont gravels. Qc deposits are poorly sorted gravelly sands to gravels, with gravel sizes, clast suites, and rounding reflecting upslope deposits. Where ARG deposits are clearly a part of the colluvium, e.g. where the deposit contains significant quartzite, chert, and granite or well sorted sands, it is speckled on the map to indicate their presence. Note that Qc is not delineated everywhere it is found, even if it is mappable. This is simply to aid with map clarity. The bases of these deposits are rarely exposed, but deposits are probably 0 to 2 m thick.

In the north-central part of the map area, landslide blocks of basalt (Qls) are found on the sides of a basalt-capped hill. These blocks are no more than a few meters thick and broken up.

Apache #1-A oil test well

Also of importance to this study is the lithologic log of the Apache 1-A oil test well. This well was drilled on the BDA NWR in the mid 1920s on the west side of the river to a depth of 745 m (Figure 6). The wellbore produced hot water under artesian pressures for a number of years, producing a hot water bathing pool until the well was plugged (Barroll and Reiter, 1995). Unfortunately, the cuttings from this well could not be recovered, but the lithologic log remains (Figure 27), and here I present a possible interpretation of the lithologic units on the log.

Lithology	Bottom, feet	Interpretation
Soil	3	post-Santa Fe Group
Sand, Hole Full Water	45	
Sand and Boulders	55	
Gravel	100	
Broken Sand Rock	379	Popotosa Formation
Sand, Red and Clay	400	
Black Hard Rock	410	Basalt of Broken Tank(?)
Sand	440	Popotosa Formation
Hard Rock	449	
Sand and Clay	500	
Hard Rock	509	
Sand	535	
Hard Rock	539	
Broken Sand, Red	550	
Sand, Rock and Clay	592	
Sand Rock	608	
Hard Rock	623	
Sand Rock	645	
Hard Rock	670	
Broken Sand Rock	680	
Hard Rock	685	
Broken Sand Rock	790	
Hard Sand Rock	810	
Red Rock	824	
Broken Hard Rock	836	
Hard Rock	870	
Lime	890	
Sandy Lime and Clay	915	
Shale and Clay, Sandy	980	
Sand and Boulders	1110	
Broken Rock	1208	
Rock and Clay	1294	
Clay	1300	
Rock and Sand	1325	
Rock	1385	
Yellow Clay	1410	
Sand and Boulders	1495	
Sandy Shale	1575	
Gumbo	1587	Fault zone
Sand Shale and Shells	1715	Cretaceous
Gumbo	1780	Fault zone
Sandy Shale, and Shells	1940	Cretaceous
Shale, Pink	1955	Fault?
Salt	2020	Permian
Anhydrite	2030	
Salt	2075	
Salt and Anhydrite	2085	
Salt	2100	
Anhydrite	2110	
Salt	2185	
Salt and Anhdrite	2285	
Salt	2310	
Anhydrite	2320	
Red Rock	2330	
Salt	2350	
Anhydrite	2400	
Red Rock and Salt	2445	

Figure 27 - Simplified lithologic log for the Apache 1-A oil test well with the interpretation presented here.

First, though, it is important to note the difficulty of interpreting a lithologic log with such ambiguous terms as "hard rock." I freely admit the log could be interpreted multiple ways, and here I present a simplest explanation interpretation. The goal is not to give a definitive interpretation of the log, but instead to document a maximum possible thickness of Santa Fe Group strata in the area based on the probable occurrence of Cretaceous strata and certain presence of Permian strata in the log.

The lithologic log is simplistically divided into post-Santa Fe Group, Popotosa Formation, Cretaceous, and Permian, with two major fault zones also inferred. The base of the post-Santa Fe is here placed at 100 feet, at the base of a 45-foot thick gravel layer. Below this is the first occurrence of a "rock" layer, suggesting the strata below are cemented early basin fill, while the strata above is uncemented Quaternary fill.

Below the post-Santa Fe fill, the Popotosa Formation is interpreted to encompass all units down to the first appearance of "gumbo." This is supported by the dominance of "sand" and "sand rock" in the unit descriptions throughout this part of the log, as although there are thin sedimentary intervals in the Mogollon Group (Eggleston, 1982) and local Datil Group (Chamberlin and Cikoski, mapping in progress), they are far thinner than the volcanic units in those Groups, such that if the well had penetrated through the Popotosa into the Mogollon there would be an interval with very little sand. In this interpretation, the "hard rock" entries are thought to be well-indurated conglomeratic intervals, and the "black hard rock" could be one of the basalts known to locally intercalate with the Popotosa; here I suggest it is most likely to be the basalt of Broken Tank, as this same basalt is known to occur amongst Popotosa strata to the northwest along the BDA fault. The "lime" is perhaps a small limestone deposit, possibly

from a local spring or cienega.

The anhydrite, salt, and "red rock and salt" must belong to the Permian Yeso Formation, as no other unit in the area contains such a thickness of evaporites (in this case, almost 150 m thick). The "shale, pink" entry above the salts is also thought to belong to the Permian, as the Yeso contains numerous "red bed" shales and sandstones on either side of the evaporite section. The "sandy shale and shells" entries are less certain, but possibly belong to the Cretaceous section (R.M. Chamberlin, pers. comm.). These interpretations raise some issues, however, as the regional stratigraphy also includes Oligocene volcanics, Eocene sediments, Triassic continental fluvial sediments, and uppermost Permian limestones, mudstones, and sandstones (Figure 10), which are not present in this interpretation. These units could be missing due to local erosion or, more likely, faulting.

The log also includes two entries of "gumbo," which generally refers to heavy, expanding clay soils. Here, "gumbo" is interpreted to refer to the fault gouge of large normal fault zones. This interpretation partially alleviates the issue of missing stratigraphy, as normal faulting removes units from vertical sections. This interpretation fits fairly well with the observed gravity data, which locates a steep gravity gradient near to the oil test well (Figure 6); the "gumbo" gouge may be a part of the fault zone(s) creating the gradient. The inferred faults are therefore presumed to be northeast-striking with down-to-the-northwest slip sense, as indicated by the gravity gradient.

At odds with this interpretation is the significant thickness of the "gumbo" units, in particular the lower "gumbo," which is almost 20 meters thick vertically. In part, these thicknesses can be explained by the attitude of the drill hole relative to the fault plane.

True thickness is only recorded in the drill hole when the hole is perpendicular to the plane it is cutting; otherwise the hole cuts across the plane at an angle and results in a thickened apparent thickness. Should the fault plane dip about 60° relative to the drill hole, the true thickness of the lower "gumbo" would only be about 10 m; for a 40° dip, the true thickness would be about 15 m. In addition, the gouge zone is probably thicker than normal due to the units juxtaposed by the fault. Since shale is generally clay-rich to begin with, it should not be surprising that a fault juxtaposing shale units would have an unusually thick gouge.

The gumbo units cannot explain the lack of Triassic or uppermost Permian rocks, however, as neither gumbo unit lies between the "sandy shale and shells" Cretaceous rocks and the evaporite section. I suggest there may be another fault between the two, one with a gouge too thin to be noted on the lithologic log.

PROVENANCE STUDIES OF POPOTOSA STRATA

I conducted two forms of provenance studies on Popotosa strata: clast counts on conglomerate beds and thin section analyses of sandstone beds.

Clast suites

Clast count data are presented in tabular form in Appendix 2, and pie diagrams of clast count data can be found on Plate 3. Clast count trends for individual units are summarized in each unit's description, above. Here, the clast count trends are reviewed and interpreted.

Both temporal (stratigraphic) and spatial (lateral) variations in clast suite are recognized in the field area, and in some instances the nature of clast suite variation cannot be determined with certainty. Examples of stratigraphic trends are the clast suite changes in map units Tpt1, Tpt2, and Tpa. Spatial variations in clast suite are seen between map units Tpa, Tpfi, Tpft1, and Tpft2. Ambiguous changes are found in map unit Tps.

Unroofing likely plays a role in the up-section clast suite changes in Tpt1, Tpt2, and Tpa. A complete unroofing sequence of the stratigraphy to the east would produce basalts, then ignimbrites, andesites, Mesozoic clastic sedimentary rocks, then "red beds" and limestones of the Permian and Pennsylvanian (see Figure 10). Parts of these trends are apparent in up-section changes in the clast suites of Tpt1, Tpt2, and Tpa. The Tpt_

units are both tuff-dominated throughout, but the minority elements change from the bottom of Tpt1 to the top of Tpt2 from rare basalts to andesitic lavas that become increasing more common toward the top (Plate 3). Tpa, meanwhile, is andesitic lava-dominated throughout, but again trends in the minority elements reflect unroofing: the abundance of tuff clasts decreases up-section, while non-volcanic "red bed" and limestone clasts become more common (Plate 3). Mesozoic clastic rocks do not appear in the clast suites of any conglomerates. This may be in part due to these clasts breaking down rapidly during transport, limiting their preservation in deposits. Well indurated concretions and clasts from the Cretaceous Dakota Sandstone are known to survive dozens of kilometers of transport down modern streams, however (D.W. Love, pers. comm.), suggesting break down during transport cannot completely explain the lack of Mesozoic clasts. Another possibility is that the Mesozoic was stripped from the source area during the Laramide, much like the Mesozoic and Permian was removed from the Chupadera Mountains area. I cannot conclusively explain the lack of Mesozoic clastics in the Popotosa clast suites.

Unroofing cannot explain all clast suite variability, however, as age controls across the Popotosa indicate that both lava- and tuff-dominated conglomerates were delivered to the basin from different parts of the source area at the same time. The oreodont fossil found amongst lava-dominated Tpa beds indicate that at least part of the source area to the east had unroofed to the andesite lavas below the ignimbrites by 11 to 9 Ma (age from Morgan et al., 2009a). The Tpft1 conglomerates found surrounding the 8.57 Ma basalt of Broken Tank (age from Chamberlin et al., 2006), however, are nearly exclusively composed of tuff clasts, indicating that not all of the source area had unroofed

to the lavas at the same time. In particular, it seems the southern part of the source unroofed to the lavas sooner than the northern part. The interbedded tuff- and lava-dominated conglomerates of Tpfi could reflect an overlap zone where conglomerates from the two source areas interfingered, and the roughly 60/40 tuff/lava clast suite of Tpft2 could be from mixing of the two end-member clast suites, as this map unit geographically lies between the tuff-dominated Tpft1 and lava-dominated Tpa.

Two possible reasons for concurrent tuff-dominated and lava-dominated regions in the eastern source area are illustrated in Figure 28. In the first (Figure 28a), faulting lifts the lavas in the southern part of the eastern highland relative to the northern. In the second (Figure 28b), paleotopography results in a thinner tuff deposit in the southern part relative to the northern part. This could result if an andesitic lava complex existed to

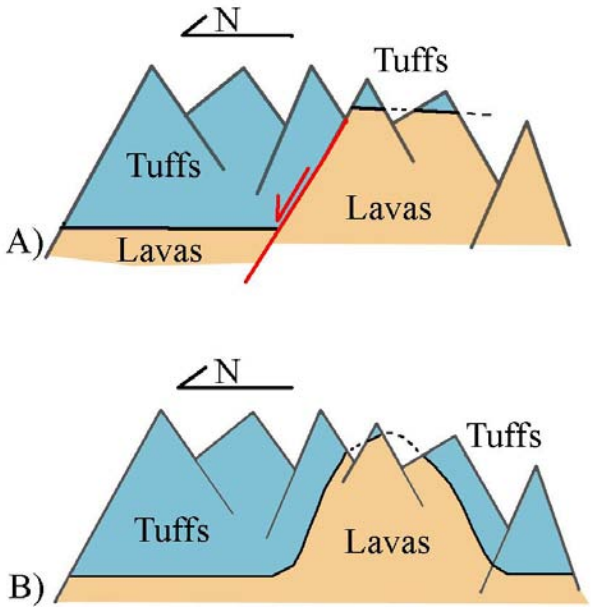

Figure 28 - Schematic diagrams depicting two scenarios that could explain the juxtaposition of tuff-dominated and lava-dominated regions in the eastern highland source area for the upper Popotosa Formation. a) Normal faulting could down-drop tuffs against lavas, or b) paleotopography could have resulted in juxtaposed tuff and lava deposits.

the south that was thinly buried by the ignimbrites. This later hypothesis is preferred, for reasons discussed in detail under the "Pre-Santa Fe Group" heading in the "Paleogeography" section. Alternatively, the different clast suites could be derived from completely separate highlands. I have no way of truly evaluating this possibility, except to say there is no evidence of extrabasinal sediments in the Popotosa. For simplicity, I will not consider this hypothesis further.

The clast suite trend across map unit Tps is ambiguous, but most likely results from unroofing. This trend consists of a steady, continuous increase in lava content from northwest/base of section to southeast/top of section. Although this trend parallels an unroofing sequence, it may instead be the result of changing geographic location, as the northwestern beds are presumably closer to the tuff-dominated Tpft1 conglomerates and the southeastern beds closer to the lava-dominated Tpa conglomerates. The gradual change in clast suite could reflect a gradual increase in lava content of alluvial streams emanating from the eastern highland from north to south. I prefer an unroofing explanation, however, as it is the simpler explanation.

Sandstone petrography

I performed visual estimates of modal abundances of minerals and lithics in eleven sandstone thin sections: nine from a transect along Cross-section A-A', and two from stratigraphically higher positions around the basalt of Broken Tank and from sandstones associated with the transitional unit Tsp (Figure 29; Appendix 3). Of the thin sections from the transect, I took the stratigraphically lowest sample from Tpt1, and examined two uppermost samples from unit Tpa, one I sampled and a second donated to

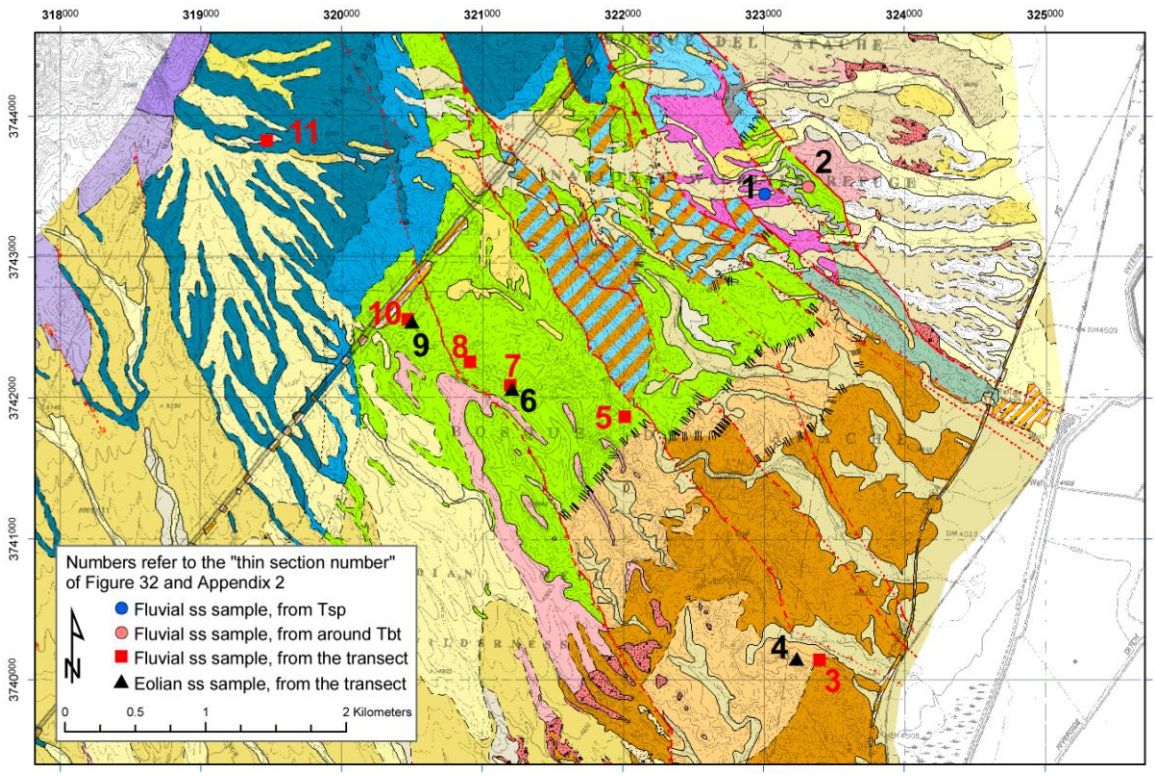

Figure 29 - Thin section locations overlain on the geologic map. Numbers correspond to the "thin section numbers" of Figure 30 and Appendix 2. 1000-meter UTM NAD27 grid.

me by R.M. Chamberlin. All other samples were taken from map unit Tps. Most samples were from alluvial sandstone beds, though three from along the transect were from eolian sandstones. The goal of this petrography was to address the source of the sandstones (i.e., from the same eastern source as the conglomerates or a more distant fluvial system), to examine stratigraphic changes in mineralogy, and to compare the eolian and fluvial sandstone compositions.

Unfortunately, the usefulness of the dataset is limited by the lack of coarse sandstones and lack of grain-size control. Optimally, for differentiating between rhyolitic versus andesitic versus exotic provenances, grain size should be coarse and uniform to

maximize lithic content and recognition and normalize grain size effects. Unfortunately, coarse sandstones are not common, and where present they are typically associated with conglomerate beds. These I avoided, as I was in part testing the idea that the sandstones and conglomerates may have different source areas, and did not want to sample sandstones that may have been contaminated by sediments from the conglomerate source. As a result, the thin section set consisted of medium- and fine-grained sandstones with limited lithic contents. Also, since grain size was not controlled in sampling, the lithic content varies considerably, which impairs interpretation. Grain size effects are apparent, for example, in Figure 30b, where the coarser-grained alluvial sandstones demonstrate a steady increase in andesitic lithic content but the finer-grained sandstones have uniformly low contents.

Appendix 3 contains the modal abundance data in tabular form; Figure 30 contains scatter charts intended to demonstrate stratigraphic trends in mineral and lithic content. Fourteen phases were examined, but only those demonstrating up-section trends are presented in the figure. The rest are included in the appendix, but not discussed here.

The clearest trend appears in the potassium feldspar content (Figure 30a**)**, which monotonically decreases through the transect, then jumps again in the uppermost two samples that are stratigraphically above the transect. This is consistent with a gradual shift from rhyolitic tuff to andesitic lava provenance along the transect, as seen in the conglomerate clast suites. The relatively high potassium feldspar content in the uppermost two samples is also comparable to nearby conglomerate clast suites, which are both rich in rhyolitic tuff clasts.

A less clear trend is evident in the andesitic lithic content data (Figure 30b), in

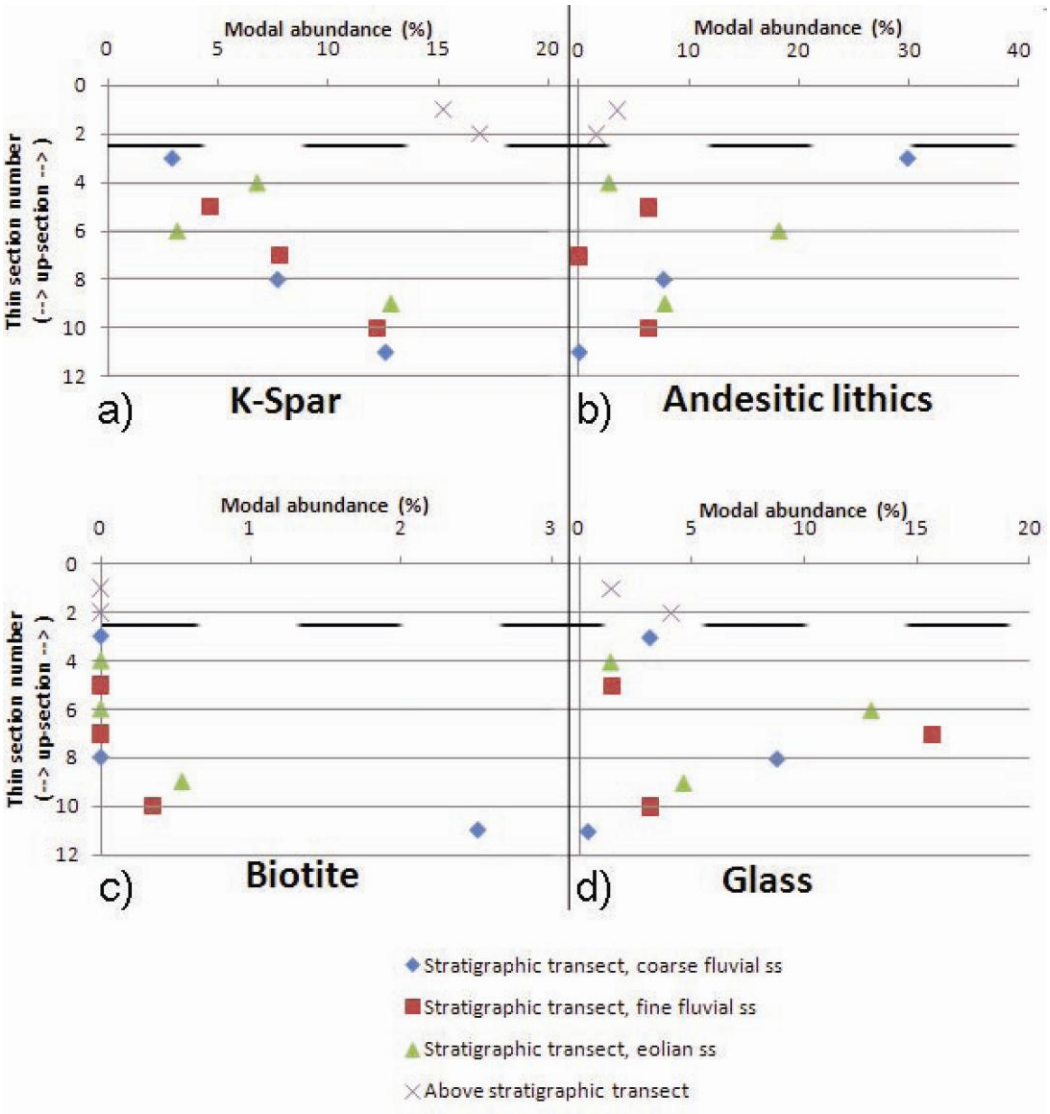

Figure 30 - Scatter plots showing the modal abundances of four phases in the thin sections described in the text. "Thin section number" refers to the numbers used in Figure 29 and Appendix 2. Dashed line separates samples from the transect (below) from samples above the transect (above).

which the coarser alluvial sandstones and the eolian sandstones demonstrate a general increase in lithic content up-section along the trend, whereas the uppermost samples have low andesite contents. The finer-grained alluvial sandstones and the uppermost eolian sandstones do not follow this trend, however. I suggest the reason the finer-grained

sandstones do not follow the trend is that the smaller grain size results in fewer lithics overall, and does not reflect a change in the andesite content of the provenance. I cannot explain the lack of andesitic lithics in the uppermost eolian sandstone. Like that in the potassium feldspar data, the apparent trend in the andesite content data parallels changes in conglomerate clast suite. Andesitic lava clasts increase in abundance up-section along the transect, but are minor components of the conglomerates near the uppermost sandstones, similar to the trends in the sandstone modal abundances.

Biotite shows a clear trend of dropping off rapidly over the lowest four samples (Figure 30c), which could be the result of several factors. First, this could reflect the transition from rhyolitic tuff to andesitic lava provenance, as biotite is more common to rhyolitic than andesitic rocks. Second, since biotite is not particularly chemically or mechanically resistant, the drop in biotite content may reflect up-section increasing mechanical weathering during transport or chemical weathering after transport. Alternatively, the biotite crystals may simply have been blown away from higher strata, as the presence of eolian sandstone beds mixed with alluvial beds in map unit Tps suggests these sands were actively reworked by winds.

The (devitrified) glass content shows an unusual bell-shaped trend (Figure 30d), one which I am not able to explain. Unfortunately, one possibility to consider is that the glass content may be misrepresented. I identified glass based on the presence of axiolitic texture, a product of devitrification that should not be present in non-glassy clasts. However, axiolitic texture may not be present in all glass clasts, such that I may have included some glass in the “Fine-grained Lithics” category, which may have affected the apparent trend. Regardless, the trend appears real, as both the coarser- and finer-grained

alluvial sandstones as well as the eolian sandstones show the same bell-shaped curve. These clasts are most likely derived from weathering of ignimbrite gravels, which contain variable amounts of volcanic glass in their matrices and as pumice clasts. This trend probably reflects a combination of factors, such as unroofing, changing degrees of mechanical weathering during transport, reworking, and possibly climate change, as these would all affect the presence and preservation of glass in the sedimentary environment. Note that the glass most likely all devitrified prior to transport and not after reworking and sedimentary deposition.

Each of these trends is comparable to the observed changes in conglomerate clast suite, suggesting the conglomerates and sandstones are sourced from the same provenance(s). In addition, the eolian sandstones show the same trends as the alluvial sandstones, suggesting they are related; in fact, in the "Paleogeography" section, below, I suggest they are the product of opposing transport processes reworking the same sands. There is no evidence of exotic minerals or lithics in the sandstones, arguing against a distant source for the sand.

PALEOGEOGRAPHY

An important aspect of this work is deciphering the change in basin structure and geometry through time. Here, regional literature and the characteristics of the Santa Fe Group sediments on the quadrangle are interpreted for changes in depositional environments and basin geometry.

Pre-Santa Fe Group

Evidence suggests that, prior to deposition of the Santa Fe Group, the field area lay on a Laramide-age highland that was buried by volcanic deposits of the Datil and Mogollon Groups. Paleogeographic maps by Cather (2004, 2009) locate the study area on the Laramide Sierra uplift of Eardley (1962), during which time Mesozoic and Permian strata were stripped from the area (Eggleston, 1982). Stratigraphic data suggests this highland largely persisted through lower Datil Group-time (upper Eocene), but then was mostly or entirely buried by upper Datil Group volcanics and associated volcaniclastic detritus (Cather, 1990, 2004).

On-going mapping by Chamberlin and Cikoski suggests that one of these Datil-age andesitic volcanic complexes existed near to the field area, most likely centered on the steep gravity gradient to the southeast of the study area. Andesitic lavas dominate the southern tip of the Chupadera Mountains, with intercalated matrix-supported debris flows and rare dikes suggesting a proximal source area. Although little of this volcanic complex

has been found as of yet, I suggest it was likely centered on the northeast-trending portion of the steep gravity gradient to the east of the field area (Figure 31). This gradient has been attributed to the large (offset of ~26 km), right-lateral strike-slip Hot Springs fault system (Harrison and Cather, 2004), which could have served as a focal point for volcanism. The short northeast-trending portion of the gradient would be particularly favorable for focusing volcanism as this right-lateral jog in the trend of the fault could have acted as a releasing bend, and such bends are particularly favorable for the rise of magma (R.M. Chamberlin, pers. comm.). In Figure 31, I made no attempt to delineate the extent of this complex due to my very limited dataset.

At 32.3 Ma, the Socorro caldera erupted to the immediate northwest of the field area (Figure 31), ejecting the Hells Mesa tuff. Presumably, much of this topography was then blanketed by a series of ignimbrites emanating from five more caldera eruptions in the area, creating an ash-flow plateau (Chamberlin, 1980). Rift faulting then dissected this plateau, most likely starting in the Oligocene, but I know of no study of deformation of this age in the southern Socorro basin area. Early rift faults were commonly reactivated Laramide structures, such that the Hot Springs fault likely became a rift fault. The gravity gradient, which is decreasing to the west to a low under basin fill sediments to the north of the IWW quadrangle, suggests it reactivated as a major down-to-the-west fault that formed the eastern margin of the basin.

Syn- and post-Santa Fe Group

Santa Fe Group paleogeographic maps are divided into time intervals based on formation, i.e. Popotosa, transitional, and Sierra Ladrones paleogeographies are discussed

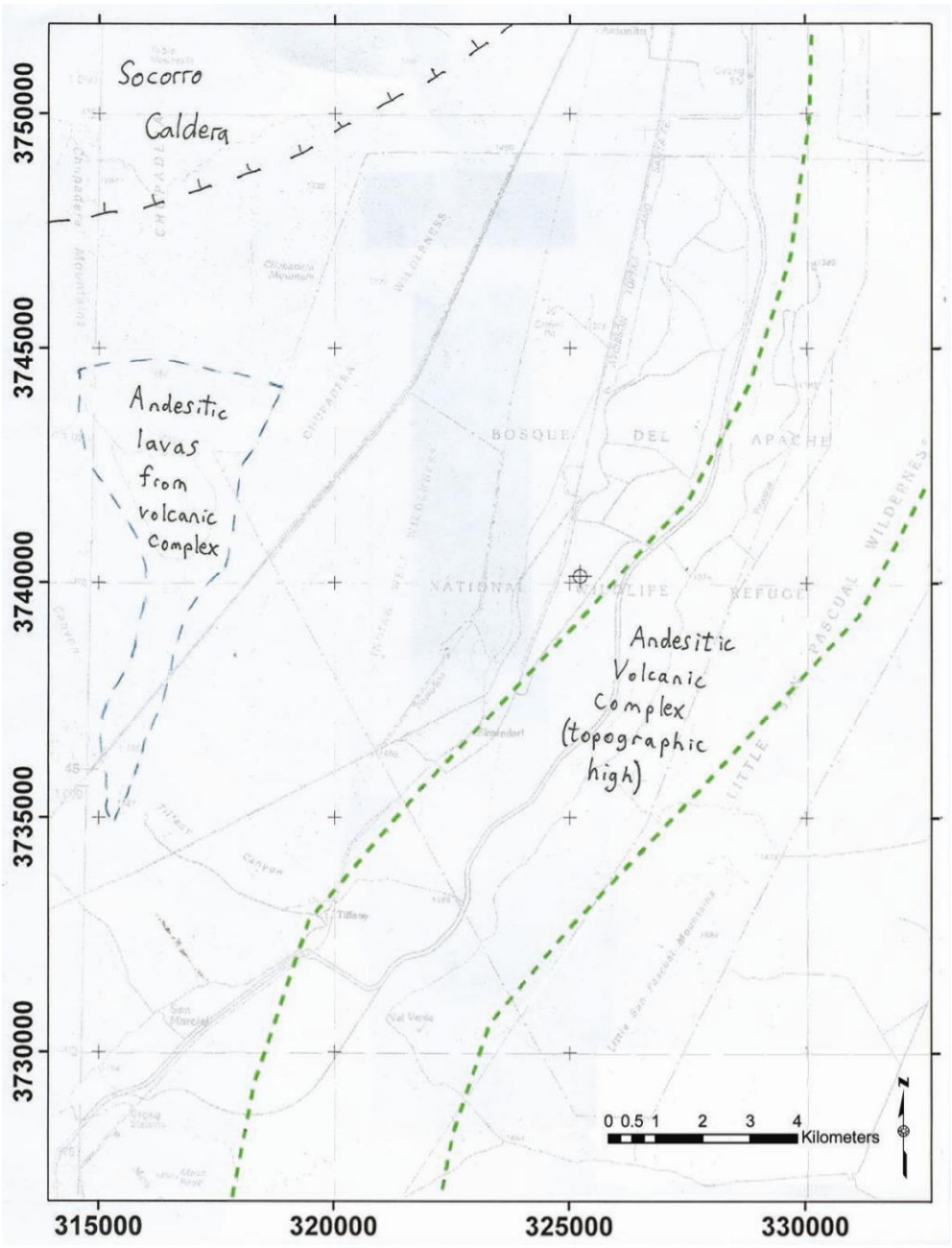

Figure 31 - Inferred paleogeography for the area in the early Oligocene. Bright green dashed lines approximately bound the steep gravity gradient found at the base of Little San Pascual Mountain, and the cross-hairs mark the location of the 1-A oil test well. Blue dashed lines bound the known extent of deposits from this paleogeography, namely an area of andesitic lavas presumably derived from the volcanic complex. The extent of the complex is unknown, but suspected to be centered on the right-lateral 'jog' in the trend of the gravity gradient. Topographic rim of the Socorro caldera after Chamberlin et al. (2002). 5000-meter UTM NAD27 grid.

separately.

Popotosa paleogeography

Popotosa time can be divided into early (Figure 32) and late (Figure 33) periods. Tpt1 and Tpt2 comprise the deposits of the earlier period; no other map units can be shown to be coeval with these two. All other Popotosa units are a part of the late period, as they all appear to occur relatively synchronously, as described below, and be a part of a single, complicated depositional setting.

The sedimentation of both time periods was dominated by piedmont gravels of an ancestral Little San Pascual Mountain (LSPM) highland. A piedmont depositional setting for the Popotosa conglomerates is suggested by the coarse nature, relatively poor sorting, lack of structures, and lack of overbank facies in the deposits. Admittedly, "piedmont" is not a typical depositional setting; usually conglomerates from this sort of setting are classified as alluvial fan or braided river/braid plain deposits. I do not use either of these terms, however, as most of the conglomerates lack critical features typically associated with these environments. For example, alluvial fan deposits typically include significant debris flow or sheetflood couplet components. Debris flow deposits are rare here, however, and I identified no couplets. Braided streams, on the other hand, typically have relatively common cross-stratification and commonly some sort of overbank facies. Except locally, such as the top of Tpa and in Tpt2, cross-strata are not common, and I identified no overbank facies. Even though the characteristics of the deposit do not fit either of these environments, the coarse nature and relatively poor sorting still suggest some sort of source-proximal deposit, however. Thus I use the term "piedmont" to

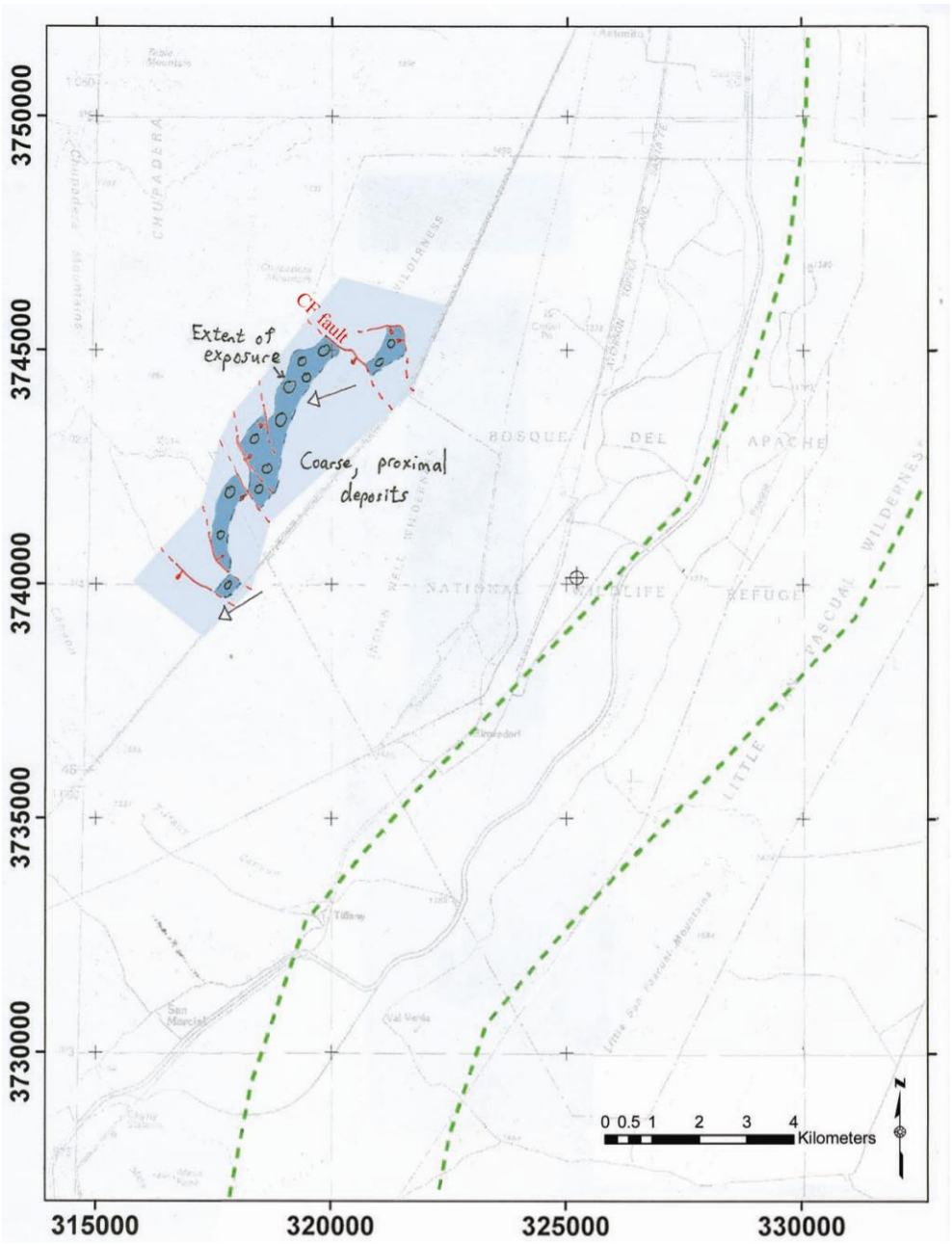

(a)

Figure 32 - a) Interpreted paleogeography for basal Popotosa time, between about 16 and 15 Ma. During this time, local fault blocks contributed coarse, often bouldery detritus to the eastern piedmont. Both source areas delivered mainly rhyolite tuff clasts of the Mogollon Group. The number of faults active during this time is uncertain, but I suspect many of the basal faults were active. Note that everything shown outside of the extent of well-exposed Popotosa is inferred. b) key to symbols used in part a) as well as in Figure 33 through 35. 5000-meter UTM NAD27 grid.

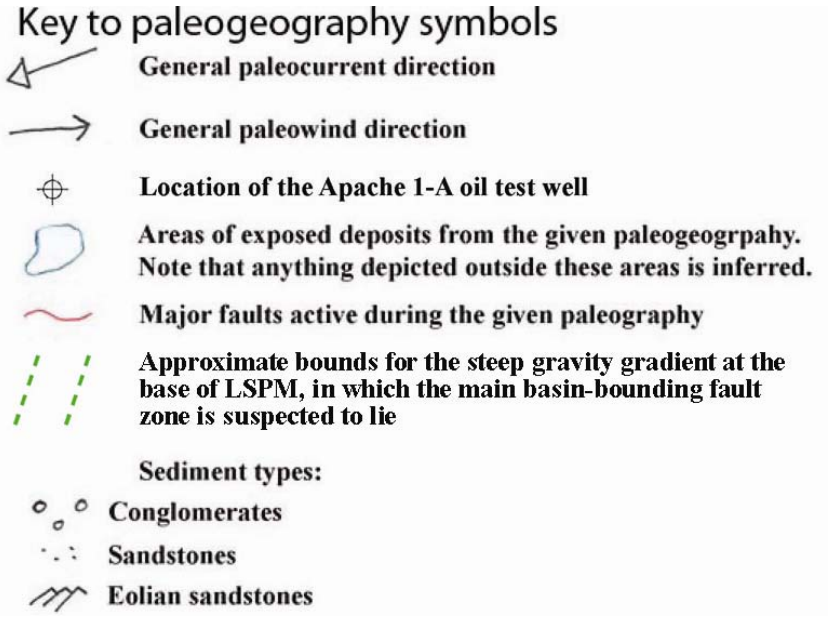

Figure 32b (continued from last page)

describe the depositional environment, as it is conveniently broad and intuitively suggests an environment similar to but somewhere between the classic alluvial fan and braid plain settings. It also captures the important aspect of these deposits, which is that they are proximal deposits derived directly from a nearby highland.

That these deposits originated from an ancestral LSPM highland is indicated by paleocurrent data and by the presence of "red bed" clasts in the younger strata. Paleocurrent indicators from conglomerates throughout the Popotosa indicate that the alluvial systems transporting the gravels originated to the east, suggesting the presence of some eastern highland large enough to shed relatively coarse sediments up to 10 km into the basin. The "red bed" clasts further suggest an eastern source, as these are almost certainly from Permian strata, and no such strata are found to the west.

These observations are important as they suggest the LSPM area in the Miocene

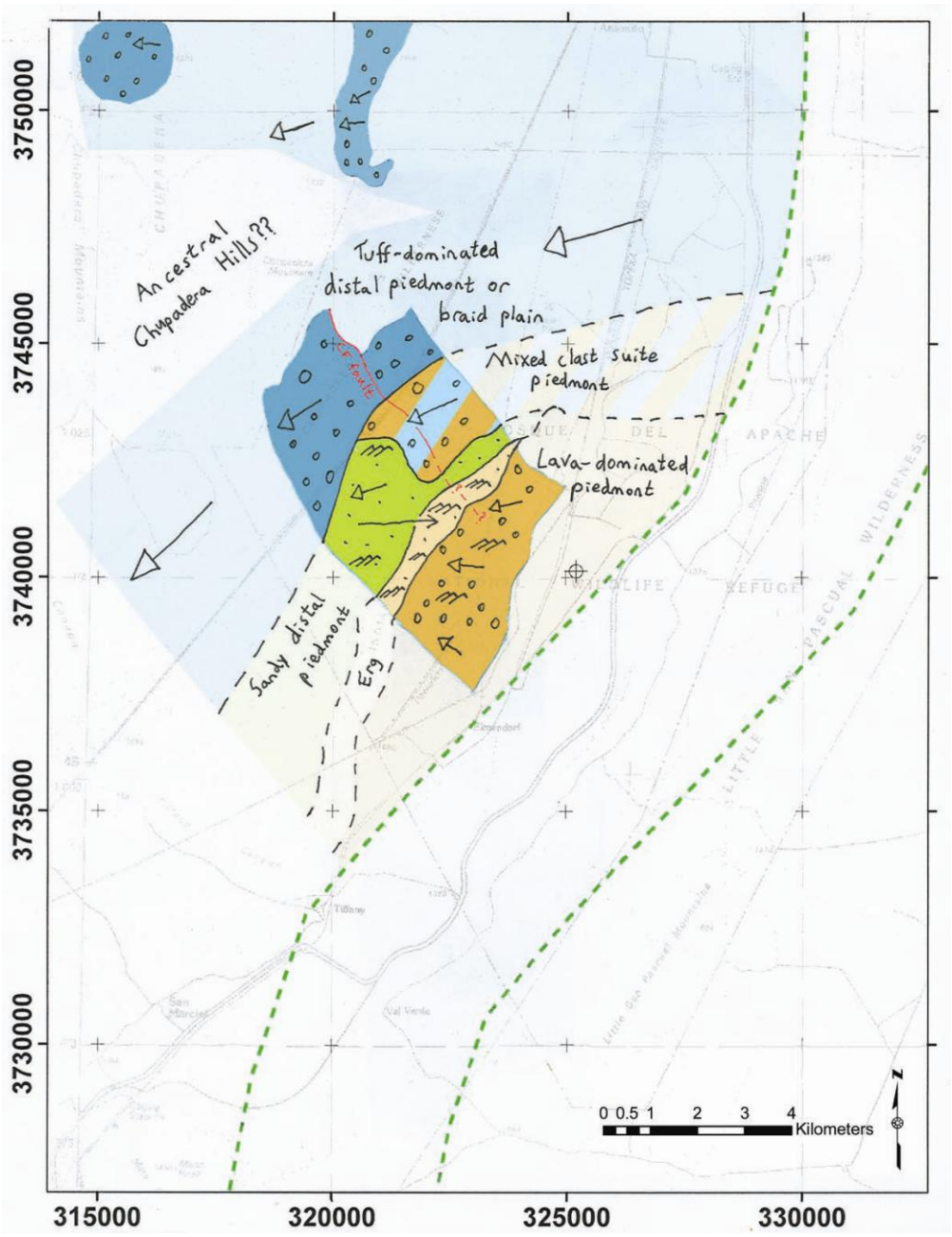

Figure 33 - Interpreted paleogeography for the study area and surroundings in later Popotosa time, between about 15 and 8 Ma. Key to symbols given in Figure 32b. Note that everything outside of the extent of well-exposed Popotosa is inferred and questionable. 5000-meter UTM NAD27 grid.

was a much more significant highland than it is today. LSPM today is a relatively small mountain, having both lower elevations and smaller lateral extent than both the Chupadera and Magdalena Mountains to the west. It is not the sort of mountain that could deliver coarse sediment 10 km across a basin. In order for its piedmont to dominate sedimentation in the area, the highland must have been significantly larger in Popotosa time. This interpretation is also suggested by the gravity data (Figure 6), which suggests a large, down-to-the-west basin-bounding fault lies at the base of LSPM. Such large, basin-bounding faults are generally found at the foot of large mountain blocks, suggesting that at some point the LSPM area may have been a significant footwall mountain block.

Deposits from early Popotosa time (Figure 32) are marked by a bouldery base that fines upwards to cobbles and pebbles. I suggest the pebbles and cobbles belong to the aforementioned ancestral LSPM piedmont, as paleocurrent indicators from throughout Tpt1 and Tpt2 indicate an eastern source. The boulders, however, could either be far-flung debris flows originating from the same eastern source or locally-derived detritus from nearby fault blocks. Local fault blocks probably did exist to supply sediment, as at least one fault in the area, the Chupadera Foothills (CF) fault, clearly was active during deposition as Tpt1 and Tpt2 both thicken across the fault. Although I cannot prove that the boulders were derived from these local blocks, it is my preferred hypothesis for their origin. Locally, these boulders are found mixed with moderately sorted pebbles, suggesting they were reworked by the alluvial streams from the east to become a part of the piedmont alluvium.

Stratigraphic changes in the early Popotosa deposits suggest the piedmont may have retreated through this time. From the bottom of Tpt1 to the top of Tpt2, sorting

improves, average grain size decreases, the abundance of sandstone beds increases, and the frequency of cross-bedding and paleochannels increases, all of which are suggestive of a progressive change from more proximal to more distal piedmont deposition. This suggests the piedmont retreated eastward through early Popotosa deposition. Possible reasons for retreat are discussed below under the "Piedmont replacement" heading.

Late Popotosa time paleogeography (Figure 33) is a much more complicated picture. Age constraints and the relationships between map units suggest most were deposited synchronously and interacted with each other. As noted under the "Clast count" heading in the "Provenance studies" section, the 11 to 9 Ma oreodont fossil (Morgan et al., 2009a) and the 8.57 Ma basalt of Broken Tank (Chamberlin et al., 2006) indicate that Tpa and Tpft1 deposited at about the same time. As Tpfi and Tpft2 are interpreted to be mixture facies of the Tpa and Tpft1 deposits, they, too, must have deposited at the same time. Also, lateral contacts are interpreted between Tps, Tpe, and Tpa, which suggests these three deposits are related and coeval as well. If these interpretations are true, then there existed a basin fill with an impressive range of characteristics during the late Miocene that accumulated in a complex depositional setting of interacting environments (Figure 33).

Above, under the "Clast counts" heading in the "Provenance studies" section, I suggested how Tpa, Tpft1, Tpfi, and Tpft2 may be genetically related. Each appears to come from the same eastern highland, which has two distinct source areas. The northern source area is dominated by rhyolitic tuffs, and the southern source by andesitic lavas. These source areas delivered the bulk of the sediment for map units Tpft1 and Tpa, respectively. Tpfi and Tpft2 geographically lie between Tpft1 and Tpa, and their mixed

clast suites are interpreted to result from mixing of sediment from the two source areas.

Furthermore, in the earlier section I illustrated two scenarios that could explain the juxtaposition of distinct source areas (Figure 28). Here I suggest the cause is exhumation of a buried volcanic complex (e.g., Figure 28b), which occurred in this late Popotosa time. Under the "Pre-Santa Fe Group" heading, above, I suggested that an andesitic volcanic complex may have existed to the southwest of the study area (Figure 31) that was buried by later ash-flow sheets. Ash-flows smooth topography, forming thick deposits in valleys and thin deposits on topography highs, such that above the volcanic complex would be thinner ignimbrite sheet than would be on the lowlands surrounding the complex. Thus, as streams incise into these volcanic deposits, the lavas would be exposed to erosion and transport in the south of the eastern highland source earlier that in the north (Figure 28b). This would explain the coeval lava-dominated southern piedmont deposits of Tpa and tuff-dominated northern piedmont deposits of Tpft1.

Two lines of evidence suggest the alluvial and eolian systems of map units Tpa, Tpe, and Tps were related and interacted. First, deposits of Tps interfinger with those of Tpe which interfinger with those of Tpa, suggesting the three depositional settings interacted with each other. Second, the paleocurrent indicators of Tpa and the paleowind indicators of Tpe indicate that stream flow down the Tpa piedmont was directed towards the dune field, while the dunes were blown toward the piedmont (Figure 33). Also, paleocurrent indicators from unit Tps suggest flow came from, or more likely across, the dune field. These observations further suggest the three environments strongly interacted.

I suggest the three may have formed a similar depositional setting to that seen in the Great Sand Dunes area of Colorado today. There, Langford (1989) observed that

west-heading streams from the Sangre de Cristo Mountains carrying coarse sediment dropped their coarse bedload upon entering the sand dunes and entrained sand. The streams continued through the dune field with this sand load, redepositing it on the lee side of the field as alluvium. Westerly winds then reworked this sandy alluvium into eolian dune deposits, effectively returning the sand to the dune field. These same eolian/alluvial interactions could have occurred in this study area during the late Miocene, as the paleocurrent observations from Tps and Tpa, paleowind data from Tpe, and geographic locations of the three units are all comparable to the Great Sand Dunes modern analogy. In this hypothesis, the rare, often channel-shaped conglomerate beds found in units Tps and Tpe could be the product of unusually strong flooding events that delivered coarse sediment into and through the dune field. This hypothesis is also consistent with the clast count and sandstone petrography data, which demonstrate that the clast suites of conglomerate beds and modal abundances of both alluvial and eolian sandstones all follow comparable stratigraphic trends, which should be expected if the three types of beds are linked by eolian/alluvial interactions reworking the same sediment.

Transitional paleogeography

Tuff-dominated gravels with southeastward paleocurrent directions overlying Popotosa strata with westward paleocurrents indicates a significant change in basin geometry sometime after the eruption of the basalt of Broken Tank (Figure 34). Unfortunately, exposures of strata from this time are rare, and no control exists for the

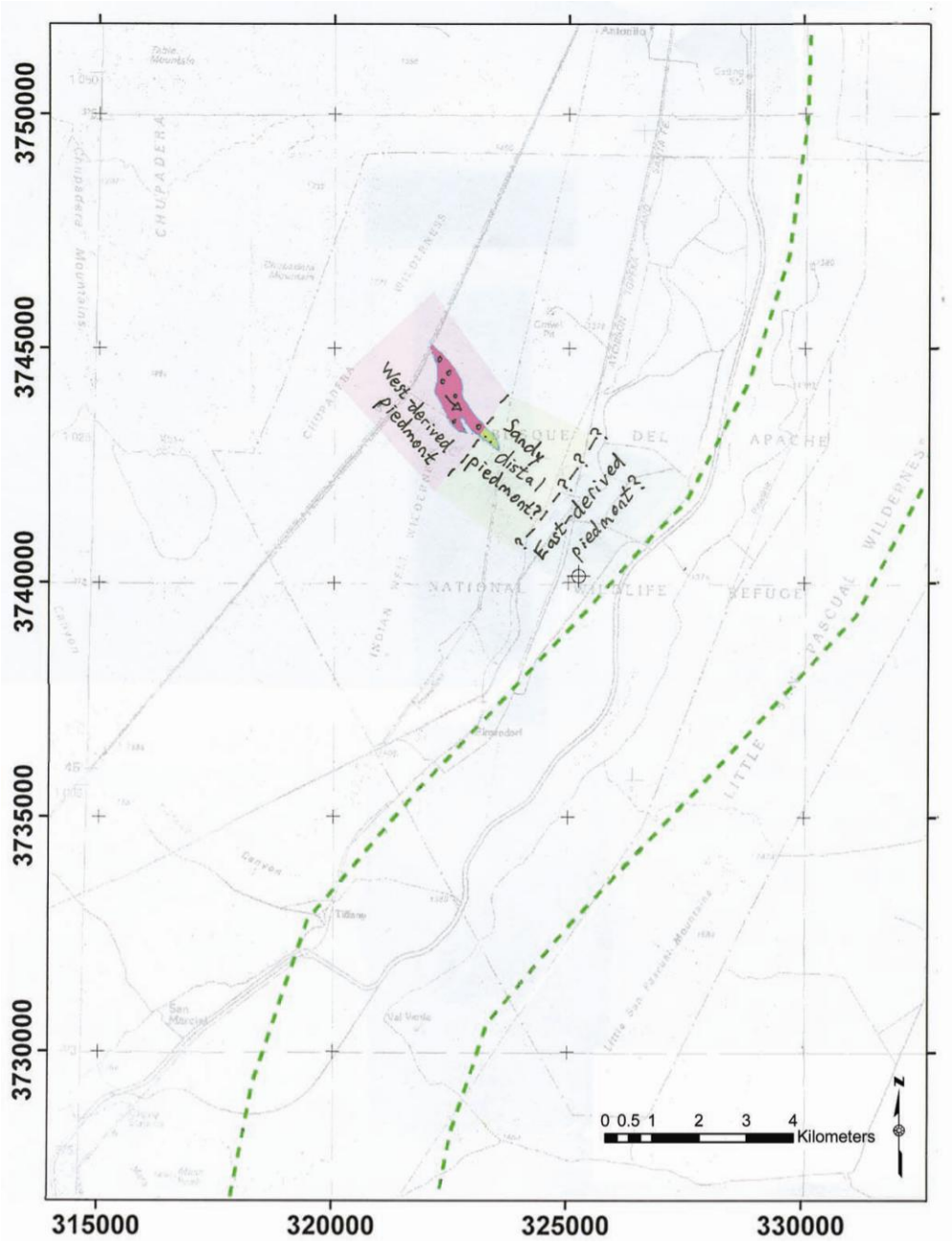

Figure 34 - Interpreted paleogeography for the study area and surroundings during the transitional period, between about 8 Ma and the time of the arrival of the ancestral Rio Grande between 4 and 7 Ma. Key to symbols given in Figure 32b. Note that everything outside of the extent of well-exposed deposits is inferred and questionable. 5000-meter UTM NAD27 grid.

geography away from the BDA fault. This discussion is thus resulting from examination of relatively few exposures.

Although progradation of the western piedmont could be the product of any of a number of causes (see "Piedmont replacement" section, below), the simplest explanation is continued retreat of the eastern piedmont. Since I could not find evidence of an ancestral Rio Grande during this time, nor could I attribute the southeast-transported transitional deposits to any local fault blocks, there is no reason to suggest any major change in basin geometry occurred to cause progradation of the western piedmont. I suggest that eastern-piedmont retreat and western-piedmont advance during the transitional period is the result of a combination of mountain front tectonism and degradation of the eastern highland, as discussed in the "Piedmont replacement" section, below.

Sierra Ladrones to present (paleo)geography

From Sierra Ladrones time to now, the depositional setting appears relatively constant (Figure 35). Piedmont deposits from the Chupadera Mountains travel eastward to southward to intertongue with a through-flowing axial stream that meandered as far west as about 3.5 km from the present-day floodplain. To the south of the area, where the Chupaderas terminate and the basin widens, a transitional distal fan/floodplain area developed. This pattern largely persists to today, albeit at a more entrenched level.

Piedmont replacement through Santa Fe Group time

One purpose of this study was to examine the shift from eastern piedmont-dominated to western piedmont-dominated deposition. Here, stratigraphic changes within

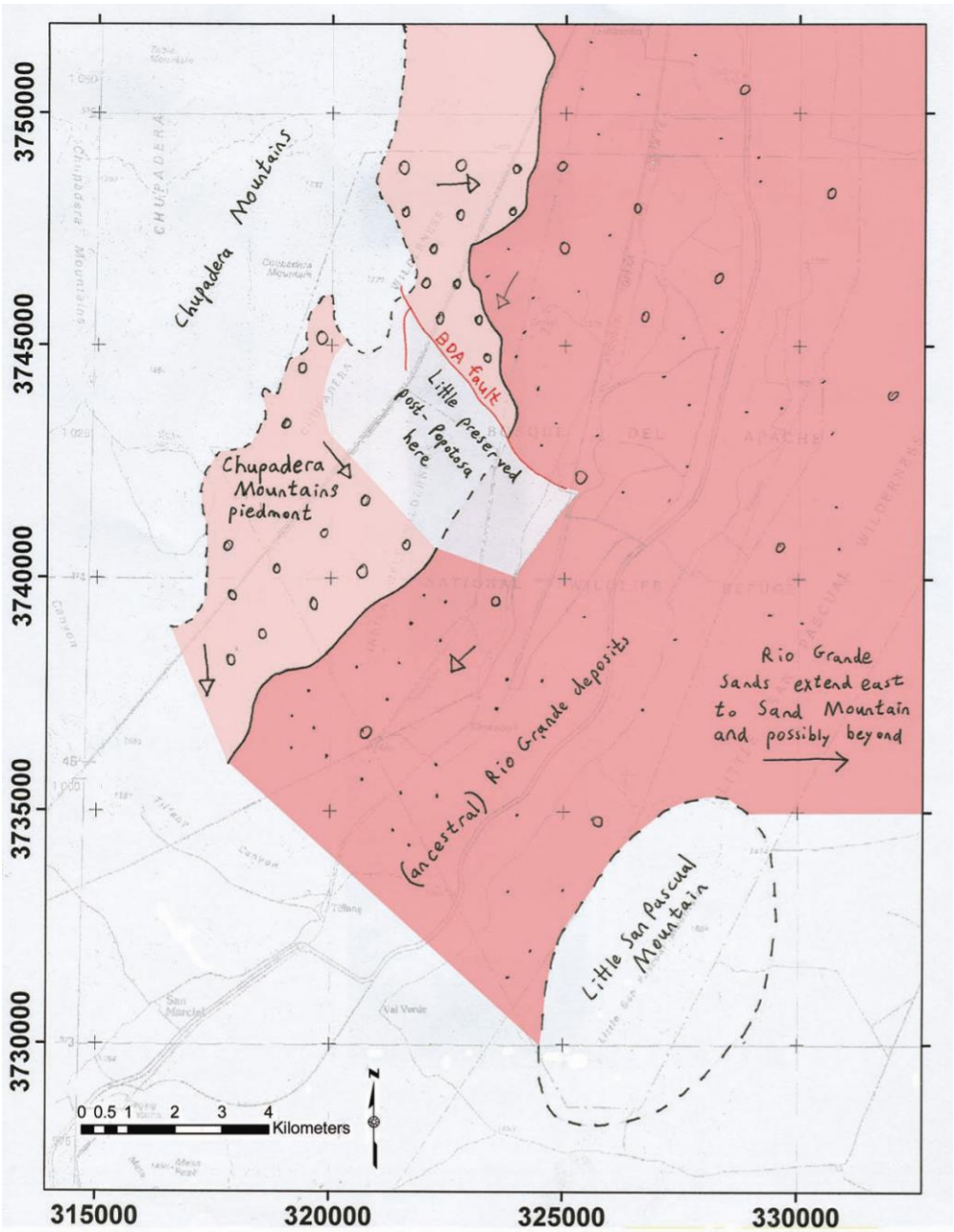

Figure 35 - Generalized paleogeography for Sierra Ladrones and post-Santa Fe Group times, beginning between 4 and 7 Ma. Note that piedmont deposits extend eastward into the area of ancestral Rio Grande deposits, and their eastern extent has not been documented. Eastern extent of ancestral Rio Grande deposits given by D.W. Love (pers. comm., 09/2009). Key to symbols is given in Figure 32b. 5000-meter UTM NAD27 grid.

and between map units are interpreted to narrow down the cause of this piedmont replacement.

Piedmont replacement could be the result of gradual, sudden, or oscillatory retreat of the eastern piedmont and advance of the western piedmont. An oscillatory shift, where the two piedmonts advance and retreat episodically but overall change from eastern- to western-domination, would result in intercalated west-transported and east-transported deposits; this is not observed anywhere in the field area, so if there was any episodic advance and retreat it is not at the right scale to be apparent. This scenario is therefore rejected.

A gradual shift is suggested by up-section changes in the Tpt_ units. From the bottom of Tpt1 to the top of Tpt2, sorting improves, the overall clast size decreases, and the abundance of sandstone beds increases, suggesting gradual retreat of the eastern piedmont during this time. This gradual retreat may have continued throughout Santa Fe deposition, resulting in the complete retreat of the eastern piedmont from the area and its replacement by an advancing western piedmont. A gradual shift is also suggested by the local south-directed clast imbrications in the area around the contact between Tpft1 and Tsp and in the upper Tpfi beds. These suggest that local paleocurrents in the area gradually changed from west-southwest- to southeast-directed, rather than 'jumping' suddenly from one orientation to the other. These local south-directed paleocurrents could reflect the axial zone between the two piedmonts, where a southwest-facing piedmont and a southeast-facing piedmont interacted to create a small south-directed axial stream. As the one piedmont retreated and the other advanced, this axial stream would traverse the area, leaving local southward paleocurrents at the contact between the two deposits.

Neither of these lines of evidence is indicative of a gradual piedmont replacement, however.

A sudden shift is suggested by the apparently irregular and unconformable nature of the Tsp basal contact. One would expect that any gradual change would result in conformable, relatively planar contacts, not result in erosive contacts with map-scale paleorelief and up to 10° of angular discrepancy. The nature of the contact is not indicative of a sudden shift, however, as the uplift and tilting of the Popotosa strata that resulted in the irregular and unconformable contact could have been gradual and concurrent with gradual advance of the western piedmont.

Piedmont replacement could have one or more of any number of physical causes; for example: 1) tectonic surface tilting-driven migration of facies, such as described by Blair and Bilodeau (1988; Figure 36); 2) degradation of the eastern highland causing retreat of the eastern piedmont; 3) exhumation of the Chupadera Mountain block, creating a source of gravels for the western piedmont that is close to the field area; 4) rise of the ancestral Magdalena Mountains to the west, causing advance of the western piedmont; and/or 5) local faulting influencing depositional environments. Note that none of these possibilities are exclusive, and that most only cause either eastern piedmont retreat or western piedmont advance, not both. In addition, different factors may have occurred together or separately at different times.

Tectonic surface tilting (Figure 36) is an attractive idea, as syndepositional fault block tilt is also suggested by apparent fanning of strata evident in the dip magnitudes to the southwest of the Solitude fault (fanning of strata is discussed in more detail in the "Structure" section, below). In addition, the radiometric age controls for the Popotosa,

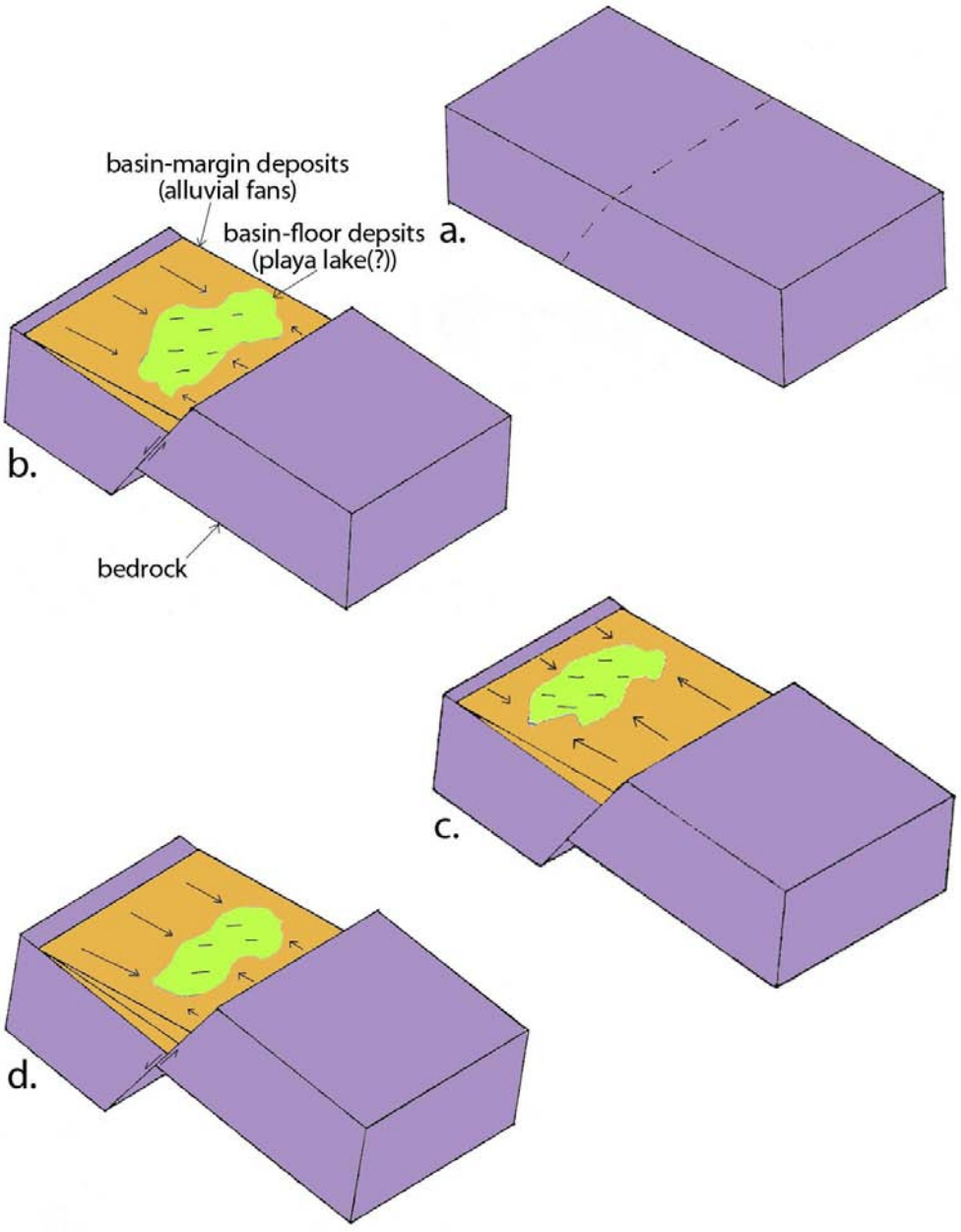

Figure 36 - Block diagrams depicting the lateral migration of sedimentary facies due to tectonic surface tilting in a half-graben, after Blair and Bilodeau (1988) and Cather et al. (1994a). Notice that the basin-floor deposits migrate closer to the master fault after slip events (blocks b and d), then migrate away from the fault during quiescence (block c).

specifically the 14.59 Ma age for the base of Tpt2 and the 8.57 Ma age on the basalt of Broken Tank toward the top of the section, constrain the timing of the bulk of deposition for the Popotosa to be during the 16 to 10 Ma surge in extension rate and tectonic activity described by Cather et al. (1994a) for the northern Socorro basin. Cather et al. suggested this surge was regional in extent, and therefore may have occurred in the Bosque basin area as well. Rapid extension would likely result in significant slip along the basin-bounding faults and possibly in major surface tilting as well. Thus, a tectonic surface tilting-driven hypothesis is a reasonable explanation for the retreat of the eastern piedmont as well as the advance of the western piedmont, at least during Popotosa time.

Unfortunately, footwall-ward migration of facies is only half of Blair and Bilodeau's (1988) model; the other half is later progradation of the footwall piedmont back into the basin after fault block tilting ceases (Figure 36c). As no progradational deposits from the east have been recognized in the area, the stratigraphy may not perfectly match the Blair and Bilodeau model. In addition, surface tilting is usually concurrent with rejuvenation of the footwall mountain block. Thus, if surface tilting is the primary cause of piedmont replacement throughout Santa Fe time, the footwall mountain block, in this case LSPM, should be a major highland. Today, LSPM is a relatively minor mountain block, being smaller both in terms of relief and lateral extent than the Magdalena and Chupadera Mountain ranges on the hanging wall side of the basin. This is not consistent with a hypothesis involving a long period of extension and fault block tilt.

These issues do not rule out the surface tilting hypothesis, however. First, the eastern piedmont may have in fact prograded into the area, as dictated by the Blair and

Bilodeau model, but the deposits could either have been removed by erosion or simply not recognized as a prograding piedmont. It is entirely possible, for example, that the Tpt_ map units represent the retreating phase but Tpa is a part of the prograding phase. Alternatively, the dune field of unit Tpe may have acted as a topographic barrier to eastern piedmont advance, preventing progradation. In addition, the footwall mountain block may have been much larger prior to the arrival of the ARG, the transport capacity of which may have contributed to unusually rapid degradation of the highland. Finally, surface tilting only requires that the hanging wall of the basin-bounding fault subsides; it does not require the footwall to concurrently uplift. Although it would be highly unusual for the hanging wall to subside without uplift of the footwall, it is a possibility, and would result in footwall-ward migration of basinal facies without rejuvenation of the footwall mountain block or later progradation of the footwall piedmont.

The second possible cause of retreat of the eastern piedmont, degradation of the ancestral LSPM highland, is also plausible as it is consistent with the present-day relatively diminutive stature of the eastern highland. No other datasets or lines of evidence exist to support this hypothesis, however. Thermochronologic data might be able to resolve periods of denudation in the history of LSPM, but I found no such dataset.

Exhumation of the Chupadera Mountain block as a cause of western piedmont progradation is also an attractive hypothesis due to timing. The youngest east-transported deposits in the area, which are presumably a part of the western piedmont, are those belonging to map unit Tsp. This unit is believed to stratigraphically lie just above the basalt of Broken Tank, placing an upper bound on the age of the unit at 8.5 Ma. Previous work in the mountains around the northern Socorro basin, meanwhile, suggests the

Chupadera-Socorro-Lemitar Mountain chain exhumed between 4 and 8 Ma (Chamberlin, 1982; Kelley et al., 1992), such that the timing would be appropriate for progradation of the western piedmont to be the result of exhumation of the Chupadera Mountains. However, work elsewhere in the rift suggests exhumation was the result of integration of a through-flowing ancestral Rio Grande (R.M. Chamberlin, pers. comm.), and since there is no evidence of an axial fluvial system during Tsp-time it is more likely that deposition of Tsp, and hence progradation of the western piedmont, predated exhumation. In addition, Tsp deposits lack any clasts definitely derived from the Chupaderas, precluding a direct connection between the deposits and the mountain range.

I did not found a way to evaluate the other two possibilities. Rise of the ancestral Magdalena Mountains may be preserved in thermochronologic data, but the work of Kelley et al. (1992) suggests the thermal history of these mountains is dominated by intrusive events, not the exhumational history. I also did not find any faults that I could attribute local depositional environments to.

My preferred hypothesis invokes both tectonic surface tilting and degradation of the ancestral LSPM highland as causes of gradual eastern piedmont retreat and concurrent western piedmont advance. These hypotheses best fit all the observations, including fanning of strata, timing of deposition, the stratigraphy, and the current topography. The lack of a progradational sequence capping the retreating deposit is, admittedly, an issue with invoking tectonism as a cause of eastern piedmont retreat, but I do not believe this issue disproves the hypothesis for the reasons outlined above.

STRUCTURE

The Socorro basin region has been subject to several phases of major structural development, starting with Precambrian continental accretion and continuing today with rifting. As Precambrian, late Paleozoic, and Cenozoic rocks are all present within the bounds of the field area, structures from throughout the history of the region are potentially present. In addition, each phase influences later phases, such that the Tertiary extensional features mapped in this study could be controlled in part by events throughout the area's history. Despite this, only the Laramide to present history is discussed below in any detail. Some features of nearby Precambrian outcrops are also described for later comparison to rift structure attitudes.

For more information on pre-Laramide structures and tectonism in the area and in New Mexico in general, the reader is referred to Karlstrom et al. (2004), Kues and Giles (2004), Beck (1993), and references therein.

Review of local structure

Precambrian

Kent (1982) mapped the Precambrian rocks of the central Chupadera Mountains exposed just northwest of the field area. Although she does not discuss the history of the area, her map does show the basement fabric that presumably underlies the study area.

Foliations vary from dominantly north-northwest-striking in the northwest of her area to mainly west-northwest-striking in the southeast, the corner closest to the basin-fill study area. Overall, foliations vary from north- to west-southwest-striking. In addition, the area is cut by east-northeast-striking carbonatite dikes.

Laramide, excluding volcanism

From approximately 80 to 36 Ma, northeast-southwest compression of the Laramide orogeny affected the area, producing the Sierra uplift of Eardley (1962) that encompassed the field area (Cather, 2004, 2009). Major structures in the area associated with this period include anticlinal folding of Little San Pascual Mountain (LSPM; Geddes, 1963) and the Hot Springs fault, which most likely co-locates with the present-day steep gravity gradient lying at the base of LSPM (Harrison and Cather, 2004). Erosion associated with uplift stripped the area down to late Paleozoic and Precambrian rocks (Eggleston, 1982; Cather, 2004).

Geddes (1963) mapped Pennsylvanian and Permian strata on LSPM, which are folded into a range-spanning anticline. The anticline strikes north-northeast, is concave westward, and plunges to the southwest. It is cut on both the north and south ends by northwest-striking normal faults. Numerous smaller northwest striking faults also cut the LSPM area. Geddes suggested the anticline to be Laramide in age and the northwest-striking faults to be reactivated joint sets from Laramide deformation, but did not have age controls for either structure. The only line of reasoning presented is that the folding is similar to Laramide structures seen in the Caballo, Fra Cristobal, Manzano, and Sandia Mountains and in the Joyita Hills.

Harrison and Cather (2004) proposed the steep gravity gradient along the west flank of LSPM (Figures 6) correlates with the Laramide Hot Springs fault system, exposed near Truth or Consequences. They make a case for a north-northeast-striking, dextral strike-slip fault system with approximately 26 km of offset spanning the distance from at least Deming in the southwest of the state to LSPM, and possibly further into the Mesa del Yeso area, northeast of Socorro. Such a fault system should be expected to fracture the area with strong north-northeast to northeast trends, and lesser northwest and north-northwest trends (e.g., Figure 4c in Harrison and Cather, 2004). In addition, in the vicinity of the field area the gravity gradient makes a right-lateral jog, which for a dextral strike-slip fault would result in a releasing bend. This releasing bend may have focused andesitic volcanism in the area (R.M. Chamberlin, pers. comm.).

Cenozoic volcanism

In central New Mexico, Cenozoic volcanism began in the middle Eocene with dominantly intermediate eruptions, but shifted to bimodal rhyolitic/basaltic volcanism with the change from tectonic compression to extension (Chapin et al., 2004b). Possibly belonging to the earlier intermediate period are a pile of andesitic porphyry lavas and breccias found in the southwestern corner of the study area (map unit Td). These appear to be the product of an Eocene(?) volcanic complex that may have been centered immediately southeast of the study area at a releasing bend in the trend of the Hot Springs fault (Figure 31). Not much is known about this complex, however, or the structures associated with it, not has any product of the complex yet been dated.

Included in the later bimodal phase of volcanism are a series of six Oligocene

calderas that engulfed the area north and northwest of the field area (Chapin et al., 2004a; Figure 2). The furthest east and oldest of these, the Socorro caldera, lay to the immediate northwest of the area, and has been well documented by Chamberlin (1980), Eggleston (1982), and particularly by Chamberlin et al. (2004). Eggleston (1982) mapped the southern caldera wall just north of Chupadera Peak, which in turn is just northwest of the study area; unfortunately, the same structure is eroded and buried where it crosses into the field area, but it may impart an east-northeast structural grain in the area, and possibly affect structures crossing it (cf. Osburn, 1979).

Previous work on rift structures in the area

Chamberlin (1980, 1983) proposed the crust near Socorro extends by progressive domino-style extension (cf. Morton and Black, 1975), and Cather et al. (1994a) suggest extension is episodic, with two major periods of tectonism. Thickness trends and angular unconformities primarily in the Oligocene volcanic pile of the Lemitar Mountains demonstrate concurrent syn-depositional faulting and fault block rotation, characteristic of "domino-style" extension, *sensu* Chamberlin (1978; Figure 12; see also Chamberlin, 1980, 1983, and Cather et al., 1994a). Here, initially high angle (60-70°) faults progressively rotated to lower dips, and, following approximately 30° of rotation, new faults developed that overprinted the initial faults. Continued extension flattened both initial and overprinting faults, and created new sets of faults to overprint both. The result is depicted diagrammatically on the right end of Figure 12 (from Morton and Black, 1975). Today, the initial fault set is locally subhorizontal (Chamberlin, 1983, 2004), and it follows from this model that the shallowest faults in an area should be the oldest faults.

It also follows from the domino-style model that the oldest strata have the steepest dips, and that relative extension rates are preserved in the rates of stratal dip change. In the northern Socorro basin, Cather et al. (1994a) used this logic to identify two periods of rapid extension (Figure 37), one in the late Oligocene (approximately 29 to 27 Ma) and another in the middle to late Miocene (16 to 10 Ma). Cather et al. also noted that while the later period apparently correlates to rapid extension throughout the RGR, the former period does not overlap with other well-dated early periods of rapid extension

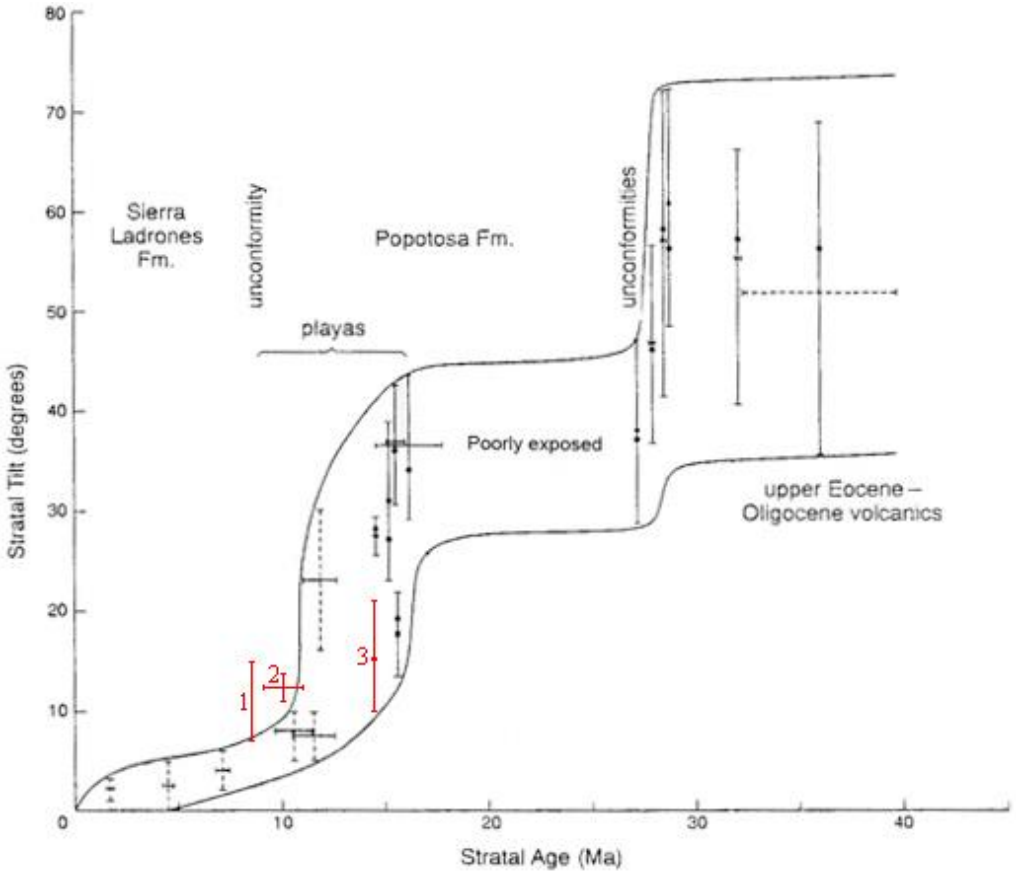

Figure 37 - Stratal tilt versus age graph of Cather et al. (1994) for strata in the northern Socorro basin. The two ages of rapidly changing tilt suggest two phases of rapid tectonism separated by relative quiescence. Red data points are additional data from this study: 1 – for beds around the 8.57 Ma basalt of Broken Tank; 2 – for beds around the 9 to 11 Ma oreodont fossil; and 3 – for beds at the base of Tpt2, from which 14.59 Ma sanidines were extracted.

documented in the rift. They suggest the early phase was localized by thermal heating associated with volcanism, while the later episode occurred throughout the rift. Finally, they note a change in fault spacing between the two phases, with the early phase characterized by narrow (2-5 km) spacing and the later by wide (5-15 km) spacing, which may be the result of progressive cooling of the crust changing its mechanical properties. Chamberlin (1983) suggests there may also be a third, youngest period of extension that is ongoing and overprints all earlier phases with largely unrotated, still-steep (60-70°) faults, such as those that presently bound the Socorro basin.

Quaternary fault scarps and active crustal magma bodies attest to continuing tectonic and magmatic activity to this day throughout the RGR but particularly in the Socorro area. Fault scarps in Quaternary sediments are found all along the RGR in New Mexico (Machette et al., 1998) though only a few have been studied in detail, and most appear to have long recurrence intervals. Most seismicity in the state results from small-magnitude earthquake swarms occurring in the Socorro to Bernardo area in the northernmost Socorro basin, generally attributed to activity of a crustal magma body underlying Socorro county (Sanford et al., 2002). The extent of this body is generally well constrained by seismic reflection studies, appearing to stretch from Ladron Peak in the north to the southern end of the field area (Figure 2). It is generally considered to be the youngest manifestation of the periodically volcanically active SAZ (Chapin et al., 2004b), with the most recent research suggesting a late Holocene age of emplacement (Fialko and Simons, 2001; Finnegan and Pritchard, 2009), though this is still under contention (cf., Love et al., 2009).

Rift structures of the IWW basin fill

All faults and folds in the Mogollon Group and basin fill mapped as a part of this study are attributed to mid-Tertiary to present east-west extension. The field area structure consists of northwest-striking normal faults, northwest-striking folds, and an apparent northeast-striking syncline that is likely the result of "fanning" of strata.

Faulting

Major northwest-striking faults exhibit both down-to-the-southwest and down-to-the-northeast slip senses, with neither sense being dominant. Rare lineations on fault surfaces suggest slight right-lateral obliquity, but mostly dip slip (rakes of 60 to 75°; Table 1). Displacements are almost everywhere poorly constrained, but cross-section reconstructions suggest they are mainly 100 to 200 meters, with two faults, the Chupadera Foothills (CF) and Bosque del Apache (BDA) faults, having over 300 meters of offset. Three faults appear to have variable displacements: the Hidden and Reversed faults have greater displacements to the northwest, and the CF fault has greater displacement down-section due to syndepositional slip (cf. Cross-sections B-B' and D-D'). Dip angles of faults range from 30° to nearly 90° (Table 1), and generally divide the faults into three groups: shallowly- to moderately-dipping down-to-the-southwest, steeply-dipping down-to-the-southwest, and moderately-dipping down-to-the-northeast.

The Chupadera Foothills (CF) fault is the main shallowly- to moderately-dipping down-to-the-southwest fault in the area, with about 50 to 700 meters of displacement, increasing down-section due to syndepositional slip. The fault is moderately dipping (50-60°) where juxtaposing the volcanic pile against Popotosa strata and shallowly (30-50°)

dipping in the center of the area where it splits into two strands. Southeast of there, exposure makes correlation difficult, but it is tentatively correlated with a moderately exposed, ~70° dipping fault. Thickening of strata across the fault is clearly expressed in map patterns in the lower Popotosa strata; Tpt1 and Tpt2 thicken by 100% and 33%, respectively. The Hidden fault, immediately northeast of the CF fault, also appears to be a shallowly- to moderately-dipping down-to-the-southwest fault, as evidenced by its sinuous map pattern. This fault may also have been syndepositional; Tpt2, the principal unit for determining strata thicknesses, is very poorly exposed in its footwall, and may easily be thinned. Also, cross-section reconstructions suggest offset on this fault increases to the northwest, or down-section, from about 140 to 200 m.

Steeply-dipping down-to-the-southwest faults are found in the far southwest of the area and in the immediate footwall of the BDA fault. The Burro fault in the far southwest is small (~25 m of displacement) and isolated. The faults near the BDA fault are intricately intertwined with moderately-dipping down-to-the-northeast faults, and are interpreted be conjugate faults forming horsts and graben with these other faults (see Cross-sections B-B' and D-D', Plate 2). Steep, down-to-the-southwest faults near the BDA fault may have offsets of about 130 to 200 meters, but these offsets are particularly poorly constrained as they rely on the thickness of the Tpf_ units, which are not known with certainty.

Moderately-dipping down-to-the-northeast faults are found throughout the field area, particularly in the immediate footwall of the BDA fault, which itself is one of these faults. They exhibit a wide range of offsets, from less than 10 m to possibly as much as 340 m. The largest offsets occur along the BDA fault and in its immediate footwall, in an

area of horst and graben structure (see Cross-sections B-B' and D-D', Plate 2). The BDA fault itself may have as much as 340 m of offset across it, as it juxtaposes Sierra Ladrones ARG facies deposits in its handing wall against upper Popotosa sandstones. Drilling near Socorro yielded a maximum thickness of 340 m for the ARG facies (R.M. Chamberlin, pers. comm. 04/2009), suggesting this much offset across the fault. This assumes, however, that the thickness of the ARG facies in the hanging wall of the BDA fault is comparable to the thickness by Socorro. This assumption is tenuous at best, such that 340 m is more of a maximum offset than an actual offset. The BDA fault also offsets the surface of a late Pleistocene piedmont deposit (Qvn3), indicating it remains active today. The seismic risk associated with this fault is discussed later.

The most notable exception to these three categories is a steeply-dipping apparent reverse fault located between the CF and BDA faults adjacent to the Chupadera Mountains, informally called the Reversed fault. This fault is interpreted to have originally been a down-to-the-northeast normal fault that rotated to a southwest-dipping apparent reverse fault. To test this interpretation, I considered the attitudes of the fault and of bedding planes on either side of the fault, then rotated them all about the same axis by the same degree in order to bring the bedding back to horizontal (Table 1). This confirmed the hypothesis by overturning the apparent reverse fault, returning it to its original, down-to-the-northeast normal geometry. This fault cannot be followed far as an apparent reverse fault, but I suggest it may correlate to a small-offset, down-to-the-northeast fault based on geographic location.

In addition to the northwest striking faults found in the basin fill itself, major north-northeast striking faults are also found in the nearby area. Eggleston (1982)

Table 1: Fault plane data, both original and rotated so as to bring nearby bedding back to horizontal

		Original fault plane data		Data location		H.W.[1]	F.W.[1]	Rotated fault plane data	
Fault name[2]	**Category[3]**	**Dip – Dip azimuth**	**Rake of lineations[4]**	**Easting (m)**	**Northing (m)**	**Dip – Dip azimuth**	**Dip – Dip azimuth**	**Dip – Dip azimuth**	**Rake of lineations[4]**
Burro	4	52 - 250	84 (L)	320627	3742673	11 - 127	14 - 095	62 - 255	77 (L)
Burro	4	69 - 244		320778	3742263	14 - 135	15 - 143	74 - 249	
Burro	4	77 - 254	76 (R)	321535	3741148	12 - 131	14 - 124	85 - 256	85 (R)
Burro	4	77 - 247		321773	3740599	07 - 114	10 - 131	82 - 248	
Burro	4	78 - 244	77.5 (L)	322380	3739195	05 - 146	10 - 146	80 - 246	73 (L)
Solitude	3	72 - 058		321293	3743105	17 - 053	21 - 081	54 - 056	
Solitude	3	43 - 068		321520	3742732	18 - 072	11 - 101	30 - 063	
Solitude	3	61 - 049		321640	3742573	25 - 084	11 - 101	51 - 029	
Solitude	3	44 - 074		321733	3742444	25 - 084	11 - 101	28 - 065	
Solitude	3	72 - 058		321919	3742168	30 - 101	16 - 112	58 - 049	
Solitude	3	61 - 034		322114	3741927	11 - 136	15 - 120	63 - 027	
CF faults	2	50 - 244	75 (R)	320825	3744348	29 - 084	51 - 122	82 - 255	85 (R)
CF faults	2	58 - 240		321471	3743447	23 - 059	22 - 119	76 - 245	
CF faults	2	57 - 255		321672	3742969	26 - 074	22 - 124	78 - 259	
CF faults	2	39 - 236		321889	3743069	22 - 124	34 - 045	62 - 244	
CF faults	2	55 - 211	61 (R)	321817	3743069	26 - 074	22 - 124	66 - 223	~90
CF faults	2	65 - 245		322932	3741561	06 - 020	05 - 355	68 - 243	
Hidden	2?	54 - 256		322017	3744032	33 - 094	30 - 113	83 - 262	
Hidden	2?	60 - 241		323395	3741541	15 - 065	13 - 051	74 - 241	
Reversed	5	81 - 251		321893	3744407	28 - 099	34 - 109	73 - 070	
Reversed	5	41 - 025		322625	3743164	07 - 050	19 - 059	31 - 013	
Reversed	5	63 - 024		322955	3742888	13 - 031	11 - 044	52 - 023	
Unnamed5	3	70 - 073		322173	3744074	34 - 080	23 - 110	45 - 067	

Table 1-continued

		Original fault plane data		Data location		H.W.[1]	F.W.[1]	Rotated fault plane data	
Fault name[2]	**Category[3]**	**Dip – Dip azimuth**	**Rake of lineations[4]**	**Easting (m)**	**Northing (m)**	**Dip – Dip azimuth**	**Fault name[2]**	**Category[3]**	**Dip – Dip azimuth**
Unnamed5	3	53 - 050		322997	3743142	03 - 175	10 - 040	49 - 050	
Unnamed5	3	55 - 036		323343	3742771	05 - 047	13 - 031	46 - 036	
Unnamed5	3	81 - 056		322832	3743392	02 - 082	03 - 175	81 - 056	
Unnamed5	3	50 - 049	63 (R)	323503	3742817	0 - 0	05 - 047	48 - 049	66 (R)
Unnamed5	4	82 - 299		323400	3743155	6 - 035	03 - 227	84 - 229	
Unnamed5	3	75 - 015		323538	3743112	8 - 067	03 - 277	74 - 014	
BDA fault	3	52 - 046		323303	3743646	0 - 0	18 - 064	44 - 043	
BDA fault	3	74 - 066		323605	3743212	0 - 0	22 - 045	64 - 068	

[1] – "H.W." – nearby hanging wall bedding attitude; "F.W." – nearby footwall bedding attitude

[2] – See Figure 7

[3] – Categories as defined in the text, plus Category 5, which refers to the apparent reverse fault

[4] – Rake here refers to the acute rake angle, regardless of obliquity. Obliquity is given by the letter in parentheses: L – left-lateral, R – right-lateral

[5] – Unnamed faults are all from the area of horst and graben structure in the immediate footwall of the BDA fault

mapped north-northeast striking faults with offsets of 600 to 2000 ft (180 to 610 m) in the southern Chupadera Mountains, to the immediate west of the field area. Eggleston also mapped northwest-striking faults in his study area, but offsets on these are limited to 150 to 400 ft (45 to 120 m). Geddes (1963) mapped a large offset down-to-the-west fault at the base of LSPM, which bounds the mountain's northwest flank, but he could not determine the magnitude of its offset. Gravity data by Keller (1983), however, suggest the fault is a major basin-bounding fault zone, as the fault lies on a steep, down-to-the-west gravity gradient (Figures 6). This fault is likely a reactivated strand of the Laramide Hot Springs fault zone of Harrison and Cather (2004).

Folding

Northwest-striking folds are broad, map-scale features found throughout the area of exposed Popotosa strata. Southwest of the Solitude fault, two anticlines and a syncline are found with about 0.5 to 1 km spacing between axes. These folds appear to diminish to the southeast, and could not be followed to the northwest due to very poor exposure of the basal Popotosa. In the area of the CF fault, a regional northwest-striking anticline separates primarily southeast-dipping Popotosa strata to the southwest from a northeast dipping domain to the east. Finally, by I-25, around the Hidden and Reversed faults, multiple axes are defined by map patterns and bedding attitudes, but are disrupted by faulting and masked by Quaternary sediments and difficult to follow over long distances.

Southwest of the Solitude fault, bedding attitudes steadily shallow to the southeast, or up-section. Dips decrease from about 20° at the mountain front to subhorizontal by NM-1, a distance of about 7 km. This is likely a result of "fanning" of

strata against the basin-bounding fault (Figure 38), but could also be a broad, inclined, northeast-striking syncline.

Interpretation of IWW basin fill rift structures

Although I lack the detailed structural data necessary to thoroughly examine the structures of the area, I present some hypotheses below that may explain the presence of four categories of normal faults in the general area, as well as the northwest-striking folds.

Faulting

Four categories of faults exist in the general area: 1) the large north-northeast-striking normal faults described by Geddes (1963) and Eggleston (1982) and defined by a

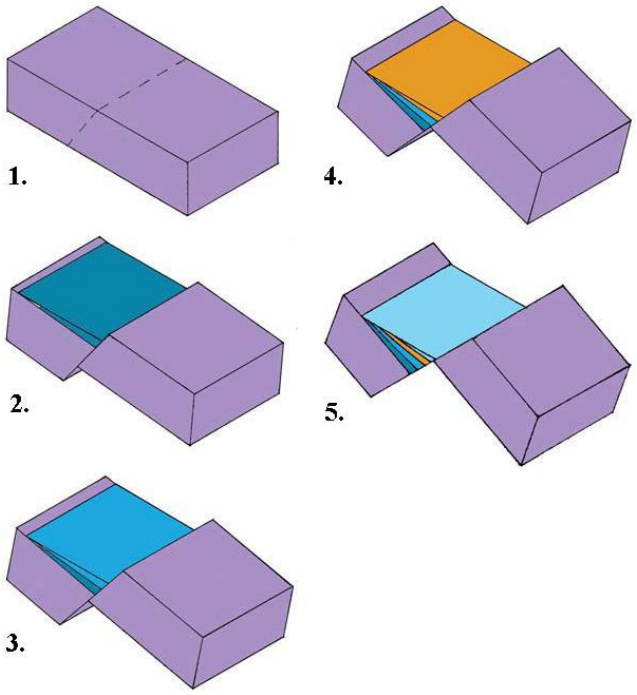

Figure 38 - Generalized block diagrams demonstrating how contemporaneous fault block rotation and deposition results in 'fanning' of stratal dips.

steep gravity gradient; 2) shallowly- to moderately-dipping, down-to-the-southwest normal faults; 3) moderately-dipping, down-to-the-northeast faults; and 4) steeply-dipping, down-to-the-southwest faults. The presence of four fault sets could be the result of one or more of 1) multiple phases of faulting; 2) reactivation of multiple planes of weakness in basement rocks; and 3) the "rift shoulder" effect. I suggest that all three contribute to the structural pattern of the area, as discussed below.

Multiple phases of faulting

Multiple phases of faulting could result in multiple fault orientations if each phase of faulting occurs under different stress conditions or under different thermal regimes. Evidence exists for multiple ages of faults in the field area in the form of fault attitudes. Assuming the area deforms by domino-style extension, as suggested by Chamberlin (1980) and Cather et al. (1994a), major faults should initially form with high dip angles of 60-70°, then progressively shallow as the faults slip and fault blocks rotate (Figure 12). In contrast, faults antithetic to the major basin-bounding faults form at high angles, then steepen and may even overturn to become apparent reverse faults. If new faults develop that overprint the older faults, they will have dips closer to 60°, as the older structures will have steepened or shallowed. Thus fault dips can define different ages of faults. A major complication in this field area is that the faults within the basin are oblique to those bounding the basin, such that the northwest-striking faults in the map area probably rotated about northeast-trending axes, and possibly about northwest-striking axes as well.

In order to study the effects of fault block rotation, I took my fault measurements and rotated them about axes and by magnitudes that would bring nearby bedding back to

horizontal (Table 1). Fault striae lineations were also similarly rotated. This process can yield the original attitude of rotated faults, provided the strata were originally horizontal when the fault formed. It can also reveal post-rotation faults, if the process yields anomalous primary dip magnitudes (i.e., dips less than 50°, or overturns a normal fault into a reverse fault). In general, down-to-the-southwest faults are steepened, while down-to-the-northeast faults shallow. Anomalously low dips measured on the CF fault are steepened to normal dip magnitudes (e.g., 39° becomes 62°), and an apparent reverse fault is overturned into a normal fault (i.e., the dip direction reverses). Moderately-dipping down-to-the-northeast faults and steeply-dipping down-to-the-southwest faults become even shallower and steeper, respectively, suggesting they may have formed after bedding rotation and be a part of a second generation of faults.

I suggest that the four fault types developed in two stages: first, concurrent slip along the northeast-trending, basin-bounding faults and dominantly down-to-the-southwest intrabasinal faults (categories 1 and 2, above), then slip along dominantly down-to-the-northeast intrabasinal faults and more minor down-to-the-southwest faults (categories 3 and 4), with or without slip along the basin-bounding faults (Figure 39). This chronology is suggested first by the apparently concurrent syndepositional slip along both the CF and basin-bounding faults, second by the seemingly conjugate nature of the moderately-dipping down-to-the-northeast faults and steeply-dipping down-to-the-southwest faults, and third by the effects of attitude rotations demonstrated in Table 1.

Syndepositional slip along the CF fault is indicated by the abrupt thickening of Tpt1 and Tpt2 as they cross the fault, while syndepositional slip along the basin-bounding

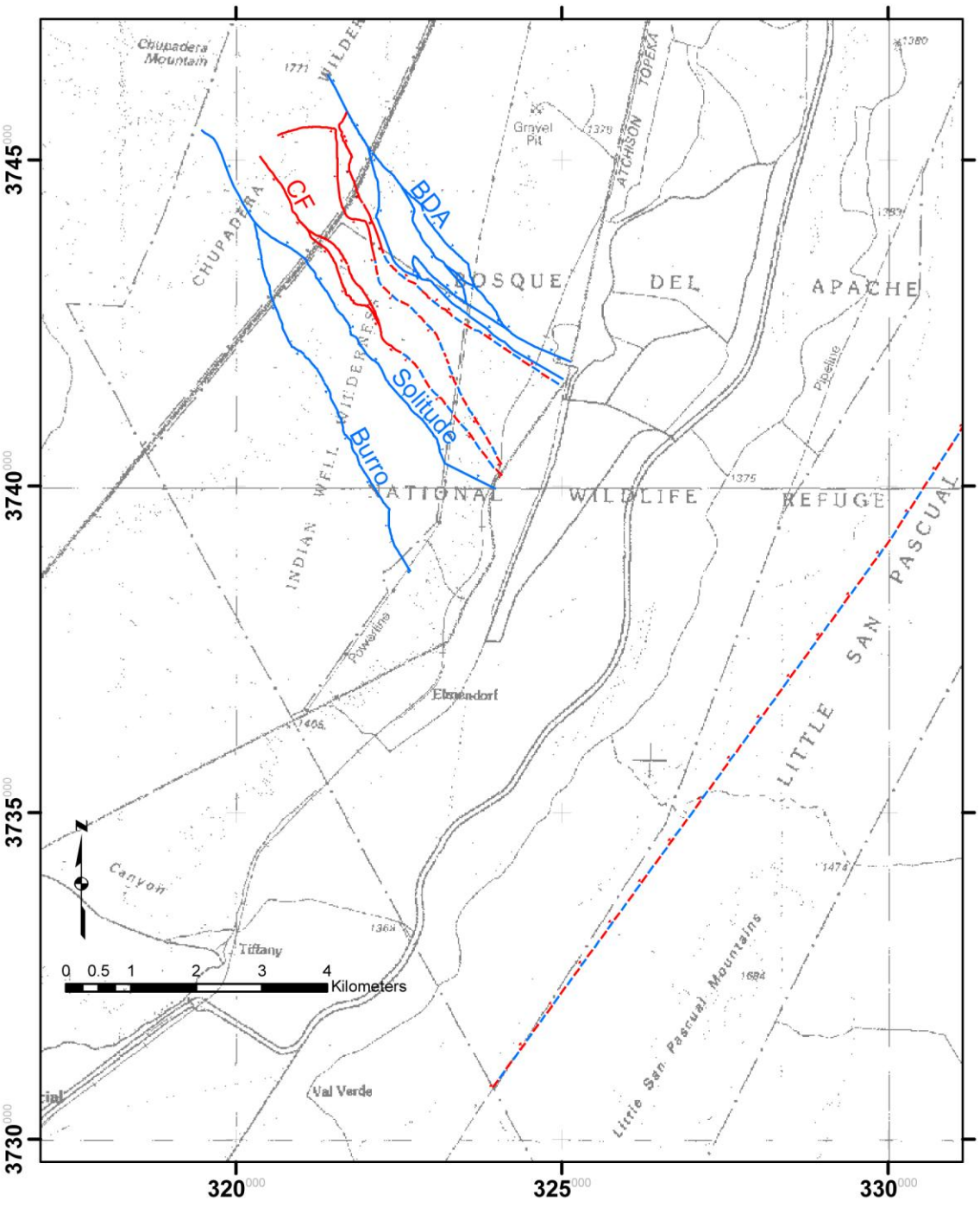

Figure 39 - Map of faults in the study area, with colors to distinguish their relative ages. Red faults belong to the earlier stage of faulting (categories 1 and 2; see text), while blue faults belong to the younger stage (categories 3 and 4). Red and blue dashed lines are fault segments that may belong to both stages. Some faults are named, as per Figure 7, for reference. 5000-meter UTM NAD27 grid.

fault is interpreted from the up-section shallowing of dips seen southwest of the Solitude fault, which is interpreted as fanning strata (cf. Figure 38). Thus the two fault sets must have been slipping together during early Popotosa deposition. This is further supported by fault and bedding attitudes and the results of fault attitude rotation (Table 1). The CF fault generally has shallow dips where the bedding is moderately dipping, and moderate dips where the bedding is shallowly dipping. This suggests the fault and bedding rotations are occurring progressively, syndepositionally, and synchronously; the oldest strata are offset by the oldest strands of the CF fault, and both are rotated more than younger strata and fault strands. Similarly, the apparent reverse fault is only overturned in the oldest strata, and is a down-to-the-northeast normal fault in younger strata. Rotation of these faults so as to bring nearby bedding to horizontal results in more typical dip magnitudes for both faults, suggesting slip occurred when bedding was still subhorizontal. On the other hand, offset along the CF fault diminishes up-section, and only minimal displacement is interpreted in the upper Popotosa, suggesting the fault slowed through time and may die up-section.

In contrast, no Popotosa-age syndepositional slip can be demonstrated along any category 3 or 4 fault, and at least one category 3 fault, the BDA fault, is still active today. In addition, these faults generally do not have anomalous dips, despite cutting strata that have been rotated by 15 to 20°, suggesting they post-date folding. In fact, rotation of these faults about axes that would bring nearby bedding back to horizontal (Table 1) would actually steepen the already steep down-to-the-southwest faults and shallow the less-steep down-to-the-northeast faults, the opposite effect one would expect if the faults

predated rotation. Thus, I suggest these categories of faults are a younger generation of faults superimposed on the older category 1 and 2 faults. I further suggest that the down-to-the-northeast faults are the dominant faults in the second generation, due to the size of the BDA fault and the possible top-to-the-southwest rotation of these younger faults. It is unclear whether or not any slip continued along the older faults at this time. The cause of the change from dominantly down-to-the-southwest to dominantly down-to-the-northeast faulting is unknown, but possibly related to heating and/or cooling of the crust changing its mechanical properties through time.

Reactivation of multiple weakness planes

As mentioned previously, the attitudes of older structures in the Socorro area can exert strong control on the attitudes of rift structures, and the diversity of pre-rift structural orientations could control the variety of fault attitudes. Nearby Precambrian rocks have dominantly north-northwest- to west-northwest-striking foliations (Kent, 1982), subparallel to the strikes of the intrabasinal faults mapped in the field area. Thus these weakness planes may underlie the northwest-striking intrabasinal faults. In contrast, the northeast-striking basin-bounding faults may follow Laramide-age weaknesses. Harrison and Cather (2004) attributed the steep gravity gradient at the base of LSPM to the Laramide Hot Springs fault, which likely reactivated as a normal fault during rifting. In addition, slip along the fault may have created a number of northeast-trending discontinuities in the crust that could also later become normal faults. Notice that neither of these attitudes is best oriented to accommodate the east-west extension (Chamberlin et al., 2007) imposed on the area. I suggest the multiple fault attitudes could have developed

so as to accommodate east-west extension while using poorly-oriented pre-existing weaknesses.

"Rift shoulder" effect

Finally, the multiple attitudes of faults could be the product of the location of the field area at a rigid "shoulder" in the RGR, where extension is being transferred southwestward from the Socorro basin to the San Marcial basin (Figures 1 and 40). East-west extension is best accommodated by series of north-trending basins, but "shoulders" occur where relatively cold and strong microplates and smaller lithospheric "stable

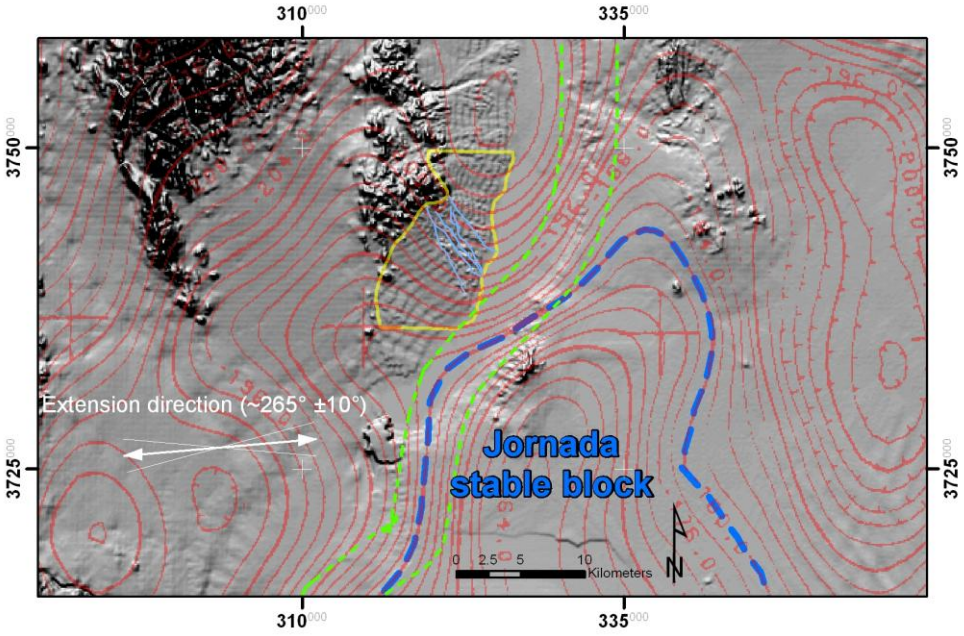

Figure 40 - Shaded relief map overlain by Bouger gravity contours from Keller (1983; red lines, interval of 2 mGal), the extent of the field area (yellow polygon), faults from the field area (light blue lines within the yellow polygon), and the approximate extent of the Jornada stable block (dark blue dashed line). The boundary of the stable block is arbitrarily placed on the -180 mGal contour; its exact location is unknown. The axes of extension of the Socorro and San Marcial basins are located by gravity lows to the north and west of the block. Dashed green lines approximately locate the steep gravity gradient that forms the eastern boundary of the Socorro and San Marcial basins. 25,000-meter UTM NAD27 grid.

blocks" (e.g., the Colorado Plateau microplate and Jornada stable block, Figure 1) obstruct this pattern. These microplates and stable blocks resist deformation and force extension to migrate around the block. One such example is the Jornada stable block, which here refers to the crust and lithospheric mantle beneath the Jornada del Muerto basin (Wilks, 2005) and parts of the surrounding highlands (Figures 1 and 40). This basin and the mountain ranges on its east and west generally constitute a broad north-trending syncline that largely resisted Cenozoic extensional deformation (Lozinsky, 1987; Reiter and Barroll, 1990), suggesting it is underlain by a block of relatively strong lithosphere, i.e. the Jornada stable block. This strong block lies to the southeast of the study area, and apparently forces extension to "jump" right-laterally between the Socorro and San Marcial basins. As defined here, the "Jornada stable block" is about 65 km wide (east-west), 65-75 km long, and perhaps 60-70 km thick, i.e. depth to top of asthenospheric mantle.

Detailed studies of similar synthetic accommodation zones (*sensu* Faulds and Varga, 1998) and "rift shoulders" in the Basin and Range and RGR provinces were conducted by Mack and Seager (1995) and Hudson et al. (1998), but neither described structural patterns similar to those in the study area. Mack and Seager examined accommodation zones in the southern RGR, including one overlapping synthetic accommodation zone linking two north-trending master faults across a right-lateral jump, similar to the field area (Figure 41). They found numerous northeast-striking faults in the zone, which they interpreted to result from local left-lateral shear causing local northwest-directed extension. They did not, however, observe any northwest-striking faulting or folding. Clearly, this is inconsistent with what is observed in this study area.

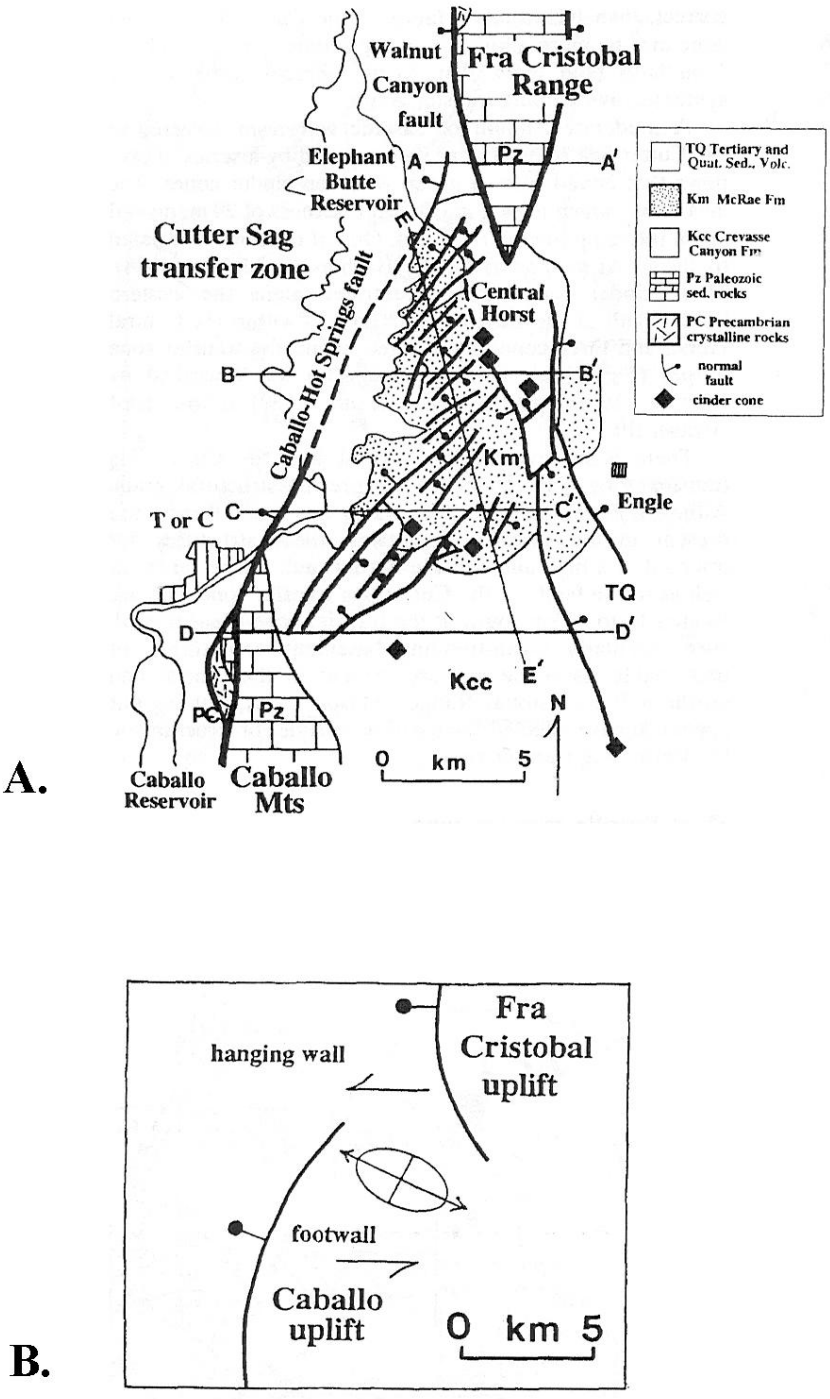

Figure 41 - A) Generalized geologic map for the overlapping synthetic accommodation zone described by Mack and Seager (1995). B) Model for the generation of NE-trending normal faults in the accommodation zone. Left-lateral shear is generated in the zone by contemporaneous westward motion of the hanging wall of the Fra Cristobal fault block and eastward motion of the footwall of the Caballo Mountains fault block.

Hudson et al. (1998) studied the Caliente-Enterprise transfer zone of southeastern Utah, which lies just west of a rigid shoulder in the Basin and Range formed by the northwestern corner ("rift shoulder") of the Colorado Plateau (Figure 42). They also interpreted left-lateral shear across their synthetic accommodation zone, but instead of northeast-trending normal faults they discovered a series of counterclockwise-rotating

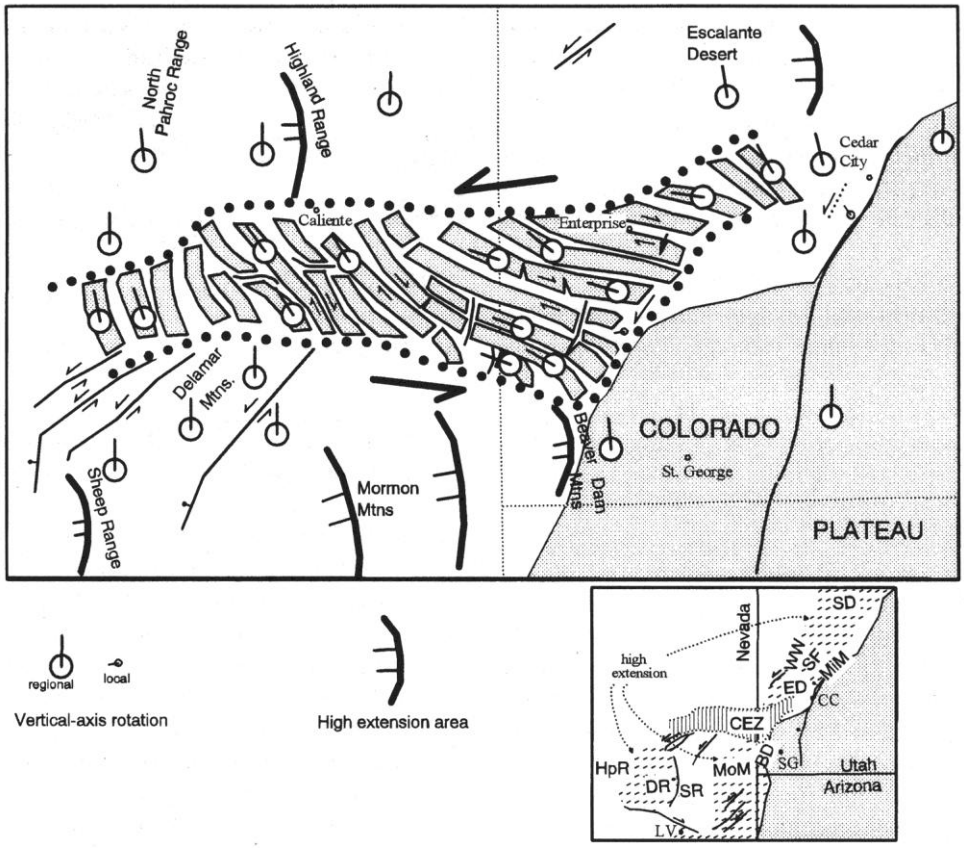

Figure 42 - Summary figure from Hudson et al. (1998), showing vertical axis rotations, derived from paleomagnetic data, of small fault blocks in a left laterally sheared transfer zone. Here the crust is being extended in an east-west direction, but the rigid Colorado Plateau has resisted extension, resulting in a heterogeneous distribution of strain. Close to the northwest corner of the Colorado Plateau, the crust to the north of the transfer zone is extended more than that to the south, resulting in left lateral strain across the zone. Abbreviations in smaller, regional figure: BD: Beaver Dam Mountains; CC: Cedar City; CEZ: Caliente-Enterprise zone; DR: Desert Range; ED: Escalante Desert; HpR: Halfpint Range; LV: Las Vegas; MiM: Mineral Mountains; MoM: Mormon Mountains; SD: Sevier Desert detachment; SF: San Francisco Mountains; SG: St. George; SR: Sheep Range; WW: Wah Wah Mountains.

fault blocks transferring strain. This is unlikely to be the case in the IWW study area, as striations in the area indicate almost purely dip-slip along major faults, in contrast to the oblique-slip necessary to cause vertical-axis rotations. Admittedly, it is possible that the dip-slip striations are the product of young movements that have obliterated previous oblique-slip striations, but without further evidence for vertical-axis rotations it is difficult to accept this hypothesis.

I suggest the principal reason the structural patterns of this area differs from those of Mack and Seager (1995) and Hudson et al. (1998) is the presence of extension-oblique weaknesses in the basement rocks exerting significant control on the style of deformation. In the two previous studies, the accommodation zones transferred strain between subparallel north-striking basin-bounding faults, which are perpendicular to the extension direction of those areas. In contrast, in the IWW area the basin-bounding faults, which have attitudes controlled by pre-rift structures, have northeasterly trends, oblique to the extension direction. Similarly, the fabric of the Precambrian rocks may be controlling the orientations of intrabasinal faults. The orientations of these basement weaknesses, I believe, result in a structural setting distinct from those of the other studies, and cause the observed fault pattern.

McClay et al. (2002) physically modeled the effect of having a rift "shoulder" using sandbox models. Their models controlled the location of extension by stretching rubber sheets at the bottom of the sandbox, and by placing several rubber sheets in a row with offsets between them that induced shoulders into their sandbox models (e.g., Figure 43a). These models were then stretched at an angle to the trend of the rubber sheets to cause oblique rifting.

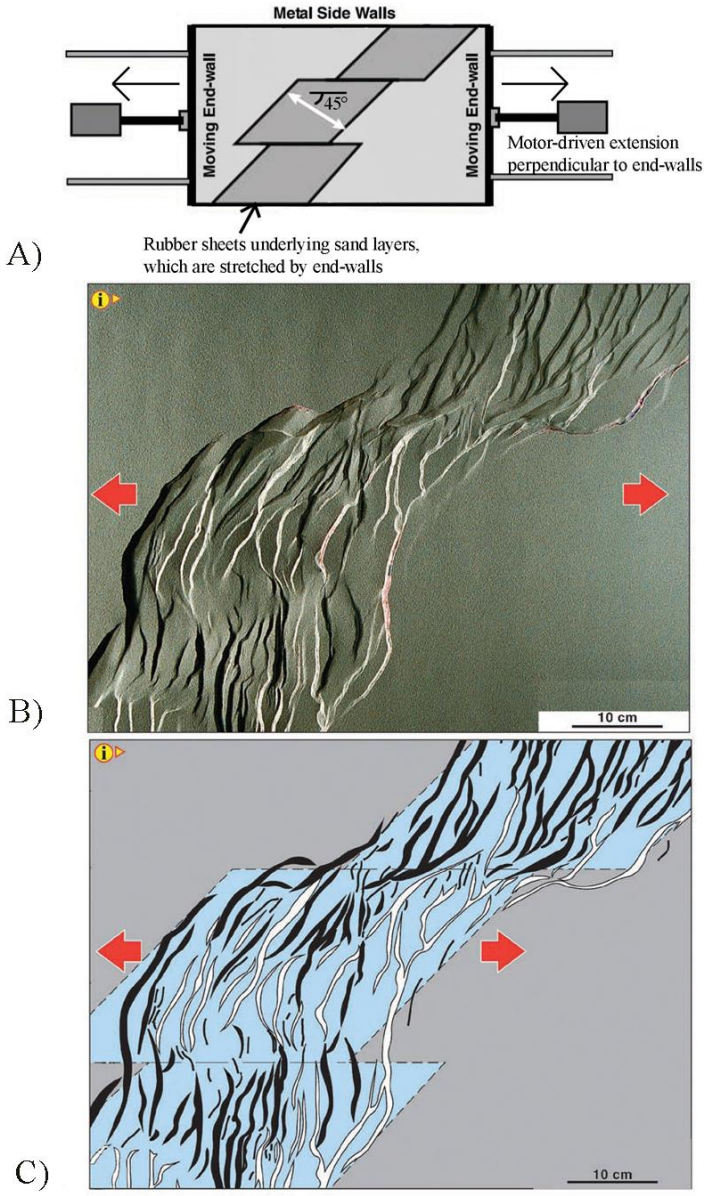

Figure 43 - a) One of McClay et al.'s (2002) experimental set-ups in plan view. The geometry of the rift is controlled at the base by the location of rubber sheets placed between two pieces of aluminum that are pulled both left and right by motors attached to the end-walls. Offsets between the rubber sheets create rift "shoulders." b and c) Results of the experiment depicted in 43a. Extension direction indicated by arrows, and the illumination direction is given by the "i" and arrow. b) Plan view picture of the top of the layered sediment extended during the experiment. Dark scarps are down-to-the-right normal faults, light scarps are down-to-the-left faults. c) Schematic drawing of the results of the experiment. Blue polygons locate the rubber sheets below the layered sediments. Black stringers are down-to-the-right faults scarps, white stringers are down-to-the-left scarps.

Figure 43b shows the results of McClay et al.'s sixth experiment, which had a right-lateral offset at one end similar to the offset observed in the study area, and produced comparable deformation. Notice in Figure 43b that faults at the far north end of the experiment are north-northeast-trending, paralleling the underlying rubber sheet margins, but that these same faults curve sharply to northeast- and even east-northeast-trends when crossing the offset. A similar situation may be occurring in this study area, but with northwest-trending structures that curve sharply into the northeast-trending basin-bounding fault zone.

Folding and stratal rotations

Three categories of folds or stratal rotations are found in the map area: broad northwest-striking anticlines and synclines, down-to-the-southeast tilting, and down-to-the-northeast tilting. Their causes are not known, but likely causes are discussed below.

Janecke et al. (1998) list known mechanisms for folding in extensional regimes, most of which could be acting in this field area. Their complete list (Figure 44) includes extension-perpendicular compressional folding, fault-drag folding, isostatic folding, longitudinal and transverse fault-bend folding, fault-propagation folding, and displacement-gradient folding. The first two are not expected to be significant in this study area. Extension-perpendicular compression is probably not a factor as the mutually perpendicular normal faults found in the area indicate extension is occurring along both northeastward and northwestward trends. Fault-drag folding, though definitely occurring in the study area, is also probably not a cause of map-scale folding, as the length scale of

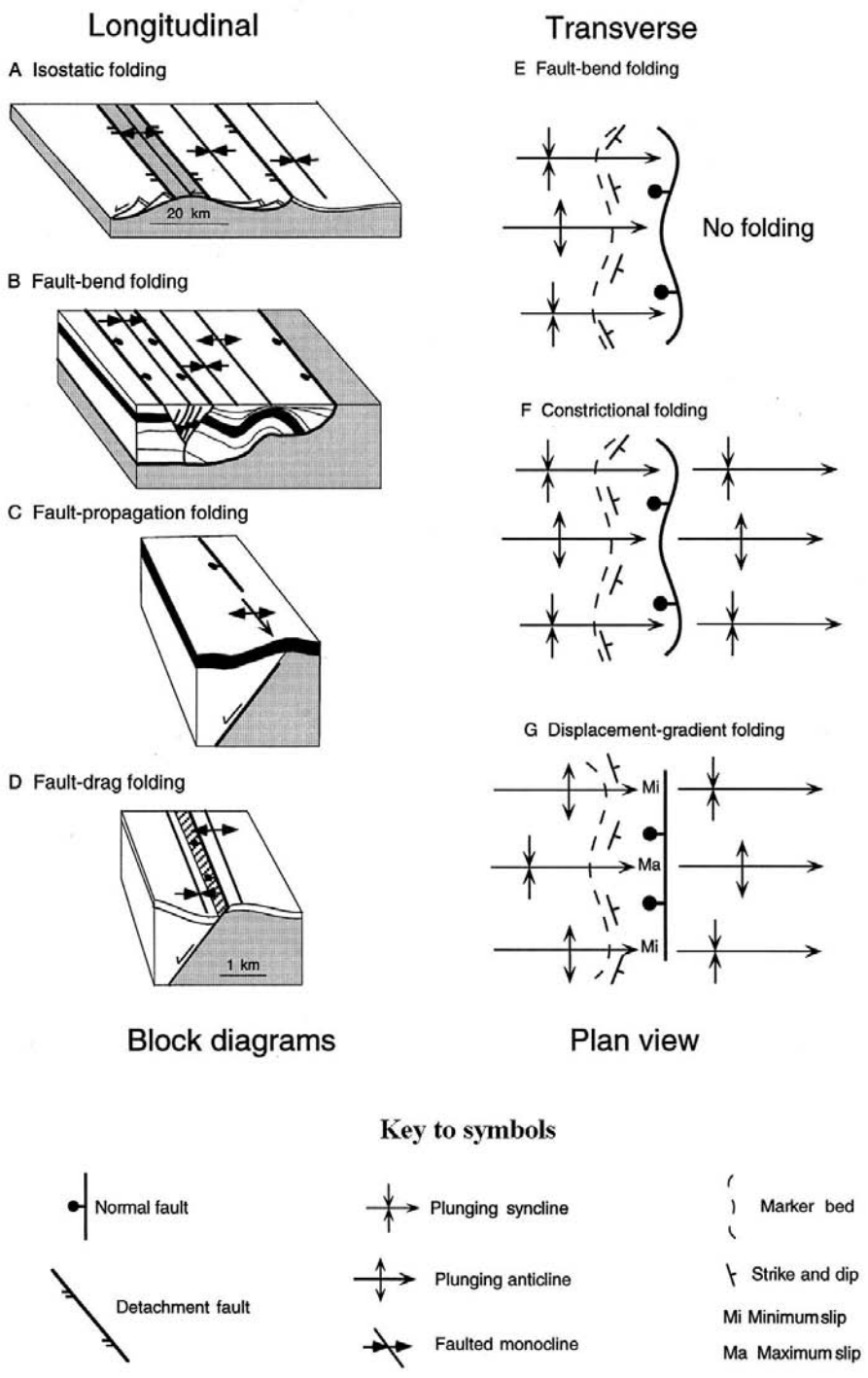

Figure 44 - Summary diagram from Janecke et al. (1998) demonstrating the most common mechanisms for generating both longitudinal and transverse folds in extensional settings. Note than all scenarios are simplified by removing subsidiary synthetic and antithetic faults.

such folding is small relative to the map scale (R.M. Chamberlin, pers. comm.). Any of the other five could be a cause of or factor in the folding seen in the study area.

I suggest the broad northwest-striking anticlines and synclines found southwest of the Solitude fault are either fault-propagation folds or fault-bend folds related to the CF fault (*sensu* Janecke et al., 1998; see Figure 44). Fault-propagation folding is reasonable given that the folds parallel the northwest-striking faults in the basin, and given that the folded strata are relatively weak and ductile compared to the underlying volcanic basement. Alternatively, the anticlines and synclines may be the product of ramp-flat geometry of the CF fault. The anticline nearest this fault appears to be a product of flattening of the fault at depth, as measured bedding attitudes approaching the fault gradually rotate into the fault (e.g., west side of Cross-section B-B'). Whether or not the other two folds are related to the geometry of the CF fault, however, cannot be determined.

I suggest the northeast-striking apparent inclined syncline southwest of the Solitude fault is the product of syndepositional southeastward rotation of strata. Figure 38 and Cross-section A-A' (Plate 2) illustrate this hypothesis. Strata are initially deposited horizontal, then progressively rotated down-to-the-southeast by fault block rotation, concurrent with more deposition. The result is the stratal dips increase in magnitude with age, forming an apparent inclined syncline in the map pattern of bedding attitudes. Alternatively, the pattern could be a fault-bend or fault-propagation fold. I do not believe this is the case, however, as the area lacks any other northeast-trending structures, which should be present if the apparent syncline is the product of one of these mechanisms.

I do not have a good explanation for the down-to-the-northeast rotations found

northeast of the Solitude fault, but suggest they may be caused by fault block rotation or fault-bend folding related to a buried fault to the northeast of the BDA fault. Alternative explanations are fault-propagation folding, or some form of displacement-gradient folding (all terms after Janecke et al., 1998; see Figure 44). My main difficulty in interpreting these rotations is the magnitude and extent of rotation. About a third of the exposed Popotosa in the area has northeastward to east-northeastward dips, suggesting a large, regional cause of stratal rotation. In addition, some of the steepest dips in the area are associated with east-northeast- or northeast-dipping strata. Dip magnitudes appear to shallow up-section, but this trend is not continuous nor well-developed throughout the area. To the northwest, the northeast-dipping strata bend synclinally back to southeast dips. Possible explanations for the northeast dips are: displacement-gradient folding, where greater slip along the basin-bounding fault to the northeast of the study area causes northeastward rotation of strata; transverse fault-bend folding, where bends in the basin-bounding fault causes rotation; and longitudinal fault-bend folding or stratal rotation caused by slip along one or more down-to-the-southwest faults. The Hidden fault is one such down-to-the-southwest faults that may contribute to the last model, and other faults may be hidden beneath the upper Santa Fe and Quaternary deposits in the hanging wall of the BDA fault. I prefer the last hypothesis, as fault-bend folding appears to cause eastward dips elsewhere in the field area (i.e., immediately adjacent to the CF fault by the Chupadera Mountains).

Flexural uplift in the footwall of the Bosque del Apache fault

The study area is unusual for the Socorro basin area in that it contains exposures of Popotosa strata along the west side of the Rio Grande extending the entire length of the western piedmont from the floodplain to the Chupadera Mountain front; most other exposures of Miocene basin fill in the area are restricted to the western highlands themselves or very near to the mountains (Figure 4). Popotosa strata crop out along a northwest-trending swath, clearly bounded on the northeast by the BDA fault but with an indistinct southwestern boundary. To the southwest, away from the Burro fault, Popotosa exposures become rarer and occur progressively lower in arroyo cuts. This pattern suggests the upper bound of the Popotosa dips to the southwest, diving into the subsurface to remove the Popotosa from the surface. This further suggests that the area may be rotated down-to-the-southwest by uplift along the BDA fault.

To test this hypothesis, I constructed a vertically exaggerated version of Cross-section C-C' (on Plate 2) in order to look for southwestward rotation of strata. On this section, the upper contact of the Popotosa with overlying ARG sediments dips approximately 5° southwestward, corresponding to about 0.5° of dip at true scale. Although this small dip could result from error in the location of contacts, it fits with a number of exposures of the contact and provides a good explanation for the disappearance of Popotosa strata to the southwest; therefore, I believe this 0.5° dip to be real. In contrast, the present-day average slope of the Rio Grande channel in this area is about 0.04° (Mussetter Engineering, 2002). Assuming the paleoslope of the ARG was

comparable to this value, this suggests some southwestward rotation of the area since the deposition of the ARG deposits directly overlying the Popotosa strata. Given the location of the field area at the south end of the Socorro magma body (Figure 2), southwestward location may be related to uplift of the crust due to inflation of the magma body. This is highly speculative, however, given the uncertainty in the magnitude, timing, and even presence of surface uplift associated with the body (see Love et al., 2009, for a summary).

The combination of these observations suggests the main process controlling exposure of Miocene basin fill on the BDA NWR is flexural uplift of the area resulting from slip along the BDA fault. Rotational uplift of the footwall block of the fault could cause southwestward rotation of the area, as well as result in exhumation of the Miocene basin fill.

APPLIED GEOLOGY

Resource potential

The field area is a potential site of groundwater, geothermal, and aggregate resources. Ancestral Rio Grande deposits, found north of the BDA fault, are known to form excellent aquifers for the region all along the Rio Grande. Unfortunately, these deposits are absent in the immediate footwall of the fault, and only return to the subsurface in the south of the area (see Cross-section C-C', Plate 2). Fortunately, both sandstone units of the Popotosa have the potential to be excellent aquifers, particularly the eolian sandstones. To my knowledge, however, neither has been explored as a groundwater resource.

A warm water well on the BDA NWR on the floodplain on the east edge of the IWW quadrangle lies just north of the projected trend of the BDA fault (Figure 45), suggesting a relationship between the shallow warm waters and the fault. Given that the fault juxtaposes highly permeable ancestral Rio Grande deposits against older, less permeable Popotosa beds, it is reasonable to believe that the fault is responsible for upwelling of deep, warm groundwater, causing the hydrothermal anomaly. Such a scenario was suggested by Barroll and Reiter (1995), who studied the temperature and chemistry of wells on the BDA NWR, but did not study the local geology and did not know about the BDA fault. Although the BDA NWR sometimes utilizes the warm water

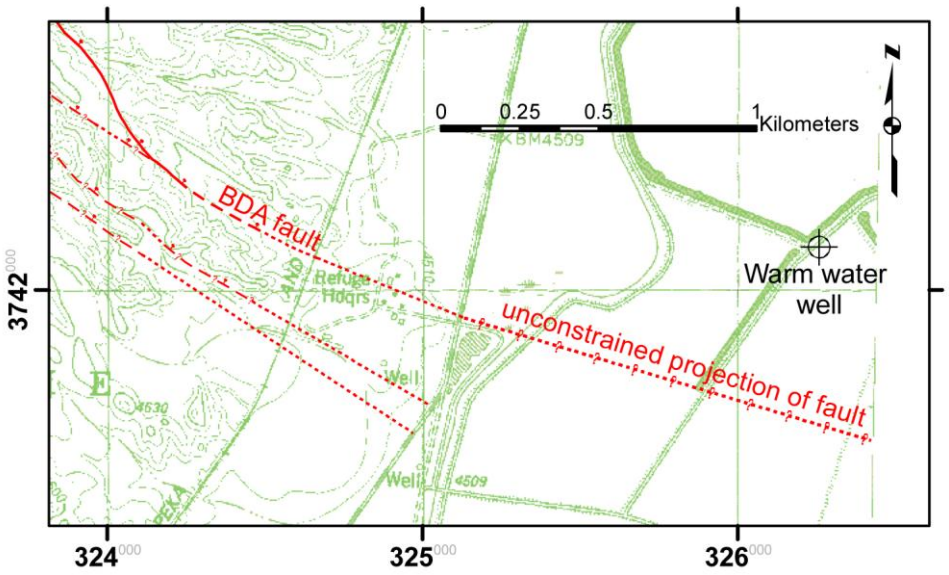

Figure 45 - Green-line topographic map of the IWW quadrangle with the BDA and nearby faults, as well as the location of a well that delivers 33°C water from 252 ft (76.8 m), which is unusually warm for the area (Barroll and Reiter, 1995). 1000-meter UTM NAD27 grid.

during winter, no exploration of the resource has been attempted.

Finally, Sierra Ladrones and younger deposits are potential sources of aggregate for construction. In fact, numerous small gravel pits all along the east end of the field area north of the BDA fault attest to previous aggregate mining, most likely during construction of the railroad and I-25.

Seismic risk

At least two faults on the quadrangle are associated with fault scarps in Quaternary piedmont deposits, indicating they are likely still active today. One fault scarp is laterally restricted, occurring adjacent to the mountain front in a Qvn3 deposit near 321600 m east, 3745400 m north. It has not been studied in detail. The other is associated with the BDA fault, and was trenched by the BDA NWR and examined by Cikoski

(unpublished data). Cikoski found three soil profiles in the colluvial wedge of the fault scarp, suggesting at least two surface-rupturing (magnitude 6 or greater) events since development of the surface. Regional mapping and soil development on the footwall side of the piedmont deposit, meanwhile, suggests the surface correlates to one dated by Phillips et al. (2003) at 122 ± 18 ka. Preliminary observations therefore indicate the BDA fault has produced at least two magnitude 6 or greater earthquakes in the past 120,000 years. Although the immediate area is sparsely populated, the BDA fault projects directly beneath the BDA NWR headquarters compound, and a large earthquake on the fault could cause serious damage to the buildings located there.

SUMMARY

Eocene to present geologic history

Initially, the area lay on a Laramide highland, which erosion stripped down to Paleozoic and Precambrian rocks (Eggleston, 1982; Cather, 2004). Andesitic volcanism then constructed large volcanoes on the erosion surface, and they and the volcaniclastic sediments derived from them buried the area (Cather, 1990). I propose that one such large andesitic volcanic center lay southeast of the IWW quadrangle (Figure 31), which later became a major source of sediment for the Bosque basin fill.

From 32.3 Ma to 24.5 Ma, a series of calderas erupted to the northwest through west of the field area, heating the upper crust and blanketing the area in rhyolite tuffs (Chapin et al, 2004a). These ash flows created an ignimbrite plateau that likely buried the andesitic volcanic highland to the southeast. Extensional faulting began shortly after eruption of the La Jencia tuff (Chamberlin, 1983) at 28.9 Ma, initially by reactivating Laramide contractional or transform faults as normal faults. This most likely includes the Hot Springs fault of Harrison and Cather (2004) to the southeast of the field area. Unfortunately, no sediments are exposed in the study area from this period of extension.

The sedimentary record of the rift begins in the mid-Miocene with deposition of an extensive piedmont with some bouldery material derived from local fault blocks (Figures 32 and 46a). This piedmont was initially dominated by rhyolite tuff clasts,

derived from an extensive ignimbrite plateau, but as the plateau degraded an older andesitic volcanic complex was exhumed, and a dual-sourced piedmont developed (Figures 33 and 46b). The northern source continued to deliver dominantly rhyolite tuff clasts but the southern source produced andesite lava clasts. Both sources also eventually delivered Permian limestone and "red bed" (including Abo Formation) clasts, rocks which are not found to the west of the field area. Streams emanating from the southern source area interacted with an erg at the toe of the piedmont, creating a dynamic eolian/alluvial boundary that likely migrated with fluctuations in climate. At this point, circa 10 Ma, the Chupadera Mountains were mostly or completely buried.

Sedimentation occurred concurrently with slip along both the northeast-trending basin-bounding fault and along northwest-striking intrabasinal faults (Figure 46c). Slip

Figure 46 (next page) - Block diagrams schematically summarizing the geologic evolution of the area. Fault planes are colored red, and the other colors correspond to those used in the geologic map. A key to the symbols used is given in Figure 33b. Attitudes and locations of geologic features are all approximated. a) A simple starting point. Leftmost dashed line will be the basin-bounding fault, while the rightmost dashed line will be the Chupadera fault of Chamberlin et al. (2002, 2004), which is the down-to-the-west fault that bounds the volcanics of the Chupadera Mountains on the west side. For clarity, in all other blocks only the middle portion of the block diagram between the two faults is shown. b) Early Popotosa time (~16 to 15 Ma), when rhyolite tuff dominated the clast suite throughout the area and local fault block-derived boulders mixed with the eastern piedmont gravels. c) Later Popotosa time (~15 to 8 Ma), when a dual-source piedmont existed that interacted with an extensive dune field. Notice that the western margin of the basin fill on-laps the ancestral Chupadera Mountain highland, nearly or possibly completely burying the highland. d) Transitional time (between ~8 Ma and the time of arrival of the ancestral Rio Grande), when the western piedmont prograded into the area, displacing the eastern piedmont. The clast suite of the transitional deposit suggests Popotosa beds are a part of the source area, suggesting off-lap of the basin. e) Sierra Ladrones and later time (beginning between 4 and 7 Ma), when the area was dominated by gravels from the recently-exhumed Chupadera Mountains, and an axial stream lay at the center of the basin.

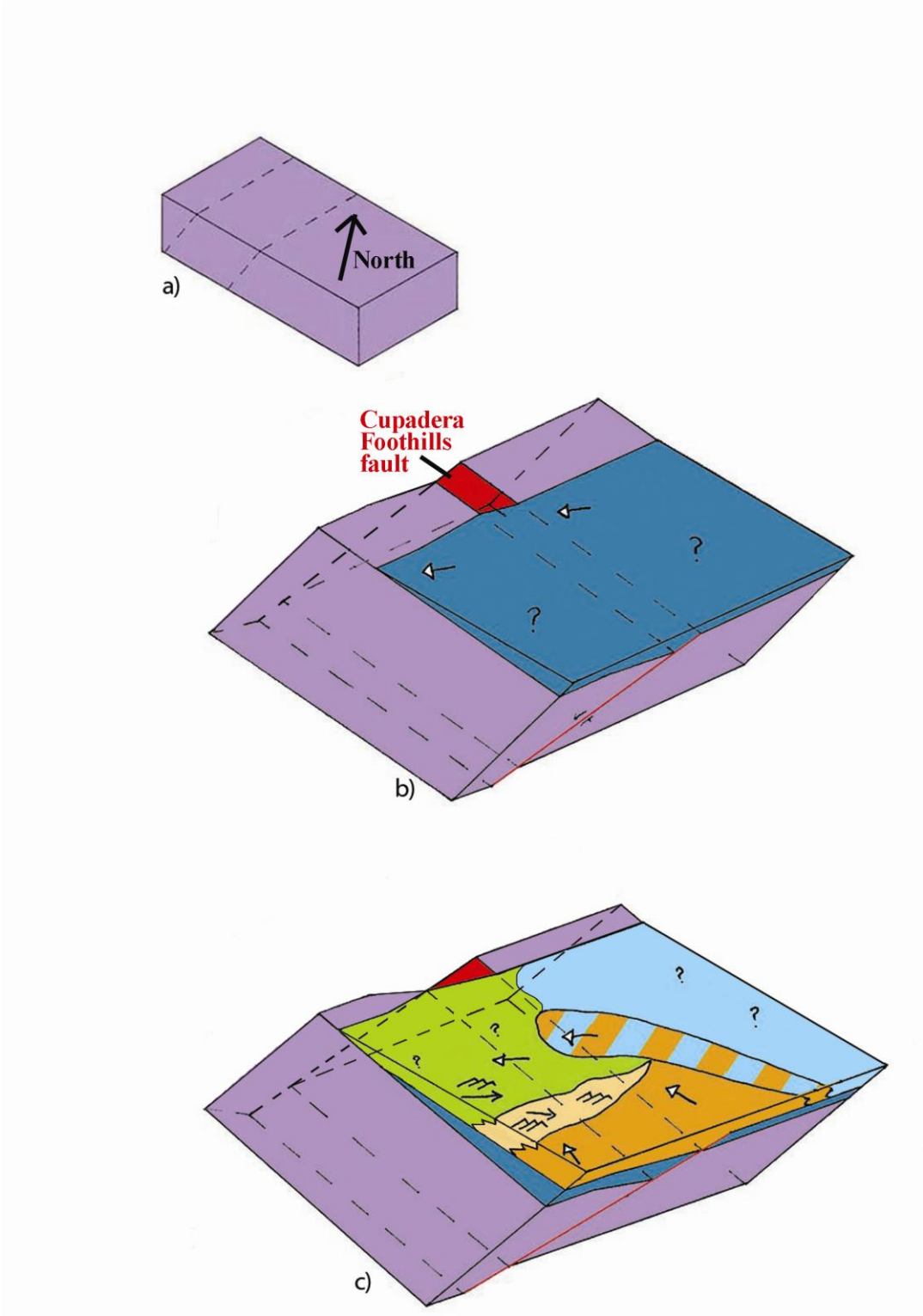

Figure 46 (caption on last page)

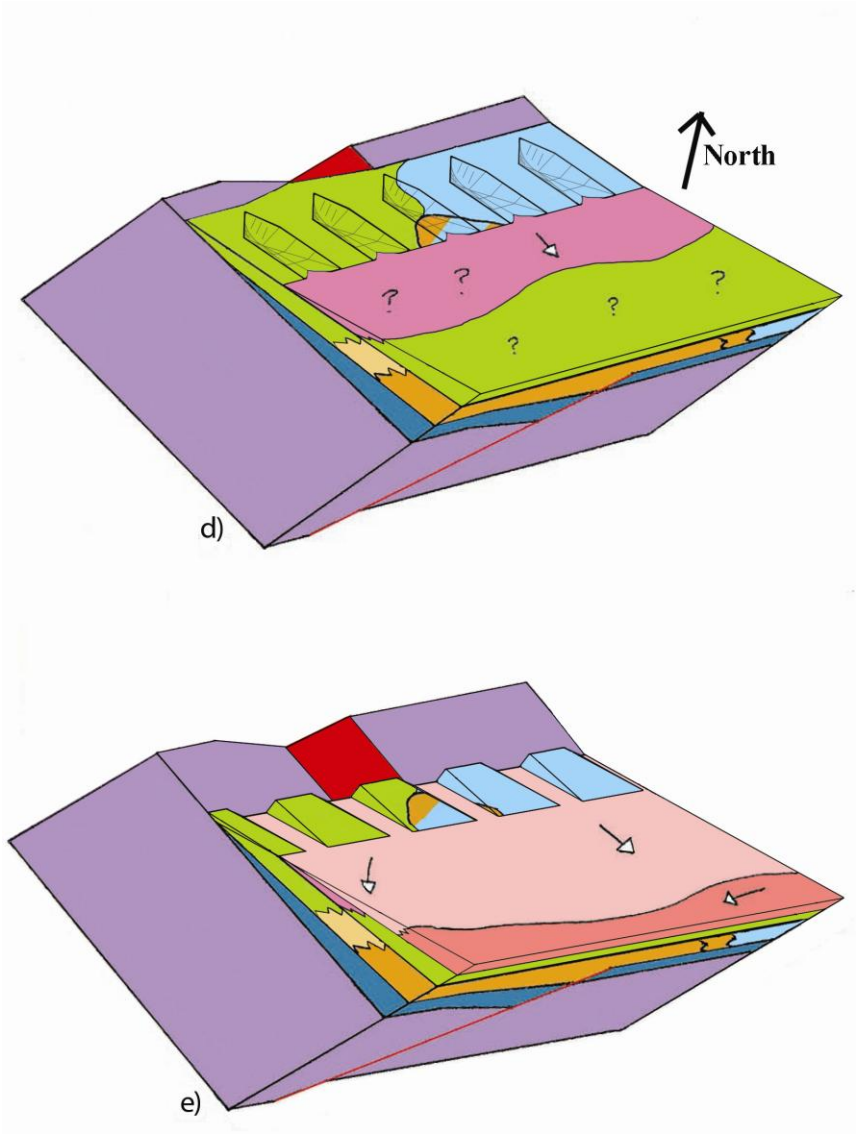

Figure 46 (continued from last page)

along the basin-bounding fault rotated strata down to the southeast, and may have caused progressive retreat of the eastern piedmont, as envisioned by Blair and Bilodeau (1988) and Cather et al. (1994; Figure 36). Retreat of the piedmont resulted in an up-section increase in sandstone abundance and fining of the conglomerates. Slip along northwest-striking intrabasinal faults caused thickness variations and northwest-trending folding of

the early basin fill.

With continued retreat of the eastern piedmont, the western piedmont migrated into the area sometime after the eruption of the basalt of Broken Tank at around 8.5 Ma (Figures 34 and 46d). The cause of this shift is uncertain, but appears to predate arrival of the ancestral Rio Grande as well as exhumation of the Chupadera Mountains. Similarities between the clast suites of the uppermost eastern piedmont deposits and lowermost western piedmont deposits suggest sediments of the eastern piedmont were exposed to erosion and reworked into the western piedmont (Figure 46d).

Around 4 to 7 Ma, the ancestral Rio Grande entered the area, and at this point the depositional setting largely resembled the present-day setting. Chupadera Mountain-derived gravels dominated the sedimentation, with a through-flowing river contributing pebbly sands and sands in the southeast of the area (Figures 35 and 46e). The basin fill continued to aggrade until about 800 ka, at which point the Rio Grande and its tributaries incised and initiated the present phase of basin fill excavation.

At some point, it appears that the intrabasinal faults switched from dominantly down-to-the-southwest to down-to-the-northeast. The cause of this is unknown, but its effect was to divide the Miocene Bosque basin into the Plio-Pleistocene to present basins of today. Flexural uplift along one of these major down-to-the-northeast faults resulted in exhumation of the Miocene fill on the BDA NWR (Figure 47). The basin continues to be tectonically active today, as evidenced by fault scarps in 120,000 year old Quaternary piedmont surfaces.

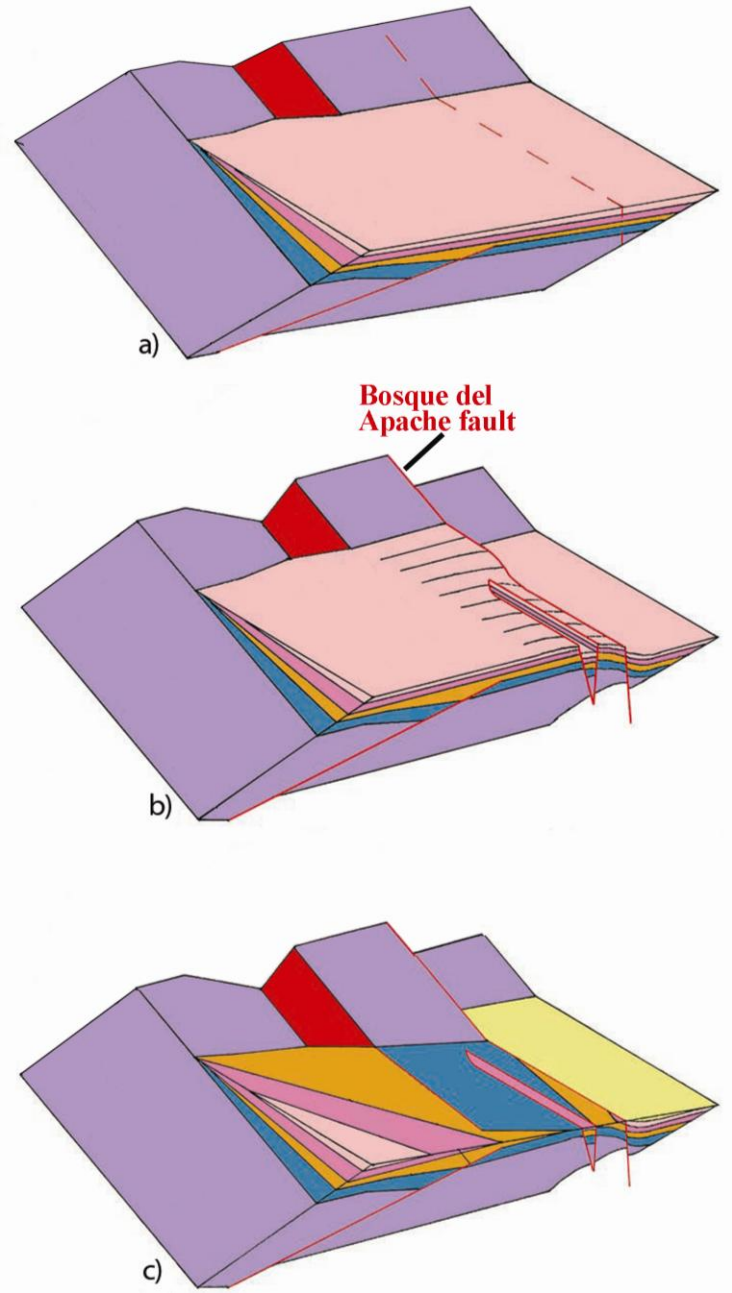

Figure 47 - Block diagrams demonstrating how flexural uplift due to slip along the BDA fault could result in exposure of Miocene basin fill in this area. Fault planes are colored red. Stratigraphy simplified from Figure 47e, and the colors no longer correspond to those of the geologic map. a) Block showing the pre-BDA fault setting. b) Slip along the BDA fault causes down-to-the-southwest rotation of strata. Horst-and-graben develop in the footwall of the fault. c) Erosion strips the post-Popotosa strata from the area, exposing the Miocene basin fill in a swath immediately adjacent to the BDA fault. Exposure decreases to the southwest due to the upper contact of the Popotosa projecting into the subsurface.

IMPLICATIONS FOR RIFT BASIN DEVELOPMENT

The results and interpretations of this study have implications for the development of rift basins in general. The structural development of the Bosque basin suggests the significant control exerted by pre-existing weaknesses and crustal properties. Also, the sediments of the study area demonstrate that dramatic changes in basin geometry can occur over the lifetime of a basin.

Structurally, the area is cut by two nearly orthogonal fault sets, both oblique to the extension direction, because of pre-existing weaknesses and spatial differences in crustal temperature and mechanical properties. Both fault sets parallel either nearby Precambrian or Laramide fabrics, suggesting the fault attitudes are controlled by these underlying weaknesses. Spatial differences in crustal thermal regime and preexisting anisotropies probably also contributed to the development of orthogonal sets by imposing left-lateral shear in the area. Neither set parallels the regional extension direction, suggesting the greater control of pre-existing weaknesses and crustal properties on rift fault attitudes than the actual direction of extension.

The results of this study also demonstrate the dramatic changes in basin geometry that can occur over the life of a basin. Between about 14 and 9 Ma, an extensive eastern piedmont blanketed the area, derived from an eastern footwall highland composed of two lithologically-distinct domains. The Chupadera Mountains were buried, and the basin

likely extended to the southwest. Sometime after 8.5 Ma, a western piedmont advanced into the area and supplanted the eastern piedmont, and later the ancestral Rio Grande entered the region. Today, the piedmont of the Chupadera Mountains dominates the area, the highland to the east is greatly diminished, and the BDA fault and similar faults close the basin in the center of the study area. These dramatic shifts, recorded in the Bosque and southern Socorro basin fills, demonstrate how greatly a rift basin can change through time.

REFERENCES

Armstrong, A.K. 1958. The Mississippian of west-central New Mexico: New Mexico Bureau of Mines and Mineral Resources Memoir **5**: 34 pp.

Balch, R.S., Hartse, H.E., Sandford, A.R., and Lin, K. 1997. A new map of the geographic extent of the Socorro magma body. *Bulletin of the Seismological Society of America* **87**: 174-182.

Baldwin, B. 1963. Part 2, Geology. *In* Spiegel, Zane, and Baldwin, *eds*. Geology and Water resources of the Santa Fe area, New Mexico. USGS Water-supply Paper 1525: 21-89.

Barroll, M.W. and Reiter, M. 1995. Hydrothermal investigation of the Bosque del Apache, New Mexico. *New Mexico Geology* **17**: 1-7.

Beck, W.C. 1993. Structural evolution of the Joyita Hills, Socorro County, New Mexico. New Mexico Institute of Mining and Technology unpublished M.S. thesis: 187 pp.

Bensing, J.P., Mozley, P.S., and Dunbar, N.W. 2005. Importance of clay in iron transport and sediment reddening; evidence from reduction features of the Abo Formation, New Mexico, USA. *Journal of Sedimentary Research* **75**: 562-571.

Blair, T.C. and Bilodeau, W.L. 1988. Development of tectonic cyclothems in rift, pull-apart, and foreland basins: Sedimentary response to episodic tectonism. *Geology* **16**: 517-520.

Bowring, S.A., Kent, S.C., and Sumner, W. 1983. Geology and U-Pb geochronology of Proterozoic rocks in the vicinity of Socorro, New Mexico. *In* Chapin, C.E. and Callender, J.E., *eds.* Socorro region II: New Mexico Geological Society Guidebook 34: 137-142.

Bruning, J.E. 1973. Origin of the Popotosa Formation, north-central Socorro County, New Mexico. New Mexico Institute of Mining and Technology Ph. D. dissertation; New Mexico Bureau of Mining and Mineral Resources Open-file Report 38: 132 pp.

Bull, W.B. 1991. Geomorphic responses to climate change. Oxford University Press: 326 pp.

Cather, S.M. 1990. Stress and volcanism in the northern Mogollon-Datil field, New Mexico: effects of the post-Laramide tectonic transition. *Geological Society of America Bulletin* **102**: 1447-1458.

Cather, S.M. 2002. Geology of the San Antonio quadrangle, Socorro County, New Mexico. New Mexico Bureau of Geology and Mineral Resources Open-file Geologic Map OF-GM-58. Scale 1:24,000.

Cather, S.M. 2004. Laramide orogeny in central and northern New Mexico and southern Colorado. *In* Mack, G.H. and Giles. K.A., *eds*. The geology of New Mexico: A geologic history: New Mexico Geological Society Special Publication 11: 203-248.

Cather, S.M. 2007. Preliminary geologic map of the Cañon Agua Buena quadrangle, Socorro County, New Mexico. New Mexico Bureau of Geology and Mineral Resources Open-file Geologic Map OF-GM-146. Scale 1:24,000.

Cather, S.M., Chamberlin, R.M., Chapin, C.E., and McIntosh, W.C. 1994a. Stratigraphic consequences of episodic extension in the Lemitar Mountains, central Rio Grande rift. *In* Keller, G.R. and Cather, S.M. *eds*. Basins of the Rio Grande rift: Structure, stratigraphy, and tectonic setting: Geological Society of America Special Paper 291: 157-169.

Cather, S.M., Chamberlin, R.M., and Ratté, J.C. 1994b. Tertiary stratigraphy and nomenclature for western New Mexico and eastern Arizona. *In* Chamberlin, R.M., Kues, B.S., Cather, S.M., Barker, J.M., and McIntosh, W.C., *eds*. Mogollon slope, west-central New Mexico and east-central Arizona: New Mexico Geological Society Guidebook 45: 259-266.

Chamberlin, R.M. 1980. Cenozoic stratigraphy and structure of the Socorro Peak volcanic center, central New Mexico. Colorado School of Mines Ph.D. dissertation; New Mexico Bureau of Mines and Mineral Resources Open-file Report 118: 395 pp.

Chamberlin, R.M. 1983. Cenozoic domino-style crustal extension in the Lemitar Mountains, New Mexico: A summary. *In* Chapin, C.E. and Callender, J.E., *eds*. Socorro region II: New Mexico Geological Society Guidebook 34: 111-118.

Chamberlin, R.M. 1999. Preliminary geologic map of the Socorro 7.5-minute quadrangle. New Mexico Bureau of Geology and Mineral Resources Open-file Geologic Map OF-GM-34.

Chamberlin, R.M. 2004. Preliminary geologic map of the San Lorenzo Spring 7.5-minute quadrangle, Socorro County, New Mexico. New Mexico Bureau of Geology and Mineral Resources Open-file Geologic Map OF-GM-86. Scale 1:24,000.

Chamberlin, R.M. and Osburn, G.R. 2006. Preliminary geologic map of the Water Canyon quadrangle, Socorro County, New Mexico. New Mexico Bureau of Geology and Mineral Resources Open-file Geologic Map OF-GM-118. Scale 1:24,000.

Chamberlin, R.M., Eggleston, T.L., and McIntosh, W.C. 2002. Preliminary geologic map the Luis Lopez 7.5-minute quadrangle, Socorro County, New Mexico. New Mexico Bureau of Geology and Mineral Resources Open-file Geologic Map OF-GM 53. Scale 1:24,000.

Chamberlin, R.M., McIntosh, W.C., and Eggleston, T.L. 2004. $^{40}Ar/^{39}Ar$ geochronology and eruptive history of the eastern sector of the Oligocene Socorro caldera, central Rio Grande rift, New Mexico. *In* Cather, S.M., McIntosh, W.C., and Kelley, S.A., *eds*. Tectonics, geochronology, and volcanism in the southern Rocky Mountains and Rio Grande rift: New Mexico Bureau of Geology and Mineral Resources Bulletin 160: 251-279.

Chamberlin, R.M., Love, D.W., and Peters, L. 2006. "Rock watching" along the Canyon Trail, Bosque del Apache National Wildlife Refuge: A pictorial guide to Neogene landscape evolution in central New Mexico. *New Mexico Geology* **28**: 63-64.

Chamberlin, R.M., McIntosh, W.C., and Dimeo, M.I. 2007. Geochronology of Oligocene mafic dikes within the southeastern Colorado Plateau: Implications to regional stress fields of the early Rio Grande rift. Poster presented at GSA Annual Meeting, October 28-31, Denver, CO.

Chapin, C.E. 1989. Volcanism along the Socorro accommodation zone, Rio Grande rift, New Mexico. *In* Chapin, C.E. and Zidek, J., *eds*. Field excursions to volcanic terranes in the western United States, Volume 1: Southern Rocky Mountain region: New Mexico Bureau of Mines and Mineral Resources Memoir 46: 46-57.

Chapin, C.E. and Seager, W.R. 1975. Evolution of the Rio Grande rift in the Socorro and Las Cruces areas. *In* Segaer, W.R., Clemons, R.E., and Callender, J.F., *eds*. Las Cruces County: New Mexico Geological Society Guidebook 26: 297-321.

Chapin, C.E., McIntosh, W.C., and Chamberlin, R.M. 2004a. The late Eocene-Oligocene peak of Cenozoic volcanism in southwestern New Mexico. *In* Mack, G.H. and Giles. K.A., *eds*. The geology of New Mexico: A geologic history: New Mexico Geological Society Special Publication 11: 271-294.

Chapin, C.E., Wilks, M., and McIntosh, W.C. 2004b. Space-time patterns of late

Cretaceous to present magmatism in New Mexico – comparison with Andean volcanism and potential for future volcanism. *In* Cather, S.M., McIntosh, W.C., and Kelley, S.A., *eds*. Tectonics, geochronology, and volcanism in the southern Rocky Mountains and Rio Grande rift: New Mexico Bureau of Geology and Mineral Resources Bulletin 160: 13-40.

Condie, K.C. and Budding, A.J. 1979. Geology and geochemistry of Precambrian rocks, central and south-central New Mexico. New Mexico Bureau of Mines and Mineral Resources Memoir 35: 58 pp.

Connell, S.D. 2004. Geology of the Albuquerque basin and tectonic development of the Rio Grande rift in north-central New Mexico. *In* Mack, G.H. and Giles. K.A., *eds*. The geology of New Mexico: A geologic history: New Mexico Geological Society Special Publication 11: 359-388.

Connell, S.D., Hawley, J.W., and Love, D.W. 2005. Late Cenozoic drainage development in the southeastern Basin and Range of New Mexico, southeasternmost Arizona, and western Texas. New Mexico Museum of Natural History and Science Bulletin 28: 125-150.

Connell, S.D., Love, D.W., and Dunbar, N.W. 2007. Geomorphology and stratigraphy of inset fluvial deposits along the Rio Grande valley in the central Albuquerque basin, New Mexico. *New Mexico Geology* **29**: 13-31.

Denny, C.S. 1940. Tertiary geology of the San Acacia area, New Mexico. *Journal of Geology* **48**: 73-106.

Dethier, D.P. and McCoy, W.D. 1993. Aminostratigraphic relations and age of Quaternary deposits, northern Española basin, New Mexico. *Quaternary Research* **39**: 222-230.

Dickinson, W.R. 2008. Conglomerate clast counts in Oligocene-Miocene strata north from the Catalina core complex to the Gila River, southeastern Arizona. Arizona Geological Survey Contributed Report CR-08-C: 34 pp.

Eardley, A.J. 1962. Structural geology of North America. Harper and Row: 743 pp.

Eggleston, T.L. 1982. Geology of the central Chupadera Mountains, Socorro County, New Mexico. New Mexico Institute of Mining and Technology M.S. thesis; New Mexico Bureau of Mines and Mineral Resouces Open-file Report 141: 161 pp.

Faulds, J.E. and Varga, R.J. 1998. The role of accommodation zones and transfer zones in the regional segmentation of extended terranes. *In* Faulds, J.E. and Steward, J.H. Accommodation zones and transfer zones: The regional segmentation of the Basin and Range province. Geological Society of America Special Paper 323: 1-45.

Ferguson, C.A. 1985. Geology of the east-central San Mateo Mountains, Socorro County, New Mexico. New Mexico Institute of Mining and Technology unpublished M.S. thesis: 118 pp.

Fialko, Y. and Simons, M. 2001. Evidence for on-going inflation of the Socorro magma body, New Mexico, from Interferometric Synthetic Aperature Radar imaging. *Geophysical Research Letters* **28**: 3549-3552.

Finnegan, N.J. and Pritchard, M.E. 2009. Magnitude and duration of surface uplift above the Socorro magma body. *Geology* **37**: 231-234.

Formento-Triligio, M.L. and Pazzaglia, F.J. 1998. Tectonic geomorphology of Sierra Nacimiento; traditional and new techniques in assessing long-term landscape evolution of the southern Rocky Mountains. *Journal of Geology* **106**: 433-453.

Geddes, R.W. 1963. Structural geology of Little San Pasqual Mountain and the adjacent Rio Grande trough. New Mexico Institute of Mining and Technology unpublished M.S. thesis: 64 pp.

Gile, L.H., Peterson, F.F., and Grossman, R.B. 1965. The K horizon: a master soil horizon of carbonate accumulation. *Soil Science* **99**: 74-82.

Gile, L.H., Hawley, J.W., and Grossman, R.B. 1981. Soils and geomorphology in the Basin and Range area of southern New Mexico: Guidebook to the Desert Project. New Mexico Bureau of Mines and Mineral Resources Memoir 39: 222 pp.

Goldstein, H.L. 2001. Spatial variation in soils developed on fluvial terraces, Socorro basin, Rio Grande rift, central New Mexico. New Mexico Institute of Mining and Technology unpublished M.S. thesis: 110 pp.

Harrison, R.W. and Cather, S.M. 2004. The Hot Springs fault system of south-central New Mexico – Evidence for the northward translation of the Colorado Plateau during the Laramide orogeny. *In* Cather, S.M., McIntosh, W.C., and Kelley, S.A., *eds*. Tectonics, geochronology, and volcanism in the southern Rocky Mountains and Rio Grande rift: New Mexico Bureau of Geology and Mineral Resources Bulletin 160: 161-179.

Hawley, J.W., Kottlowski, F.E., Seager, W.R., King, W.E., Strain, W.S., and LeMone, D.V. 1969. The Santa Fe Group in the south-central New Mexico border region. *In* Kottlowski, F.E. and LeMone, D.V., *eds*. Border stratigraphy symposium. New Mexico Bureau of Mining and Mineral Resources Circular 104: 52-76.

Hendrickx, J. and Harrison, J.B.J. 2000. Geomorphological Units, Bosque del Apache. Unpublished map submitted to the U.S. Fish and Wildlife Service, Bosque

Improvement Group, and New Mexico Tech. Scale 1:25,000.

Hudson, M.R., Rosenbaum, J.G., Grommé, C.S., Scott, R.B., and Rowley, P.D. 1998. Paleomagnetic evidence for counterclockwise rotation in a broad sinistral shear zone, Basin and Range province, southeastern Nevada and southwestern Utah. *In* Faulds, J.E. and Steward, J.H. Accommodation zones and transfer zones: The regional segmentation of the Basin and Range province. Geological Society of America Special Paper 323: 149-180.

Janecke, S.U., Vandenburg, C.J., and Blankenau, J.J. 1998. Geometry, mechanisms and significance of extensional folds from examples in the Rocky Mountain Basin and Range province, U.S.A. *Jounral of Structural Geology* **20**: 841-856.

Jones, T.A. 2006. MATLAB functions to analyze directional (azimuthal) data – I: Single-sample inference. Computers and Geosciences **32**: 166-175.

Karlstrom, K.E., Amato, J.M., Williams, M.L., Heizler, M., Shaw, C., Read, A., and Bauer, P. 2004. Proterozoic tectonic evolution of the New Mexico region: a synthesis. *In* Mack, G.H. and Giles. K.A., *eds*. The geology of New Mexico: A geologic history: New Mexico Geological Society Special Publication 11: 1-34.

Keller, G.R. 1983. Bouger gravity anomaly map of the Socorro region. *In* Chapin, C.E. and Callender, J.E., *eds.* Socorro region II: New Mexico Geological Society Guidebook 34: 96.

Kelley, S.A., Chapin, C.E., and Corrigan, J. 1992. Late Mesozoic to Cenozoic cooling histories of the flanks of the northern and central Rio Grande rift, Colorado and New Mexico. New Mexico Bureau of Mines and Mineral Resources Bulletin 145: 40 pp.

Kent, S.C. 1982. Geologic map of Precambrian rocks in the Magdalena and Chupadera Mountains, Socorro County, New Mexico. New Mexico Bureau of Mines and Mineral Resources Open-file Report 170. Scale 1:12,000.

Klein, C. 2002. The 22nd Edition of the Manual of Mineral Science. John Wiley and Sons: 641 pp.

Kottlowski, F.E. 1960. Summary of Pennsylvanian sections in southwestern New Mexico and southeastern Arizona. New Mexico Bureau of Mines and Mineral Resources Bulletin 66: 187 pp.

Kottlowski, F.E. 1963. Pennsylvanian rocks in the area around Socorro, New Mexico. *In* Kuellmer, F.J., *ed*. Socorro region: New Mexico Geological Society Guidebook 14: 102-111.

Krukowski, S.T. 1990. Conodont and foraminifer biostratigraphy of the Kelly Limestone (Mississippian), west-central New Mexico. New Mexico Institute of Mining and Technology Ph.D. dissertation: 355 pp.

Kues, B.S. and Giles, K.A. 2004. The late Paleozoic Ancestral Rocky Mountains System in New Mexico. *In* Mack, G.H. and Giles. K.A., *eds*. The geology of New Mexico: A geologic history: New Mexico Geological Society Special Publication 11: 95-136.

Langford, R.P. 1989. Fluvial-aeolian interactions: Part I, modern systems. *Sedimentology* **36**: 1023-1035.

Love, D.W., Dunbar, N., McIntosh, W.C., Connell, S.D., Sorrell, J., and Pierce, D.W. 2004. Plio-Pleistocene faults and unconformities in and between the Arroyo Ojito and Sierra Ladrones Formations and post-Santa Fe Group piedmont, Mesa del Sol and Llano de Manzano, Central Albuquerque Basin, New Mexico. New Mexico Geological Society spring meeting, abstract in New Mexico Geology **26**: 62.

Love, D.W., McCraw, D.J., Chamberlin, R.M., Reiter, M., Connell, S.D., Cather, S.M., and Majkowski, L. 2009. Progress report on tracking Rio Grande terraces across the uplift of the Socorro magma body. *In* Lueth, V.W., Lucas, S.G., and Chamberlin, R.M., *eds.* Geology of the Chupadera Mesa: New Mexico Geological Society Guidebook 60: 415-424.

Lozinsky, R.P. 1986. Geology and late Cenozoic history of the Elephant Butte area, Sierra County, New Mexico. New Mexico Bureau of Mines and Mineral Resource Circular 187: 40 pp.

Lozinsky, R.P. 1987. Cross section across the Jornada del Muerto, Engle, and northern Palomas basins, south-central New Mexico. *New Mexico Geology* **9**: 55-57.

Lueth, V.W., Lucas, S.G., and Chamberlin, R.M., *eds.* 2009. Geology of the Chupadera Mesa: New Mexico Geological Society Guidebook 60: 438 pp.

Machette, M.N. 1978. Geologic map of the San Acacia quadrangle, Socorro County, New Mexico. US Geological Survey Map GQ-1415. Scale 1:24,000.

Machette, M.N. 1985. Calcic soils of the southwestern United States. *Geological Society of America Special Paper* **203**: 1-21.

Machette, M.N., Personius, S.F., Kelson, K.I., Haller, K.M., and Dart, R.I. 1998. Map and data for Quaternary faults and folds in New Mexico. U.S. Geological Survey Open-file Report 98-521: 443 pp.

Machette, M.N., Marchetti, D.W., and Thompson, R.A. 2007. Ancient Lake Alamosa and

the Pliocene to middle Pleistocene evolution of the Rio Grande. *In* Machette, M.N., Coates, M., and Johnson, M.L. (eds.) "Quaternary geology of the San Luis basin of Colorado and New Mexico." USGS Open-file report 07-1193: 157-167.

Mack, G.H. 2004. Middle to late Cenozoic crustal extension, sedimentation, and volcanism in the southern Rio Grande rift, Basin and Range, and southern Transition Zone of southwestern New Mexico. *In* Mack, G.H. and Giles. K.A., *eds*. The geology of New Mexico: A geologic history: New Mexico Geological Society Special Publication 11: 359-408.

Mack, G.H., Salyards, S.L., and James, W.C. 1993. Magnetostratigraphy of the Plio-Pleistocene Camp Rice and Palomas Formations in the Rio Grande rift of southern New Mexico. *American Journal of Science* **293**: 49-77.

Mack, G.H. and Seager, W.R. 1995. Transfer zones in the southern Rio Grande rift. *Journal of the Geological Society of London* **152**: 551-560.

McClay, K.R., Dooley, T., Whitehouse, P., and Mills, M. 2002. 4-D evolution of rift systems: Insights from scaled physical models. *AAPG Bulletin* **86**: 935-959.

McGrath, D.B. and Hawley, J.W. 1987. Geomorphic evolution and soil-geomorphic relationships in the Socorro area, central New Mexico. *In* McLemore, V.T. and Bowie, M.R., *eds*. Guidebook to the Socorro area. New Mexico Bureau of Mines and Mineral Resources: 55-67.

McIntosh, W.C., Kedzie, L.L., and Sutter, J.F. 1991. Paleomagnetism and $^{40}Ar/^{39}Ar$ ages of ignimbrites, Mogollon-Datil volcanic field, southwestern New Mexico. New Mexico Bureau of Mines and Mineral Resources Bulletin 135: 79 pp.

Morgan, G.S., Lander, E.B., Cikoski, C., Chamberlin, R.M., and Love, D.W. 2009a. The oreodont *Merychyus major major* (Mammalia: Artiodactyla: Oreodontidae) from the Miocene Popotosa Formation, Bosque del Apache National Wildlife Refuge, Socorro County, central New Mexico. *New Mexico Geology* **31**: 91-103.

Morgan, G.S., Lucas, S.G., and Love, D.W. 2009b. Cenozoic vertebrates from Socorro County, central New Mexico. *In* Lueth, V.W., Lucas, S.G., and Chamberlin, R.M., *eds.* Geology of the Chupadera Mesa: New Mexico Geological Society Guidebook 60: 321-336.

Morton, W.H. and Black, R. 1975. Crustal attenuation in Afar. *In* Pilger, A. and Rosler, A., *eds*. Afar depression of Ethiopia: Inter-Union Commission on Geodynamics Scientific Report 14: 55-65.

Mussetter Engineering. 2002. Geomorphic and sedimentologic investigations of the middle Rio Grande between Cochiti dam and Elephant Butte reservoir. Interstate

Stream Commission technical report, available on-line at http://www.ose.state.nm.us/water-info/mrg-geomorphology-study/geomorphology.html, last accessed 01/14/10.

NMBGMR. 2003. Geologic map of New Mexico. New Mexico Bureau of Geology and Mineral Resources: Scale 1:500,000.

Osburn, G.R. 1978. Geology of the eastern Magdalena Mountains, Water Canyon to Pound Ranch, Socorro County, New Mexico. New Mexico Institute of Mining and Technology unpublished M.S. thesis: 136 pp.

Osbrun, G.R. (*Compiler*). 1984. Socorro County geologic map. New Mexico Bureau of Mines and Mineral Resources Open-file Report OFR-238.

Osburn, G.R. and Chapin, C.E. 1983. Nomenclature for Cenozoic rocks of northeast Mogollon-Datil volcanic field, New Mexico. New Mexico Bureau of Mines and Mineral Resources Stratigraphic Chart 1.

Pazzaglia, F.J. and Hawley, J.W. 2004. Neogene (rift flank) and Quaternary geology and geomorphology. *In* Mack, G.H. and Giles. K.A., *eds*. The geology of New Mexico: A geologic history: New Mexico Geological Society Special Publication 11: 407-438.

Phillips, F.M., Ayarbe, T.P., Harrison, J.B.J., and Elmore, D. 2003. Dating rupture events on alluvial fault scarps using cosmogenic nuclides and scarp morphology. *Earth and Planetary Science Letters* **215**: 203-218.

Petty, D.M. 1979. Geology of the southeastern Magdalena Mountains, Socorro County, New Mexico. New Mexico Institute of Mining and Technology unpublished M.S. thesis: 157 pp.

Reiter, M. and Barroll, M.W. 1990. High heat flow in the Jornada del Muerto: a region of crustal thinning in the Rio Grande rift without upper crustal extension. *Tectonophysics* **174**: 183-195.

Renne, P.R., Swisher, C.C., Deino, A.L., Karner, D.B., Owens, T.L., and DePaolo, D.J. 1998. Intercalibration of standards: Absolute ages and uncertainties in Ar-40/Ar-39 dating. *Chemical Geology* **145**: 117-152.

Roth, S.J. 1980. Geology of the Sawmill Canyon area of the Magdalena Mountains, New Mexico. New Mexico Institute of Mining and Technology unpublished M.S. thesis: 88 pp.

Schaetzl, R.J. and Anderson, S. 2006. Soils: Genesis and Geomorphology. Cambridge University Press: 817 pp.

Siemers, W.T. 1978. The stratigraphy, petrology and paleoenvironments of the Pennsylvanian System of the Socorro Region, west-central New Mexico. New Mexico Institute of Mining and Technology unpublished Ph.D. dissertation: 259 pp.

Smith, G.A. 2004. Middle to late Cenozoic development of the Rio Grande rift and adjacent regions in northern New Mexico. *In* Mack, G.H. and Giles. K.A., *eds*. The geology of New Mexico: A geologic history: New Mexico Geological Society Special Publication 11: 331-358.

Wilks, M.E. (*Compiler*). 2005. New Mexico geologic highway map. New Mexico Geological Society and New Mexico Bureau of Geology and Mineral Resources: Scale 1:1,000,000.

APPENDIX I – FREQUENCY DATA FOR PALEOCURRENT AND PALOWIND ROSE DIAGRAMS

Map unit:	Tpt1	Tpt2	Tpe	Tpa	Tpfi	Tsp	ARG	QTsp	Popotosa, undivided
Azimuth range	Frequency	Frequency	Frequency	Frequency	Frequency	Frequency	Frequency	Frequency	Frequency
345 - 15	0	0	0	0	0	0	0	0	0
15 - 45	0	0	3	1	0	2	1	0	2
45 - 75	1	0	7	2	0	0	0	3	4
75 - 105	0	0	14	0	0	5	1	6	1
105 - 135	1	0	16	2	0	2	0	6	6
135 - 165	0	1	8	1	3	6	1	5	10
165 - 195	3	1	0	1	3	6	2	4	12
195 - 225	4	2	1	5	5	0	3	2	23
225 - 255	8	4	2	23	7	0	5	2	52
255 - 285	4	3	1	29	3	0	1	0	49
285 - 315	3	2	0	17	0	0	1	0	31
315 - 345	0	2	0	6	0	0	2	0	11

Note – All data are paleocurrents from imbrications, except for in the "Tpe" column, which reflects paleowind data from the dip directions of eolian cross-strata. See "Methods" section for more discussion on the measurement and accuracy of paleocurrent and paleowind data.

APPENDIX II – CLAST COUNT DATA

Clast counts were performed on 67 conglomerate beds throughout the field area in an effort to evaluate temporal and spatial changes in provenance. Clast count methodology was discussed in the Methods section. Here, the modal abundances of clast lithologies are presented.

S.N.[1]	Easting (m)	Northing (m)	A. L.[2] (%)	Sc.[2] (%)	Abo[3] (%)	Ls[2] (%)	R.T.[2] (%)	Bas.[2] (%)	Other[4] (%)	N[5]
1	321933	3741928	40	4	0	0	52	0	5	176
2	321899	3741980	42	5	2	0	51	0	1	265
3	321880	3742133	48	3	0	0	49	0	1	160
4	321791	3742129	36	8	2	0	55	0	0	53
5	321696	3742141	29	5	0	0	66	0	0	217
6	321603	3742144	44	4	0	0	51	0	1	104
7	321391	3742064	32	7	0	0	61	0	1	130
8	321241	3742052	42	2	0	0	52	0	4	158
9	321207	3742087	25	8	1	0	64	0	3	117
10	320972	3742350	32	1	0	0	64	0	4	148
11	320922	3742252	25	3	1	0	68	0	4	157
12	320640	3742384	8	1	1	0	90	0	0	161
13	320537	3742472	27	1	0	0	70	0	1	151
14	320508	3742512	26	0	0	0	70	0	4	210
15	321389	3742511	36	1	1	0	60	0	2	219
16	321461	3742442	28	5	0	0	67	0	0	222
17	321473	3742354	51	2	0	0	46	0	0	232
18	321542	3742261	40	2	1	0	56	0	1	242
19	321587	3742235	26	6	0	0	67	0	0	205
20	320950	3742887	30	5	0	0	65	0	0	102
21	320965	3743047	19	5	0	0	75	0	0	129
22	320957	3743270	27	5	0	0	67	0	1	219
23	320778	3743504	20	2	0	0	78	0	0	162
24	320655	3743657	8	1	0	0	90	0	0	205
25	320489	3743662	3	1	0	0	96	0	0	149

S.N.[1]	Easting (m)	Northing (m)	A. L.[2] (%)	Sc.[2] (%)	Abo[3] (%)	Ls[2] (%)	R.T.[2] (%)	Bas.[2] (%)	Other[4] (%)	N[5]
26	320230	3743610	6	1	0	0	93	0	0	183
27	319801	3743752	3	0	0	0	96	0	0	206
28	319389	3743776	0	2	0	0	96	1	1	139
29	318905	3744022	1	2	0	0	94	2	1	160
30	322189	3741199	49	3	0	0	43	0	4	136
31	322200	3741068	33	9	0	0	57	0	1	197
32	322391	3740787	66	4	1	0	29	0	0	182
33	322751	3740709	55	6	1	0	38	0	0	154
34	322931	3740681	55	4	0	0	41	0	0	190
35	322998	3740563	51	8	1	0	39	1	1	195
36	323414	3740149	49	10	1	0	39	0	1	224
37	323536	3739854	50	4	1	0	44	0	1	149
38	323690	3742361	59	3	6	8	25	0	0	159
39	323682	3742844	40	2	4	1	50	0	3	231
40	323647	3742726	35	0	3	2	58	0	2	170
41	323362	3741440	50	8	1	0	39	0	1	206
42	323389	3741437	41	9	3	0	46	0	1	192
43	322520	3741575	28	14	2	0	56	0	1	218
44	322792	3741470	39	14	1	1	45	0	1	184
45	321909	3742167	40	15	0	1	44	0	0	124
46	322063	3742111	9	2	0	0	89	0	0	102
47	322102	3742378	56	5	2	0	37	0	0	227
48	322103	3742417	22	5	0	0	72	0	0	219
49	321824	3742794	31	3	2	0	65	0	0	119
50	321766	3743040	43	4	1	0	53	0	0	171
51	322012	3742966	20	2	2	0	77	0	0	185
52	322070	3742943	61	5	1	1	32	0	0	352
53	322078	3743081	13	5	0	0	81	0	1	187
54	322459	3743095	17	2	2	0	79	0	0	251
55	322877	3743097	28	8	1	0	62	0	1	311
56	322871	3743211	42	14	3	2	39	0	1	189
57	322811	3743393	30	0	4	0	64	0	0	210
58	322249	3744412	11	0	1	0	85	0	3	165
59	322331	3744400	12	0	1	0	87	0	0	188
60	322587	3744274	3	0	0	0	95	2	1	148
61	322177	3743988	11	3	2	0	83	0	1	108
62	322021	3744031	23	6	0	0	71	0	0	174
63	321775	3744151	13	4	0	0	83	0	0	147
64	321715	3744131	30	1	0	0	69	0	0	190
65	321802	3744842	5	6	0	0	89	0	0	181
66	321237	3745057	12	1	0	0	79	7	0	241

S.N.[1]	Easting (m)	Northing (m)	A. L.[2] (%)	Sc.[2] (%)	Abo[3] (%)	Ls[2] (%)	R.T.[2] (%)	Bas.[2] (%)	Other[4] (%)	N[5]
67	321347	3741169	66	1	2	0	27	0	4	178

[1] – "S.N." = Station number

[2] – Rock unit abbreviations: "A.L." = andesitic lava; "Sc." = scoria; "Ls" = limestone; "R.T." = rhyolitic tuff; "Bas." = basalt

[3] – "Abo" here refers to red siltstones and sandstones, with or without reduction spots, suspected of belonging to one of the Permian "red bed" units, e.g. Abo Formation or one of the members of the Yeso Formation.

[4] – Included in "Other" are volcaniclastic sedimentary rocks, chert, vein quartz, quartzite, gray siltstones, and fine-grained rocks that could not be identified

[5] – N refers to the total number of clasts examined at the station

APPENDIX III – SANDSTONE PETROGRAPHY

Modal abundances of various minerals and lithics were visually estimated in 11 sandstone thin sections. The methodology was summarized in the Methods section, their locations are given in Figure 29, and the results are presented here.

T.S.N.[1]	T.S.#[2]	Easting (m)	Northing (m)	E /A[3]?	Fine grnd?[4]	Plag.[5] (%)	K-sp[5] (%)	Qtz[5] (%)	A.l.[5] (%)	D.g.[5] (%)	F.g.l.[5] (%)	R.b.c[5] (%)
13301	1	323009	3743445	A	yes	9	15	2	3	1	24	4
13302	2	323319	3743499	A	yes	12	17	3	2	4	10	4
13303	3	323399	3740140	A	no	25	3	0	30	3	0	3
CT-1	4	323237	3740149	E	no	18	7	0	3	1	14	5
13304	5	322015	3741863	A	yes	12	5	3	6	1	18	5
13305	6	321213	3742063	E	no	13	3	2	18	13	18	3
13306	7	321201	3742087	A	yes	18	8	2	0	16	13	6
13307	8	320914	3742254	A	no	15	8	1	8	9	15	4
13308[4]	9	320504	3742542	E	no	5	13	1	8	5	10	3
13309	10	320474	3742557	A	yes	16	12	2	6	3	4	5
13310	11	319472	3743823	A	no	14	13	1	0	0	27	16

T.S.N.[1]	T.S.#[2]	Amph[5] (%)	Bt[5] (%)	Pyx[5] (%)	Opq[5] (%)	Id(?)[5] (%)	F.g.m.[5] (%)	Poro[5] (%)	Carb. cem.[5] (%)
13301	1	0	0	0	4	1	28	9	0
13302	2	1	0	0	4	0	41	3	0
13303	3	4	0	0	5	0	27	1	0
CT-1	4	4	0	0	4	0	27	5	14
13304	5	2	0	0	4	0	35	9	0
13305	6	2	0	0	4	1	1	23	0
13306	7	5	0	0	7	1	9	16	0
13307	8	4	0	1	4	2	13	18	0
13308[6]	9	4	1	0	4	0	25	23	0
13309	10	5	0	0	3	0	33	9	0
13310	11	1	3	0	5	1	0	20	0

[1] – "T.S.N." = "Thin Section Name" and refers to the code scratched on the thin sections themselves. "133--" series refers to samples collected by CT Cikoski; "CT-1" was collected by RM Chamberlin.

[2] – "T.S.#" = "Thin Section Number" and refers to the numbers used within the thesis, including Figure 29. Numbers designate stratigraphic order (e.g., 1 is highest, 11 is lowest stratigraphically).

[3] – "E/A?" = "Eolian or Alluvial?" and refers to the mode of deposition of the sandstone

[4] – Refers to thin sections that were too fine grained for accurate visual abundance estimates at 4X magnification. These thin sections were examined at both 4X and 10X. This is of importance here as lithic content was of interest to this study and lithic content is a function of grain size.

[5] – Abbreviations of phases: "Plag." = plagioclase; "K-sp" = potassium feldspar; "Qtz" = quartz; "A.l." = andesitic lithics; "D.g." = devitrified glass; "F.g.l." = fine-grained lithics; "R.b.c." = red-brown clay; "Amph" = amphibole; "Bt" = biotite; "Pyx" = pyroxene; "Opq" = opaques; "Id(?)" = iddinsite(?); "F.g.m." = fine-grained matrix; "Poro" = porosity; "Carb. cem." = carbonate cement

[6] – Thin section 13308 (number 9) had significant fracturing that I believe resulted from sampling and/or thin section preparation. Porosity given here is therefore suspected to be high compared to the in situ sandstone.

APPENDIX IV – $^{40}AR/^{39}AR$ GEOCHRONOLOGY

Summary table of $^{40}Ar/^{39}Ar$ age determinations for the Indian Well Wilderness quad

Field No.	Map Unit	Lab No.	Material Dated	Method	N	Age (Ma)	± 2 σ	MSWD	K/Ca	± 2 σ	UTM-E	UTM-N
IWW-2004-1	Tbt1	55099	groundmass	RHIF	5	8.57	0.26	1.75	0.26	nc	0322772	3744077
CTC-1	Tpt2	57746	sanidine	SCLF	12	14.59	0.05	2.76	100.7	36.8	0321323	3744229

NOTES: Method is single crystal laser fusion (SCLF) or resistance furnace incremental heating (RFIH). "N" is number of individual crystals analyzed (SCLF) or number of heating steps used to calculate weighted mean age (RFIH); K/Ca is molar ratio calculated from K-derived 39Ar and Ca-derived 37Ar. Two-sigma variance not calculated (nc) for RHIF samples. Mean sum weighted deviates (MSWD) value with asterisk(*) indicates confidence interval less than 95%.

Methods: Sample preparation: sanidine, –crushing, heavy liquid, Franz, HF; groundmass concentrate – crushing, dilute acid, heavy liquid, hand picking. Samples loaded into machined Al disk and irradiated in D-3 position, Nuclear Science Center, College Station, TX. The sanidine sample was irradiated for 7 hours while the groundmass concentrate was irradiated for 14 hours. Neutron flux monitor Fish Canyon Tuff sanidine (FC-1). Assigned age = 28.02 Ma (Renne et al., 1998); samples and monitors irradiated in alternating holes in machined Al disks.

Laboratory: New Mexico Geochronology Research Laboratory, Socorro NM. Instrumentation: Mass Analyzer Products 215-50 mass spectrometer on line with automated all-metal extraction system. Heating: sanidine – SCLF, 10W continuous CO2 laser; RFIH – 36 mg aliquot in resistance furnace. Reactive gas cleanup: SAES GP-50 getters operated at 20 °C and ~450 °C; SCLF – 1 to 2 minutes, RFIH – 9 minutes. Error calculation: all errors reported at ±2 sigma, mean ages calculated using inverse variance weighting of Samson and Alexander (1987); decay constant and isotopic abundances after Steiger and Jaeger (1977).

Analytical parameters: electron multiplier sensitivity = 4.17 x 10-16 moles/pA for the furnace sample and 5.60 x 10-17 for the laser sample; typical system blanks were 2880, 2.9, 1.3, 0.2, 9.2 x 10-18 moles (furnace) and 230, 5.4 , 1.4 , 1.1, 7.8 (laser) at masses 40, 39, 38, 37, 36 respectively; J-factors determined using SCLF of 4 to 6 crystals from each of 6 or 10 radial positions around irradiation vessel. Correction factors for interfering nuclear reactions, determined using K-glass and CaF2, (40Ar/39Ar) K = 0.0±0.0004; (36Ar/37Ar) Ca = 0.00028±0.00002; and (39Ar/37Ar) Ca = 0.00068±0.00005.

Samples: Samples are listed in apparent stratigraphic order. Collected by David Love (IWW-2004) and Colin Cikoski (CTC). Sample locations are in UTM zone 13S and based on 1927 NAD. Map units are shown on Figure 1; Tbt1 is the basalt of Broken Tank, Tpt2 is the ash-bearing member of the lower Popotosa Formation at Bosque del Apache.

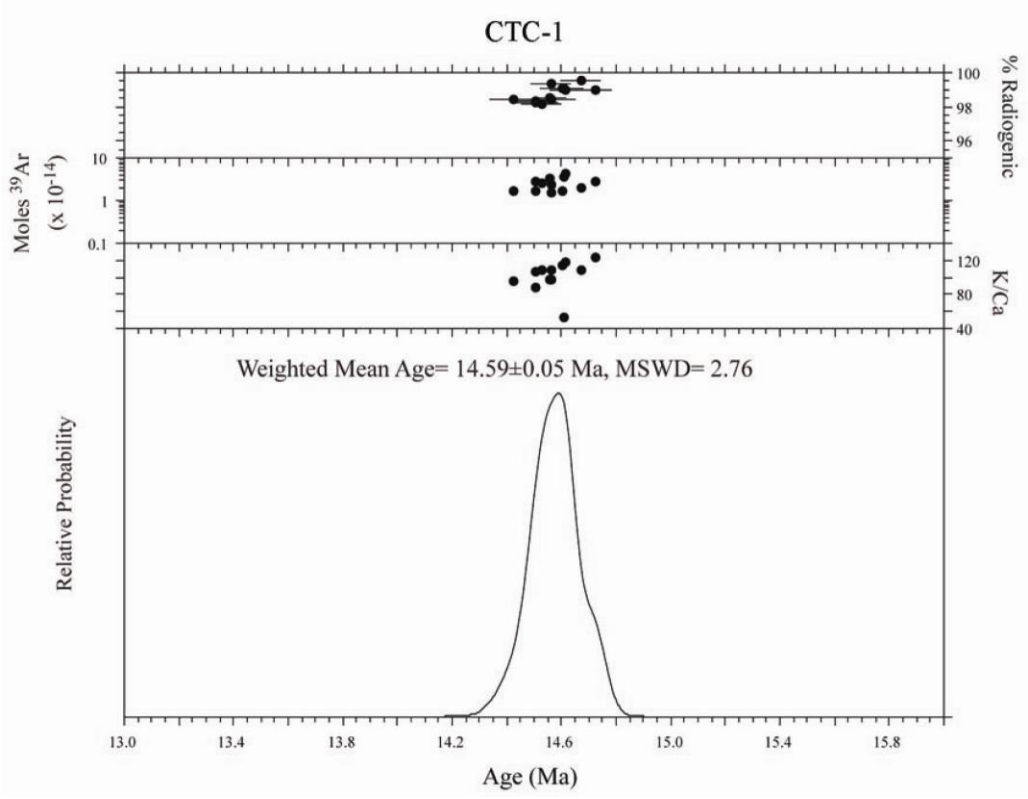

Figure A4-1 – Age probability distribution diagram for CTC-1, a sample of sanidines recovered from pumices from sandstones at the base of Tpt2. See the footnotes for Table 1 for an explanation of abbrevations. Note that the analyzed sanidine crystals came from multiple pumice clasts, such that the narrow peak in the age probability graph likely reflects a lack of sedimentary reworking (and mixing) since the eruptive event.

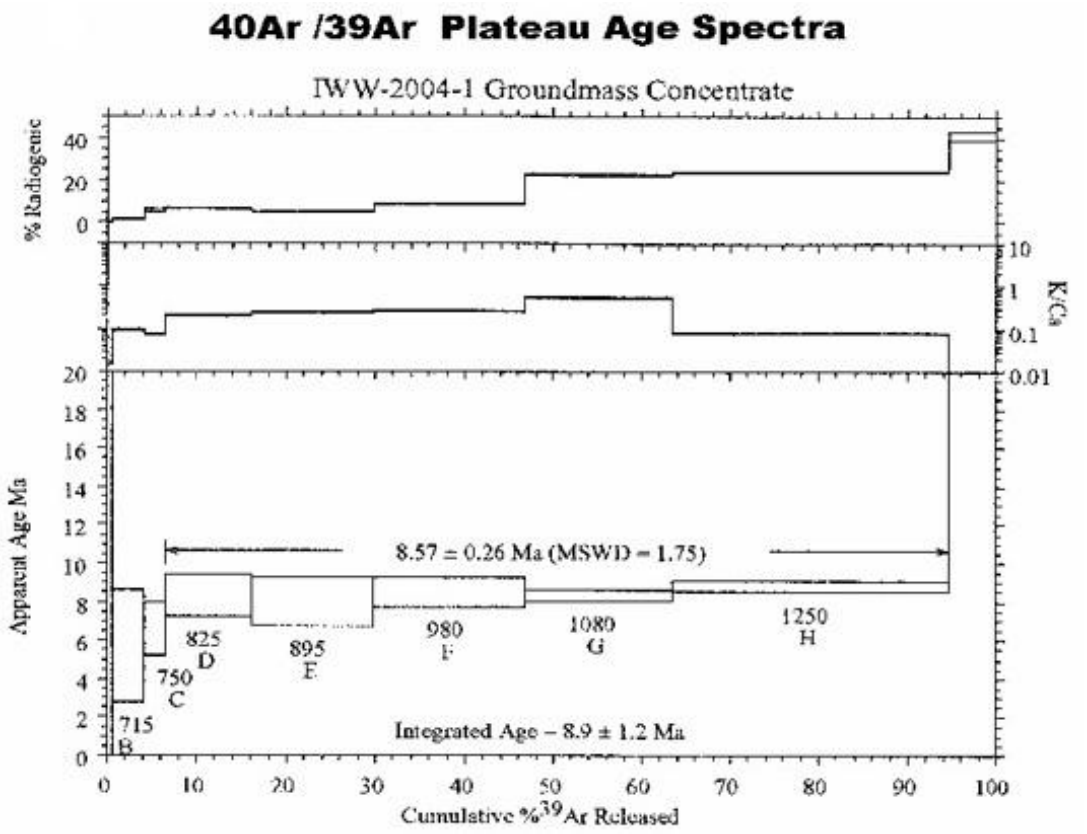

Figure A4-2 – Plateau age spectra for sample IWW-2004-1, a sample from the basalt of Broken Tank, map unit Tbt1. See the footnotes for the above table for an explanation of abbreviations.